Practical Invisibility Cloaking

by

Joseph Sung-hwoon Choi

Submitted in Partial Fulfillment of the

Requirements for the Degree

Doctor of Philosophy

Supervised by Professor John C. Howell

The Institute of Optics
Arts, Sciences and Engineering
Edmund A. Hajim School of Engineering and Applied Sciences

University of Rochester
Rochester, New York

2016

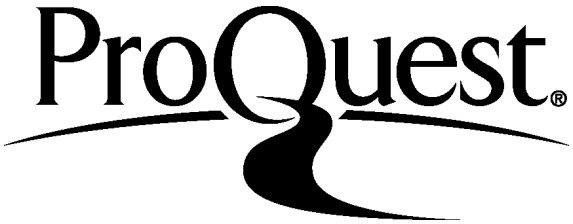

With love,

to my parents, Soo-Young and Ock-Ja Choi,

for my wife Sora Kim Choi, and my children Elly Min-ji and Clayton Min-ho.

Thank you for your faith, patience, and support.

Biographical Sketch

Joseph ("Joe") Choi was born in Hawaii, but grew up mostly in Utah and Korea. He received his Bachelor of Science degree from Brigham Young University (BYU), as a double major in Physics and Mathematics in 2001, graduating magna cum laude with University Honors. His honors thesis at BYU was in Physics, advised by Professor David Allred, where he built an ultrahigh vacuum, thin film deposition chamber. Joseph then began a PhD program in Physics at Cornell University, where he worked on high-Tc superconductor experiments with Professor J. C. Séamus Davis, and accelerator physics with Professor Georg Hoffstaetter. With an opportunity to help start a business with his brother Michael, Joseph took a break from Cornell University in 2006 after receiving a Master of Science degree in Physics.

Joseph worked on a start-up called BoomYEAH, which provided an online, visual directory for businesses, and also consulted e-commerce businesses with internet marketing. He was a business intelligence analyst for Nu Skin International as well as Xango, and was a software developer at Adobe Systems (Omniture business unit for web analytics). Through these experiences, Joseph found a strong interest in entrepreneurship and business. However, the desire to conduct research in quantum optics, which began at Cornell University, remained. This lingering passion is why he chose to enter the PhD program at the Institute of Optics at the University of Rochester.

As the recipient of a Robert L. and Mary L. Sproull Fellowship, Joseph began his PhD studies at the Institute of Optics in the fall of 2010. In 2011, Joseph received two years of additional funding through a National Science Foundation (NSF) IGERT (Integrative Graduate Education Research and Traineeship) fellowship, which had a focus on renewable energy research. By the first week of school in 2010, Joseph joined Professor John C. Howell's experimental quantum optics and quantum information group. In the Howell lab, he worked on various experimental projects that included interferometry with weak value amplification, Rubidium atomic physics, photonic crystals, optical cavities, cross-phase modulation, and invisibility cloaking.

While at the University of Rochester, Joseph served in various positions for leadership and outreach. With other IGERT fellows, Joseph visited Ghana for a month in 2013, where they helped students build and install solar energy panels in a rural village, shared the Optics Suitcase from the Optical Society (OSA) and other science demonstrations to several technical high schools, and presented to university students and faculty. He was the Senior Graduate Representative and member of the Graduate Committee for the Institute of Optics (2013-14), and Vice-President of the University of Rochester student chapter for SPIE (2015-16). He served in the conference committee for "Novel Optical Systems Design and Optimization" at SPIE (2015-), and as a member of the Future Leaders Committee and the Membership Committee of SPIE (2016-). With fellow optics and church friends, he played with and coached their basketball team "LightShots" all the way to the intramural open league championship match in March, 2014. He has also mentored students and worked with teachers in middle shool, high school, and universities, to help build their own versions of the "Rochester Cloak" for science fairs, classes, and labs.

(More details available at www.JosephSChoi.com)

Publications

[7] Joseph S. Choi, and John C. Howell, "Digital integral cloaking," *Optica* (accepted) (2016).

[6] Joseph S. Choi, and John C. Howell, "Paraxial full-field cloaking," *Optics Express* **23**, 15857–15862 (2015).

[5] Joseph S. Choi, and John C. Howell, "Paraxial ray optics cloaking," *Optics Express* **22**, 29465–29478 (2014).

[4] John C. Howell, J. Benjamin Howell, and Joseph S. Choi, "Amplitude-only, passive, broadband, optical spatial cloaking of very large objects," *Applied Optics* **53**, 1958–1963 (2014).

[3] Hanju Rhee, Joseph S. Choi, David J. Starling, John C. Howell, and Minhaeng Cho, "Amplifications in chiroptical spectroscopy, optical enantioselectivity, and weak value measurement," *Chemical Science* **4**, 4107–4114 (2013).

[2] Joseph S. Choi, and Minhaeng Cho, "Limitations of a superchiral field," *Physical Review A* **86**, 063834 (2012).

[1] David J. Starling, Steven M. Bloch, Praveen K. Vudyasetu, Joseph S. Choi, Bethany Little, and John C. Howell, "Double Lorentzian atomic prism," *Physical Review A* **86**, 023826 (2012).

Conference Proceedings

[xi] Joseph S. Choi, and John C. Howell, "Paraxial Cloaking- A 'Rochester Cloak:' Is an Ideal, Broadband and Omnidirectional Cloak Possible?," *SPIE Optics and Photonics*, San Diego, CA, Poster #9544-109 (August, 2015).

[x] Joseph S. Choi, and John C. Howell, "Multidirectional Invisibility with Rays of Light- A "Rochester Cloak"," Workshop at *AAPT (American Association of Physics Teachers) Advanced Labs, BFY 2 (Beyond the First Year II) Conference*, College Park, MD (July, 2015).

[ix] Joseph S. Choi, and John C. Howell, "Paraxial full-field cloaking," *APS DAMOP*, **60**, U8.00009, Columbus, OH (June, 2015).

[viii] Joseph S. Choi, "Cloaking from Visible Light - A "Rochester Cloak"," *Photons after Dark*, Rochester Institute of Technology, NY (February 18, 2015).

[vii] Joseph S. Choi, and John C. Howell, "Paraxial ray optics cloaking," *SPIE Photonics West*, San Francisco, CA (February 10, 2015).
(*Proceedings of SPIE* **Vol. 9371** 937110 (2015).)
(Edmund Optics Exhibitor Booth Demonstration (beginning at 4:12): "Light Matters," *Photonics Media* (February 18, 2015).)

[vi] Joseph S. Choi, "How to cloak with rays of light," Tech+Forum, Seoul, Korea (Nov. 20, 2014).

[v] Joseph S. Choi, John C. Howell, Minhaeng Cho, "Limitations of a Superchiral Field," NSF IGERT Presentation, Kwame Nkrumah University of Science and Technology (KNUST), Kumasi, Ghana (August, 2013).

[iv] Joseph S. Choi, Chanse Hungerford, Stephen Head, Amanda Preske, Tyler DuBeshter, Ryan Severins, Lenore Kubie and Rebecca Berman, "Solar Panel

Workshop in Ghana," NSF IGERT, Takoradi Technical Institute (TTI), Ghana (August, 2013).

[iii] Joseph S. Choi, Minhaeng Cho, "Limitations of a Superchiral Field," Poster session, *Energy for the 21st Century Symposium*, Rochester NY (March 15, 2013).

[ii] Joseph S. Choi, Hyun Il Cheong, Michal Maj, Minhaeng Cho, Todd D. Krauss, Kara L. Bren, "Spectrum of Zn Porphyrin Pair Under Translation and Rotation," Poster session, *Energy for the 21st Century Symposium*, Rochester NY (March 15, 2013).

[i] Joseph S. Choi, and John C. Howell, "Overview of Possible Quantum Mechanics in Photosynthesis," Poster session, *Energy for the 21st Century Symposium*, Rochester NY (October 10, 2011).

Patents

[b] John C. Howell and Joseph S. Choi, "Cloaking Systems and Methods," U.S. Provisional Patent Application 62/251,781 (Filing Date: November 6, 2015; patent pending).

[a] Joseph S. Choi and John C. Howell, "Paraxial Cloak Design and Device," U.S. Utility Patent Application 14/714,671 (Filing Date: May 18, 2015; patent pending).

Acknowledgments

First, I would like to thank God for giving me a perfect opportunity to begin and finish my PhD at the Institute of Optics. I have been blessed to have received two fellowships that have given me freedom to study what I came here to research-experimental quantum optics and quantum computing. The relatively large media coverage for some of our invisibility cloaking work was a gift as well.

I have been fortunate to have joined Professor John Howell's group, one that remains competitive to enter even today. Professor Howell seems to have an endless source of ideas and enthusiasm for physics, combined with excellent intuition and rules-of-thumb, which have been key to the success of all of our research projects. His persistence to achieve the best results possible has been an inspiring example of how to pursue research. He has especially been a role model to me on how to be an effective principal investigator, manager of a team, scientist, and researcher, while being a good father, husband, and person. If I can be more like him, my wife, children, family, and friends would be quite happy.

I would like to thank my committee members - Professor Carlos Stroud, who served as my Optics internal advisor and mentor for many years (and happens to be the advisor of Professor John Howell's advisor), Professor Nick Vamivakas, who has been a friend and advisor, Professor Andrew Jordan, who has been an example to me of a very successful theoretical physicist, and Professor Allan Greenleaf for his time and help on our cloaking research and my PhD.

I am indebted in particular, to Professor David Allred, my undergraduate advisor at BYU. He was the only professor that seemed to have faith in me when no others in academia did. While contemplating a return to graduate school, he patiently listened to me, and encouraged me to apply for a PhD program again as if I should succeed since he believed me to be one of his best students. That optimism and faith of Professor Allred, which likely led to a glowing letter of recommendation for my application, was instrumental in not only being accepted to all of the Optics schools I applied, but in receiving fellowships to attend. I am extremely lucky to have had such an advisor who cared for me long after I graduated from his group.

I have learned a lot, in knowledge and lab skills, from all of my group members. In particular, David Starling was my instructor and mentor when I first joined the lab, and continued to be such in the group. Steve Bloch was another mentor to me, who showed me how to use many of the lab equipments, seemed to have extensive knowledge of most setups and principles of the atomic physics side of the lab. Praveen Vudyasetu was always a gentleman to me whom I could ask questions on quantum transitions and other optics-related inquiries. Curtis Broadbent has been a great example to me of how to do experiments and develop theory well and deeply, through our collaborations and sharing of the lab space. Even though we only worked on one project together, and even that was cut short, Gerardo Viza has been a soft-spoken, kind-hearted friend and labmate to me. Greg Howland has been a great source of counsel, sometimes good and sometimes eccentric, but always a model to me for how to be a good researcher with solid physics intuition. I would also like to thank my other labmates for their friendship, time, and sharing of knowledge and skills: Ben Dixon, James Schneeloch, Bethany Little, Julian Martinez, Chris Mullarkey, Daniel Lum, Samuel Knarr, Justin Winkler, and Shurik (Alexander) Zavriyev.

In particular, I would like to thank my research collaborators, Professor Minhaeng Cho and Dr. Hanju Rhee from Korea University. They are tremendously successful scientists who have been very supportive in allowing me to be a part of their publications. I have really enjoyed every visit to Korea University because of their care. Also, Dr. Andrey V. Okishev from the Laboratory for Laser Energetics (LLE), who is also an Institute of Optics alumni, single-handedly helped me solve the cavity problems I had by generously lending equipment, visiting with me multiple times and sharing knowledge that helped me successfully build a confocal optical cavity for the first time, within a few weeks.

To my Institute of Optics classmates of the same year (entering PhD class of 2010), we struggled through late night homeworks, months-long prelim study sessions, and really learned our optics: Daniel Savage, Mohammad Mirhosseini, Chanse Hungerford, Mark Kasperczyk, Stephen Head, James Corsetti, Aizhong Zhang, Brandon Zimmerman, Sam Spencer, and Robert Gray. My PhD stay was much lighter thanks to my friends and colleagues at the Institute: Aaron Bauer, Kyle Fuershbach, Tony Visconti, Zachary Lapin, Cristina Canavesi, Greg Schmidt, Haomin Yao, Anthony Yee, Anthony Vella, Coby Reimers as Junior Grad Rep while I was Senior Grad Rep, Heedeuk Shin, Taek Yong Hwang, Janghwan Bae, Haewon Jung, Kye-Sung Lee, Joe Vornehm, Dan Christensen, Dustin Shipp, Luke Bissell, and many others.

The Institute of Optics staff really made things work: Lissa Cotter, Kari Brick, Lori Russell, Gina Kern, Maria Schnitzler, Per Adam, and others. I would also like to thank my professors: Lukas Novotny, Miguel Alonso, Dale Buralli, Jim Fienup, Gary Wicks, Janick Rolland-Thompson, Julie Bentley, Chunlei Guo, Nicholas George, Jim Zavislan, Joe Eberly, Andrew Berger, Robert Boyd, Thomas Brown, Todd Krauss, Kara Bren, Wayne Knox, Duncan Moore, and Director Xi-Cheng Zhang. I have also appreciated the regular help the Physics staff has given me: "Mike" Myron Culver, David Munson, Richard Sarkis, Sondra Anderson, Laura

Blumkin, Shirley Brignall, Connie Hendricks, Connie Jones, Cynthia Spencer, Caleb J. Winne, and others. Thank you for adopting me into the department.

The IGERT program has been a privilege to be a part, so I would like to acknowledge Professor Phillip Fauchet, Vicki Heberling, Matthew Yates, and my own IGERT cohort: Stephen Head, Chanse Hungerford, Tyler Dubeshter, Amanda Preske, Ryan Severins. We had a lot of fun in Ghana and in various activities. Same goes for my additional friends from IGERT: Rebecca Berman, Andrew Durney, Kenny Goodfellow, etc. Through IGERT, I was able to finish the T.E.A.M. Master of Science program, where Professor Duncan Moore, Andrea Galati, He Ba, Ahmed Khogheer, and my T.E.A.M. classmates and friends helped me finish.

I have been privileged to associate with smart scientists and friendly colleagues at the University of Rochester who have helped me learn more science: Justin Dressel, Shantanu Agarwal, Steve Gillmer, Arnab Kar, Brandon Rodenburg, Levi Neukirch, Mishkat Bhattacharya (RIT), and many more. I have also been able to serve our SPIE student chapter with Fabrizio Buccheri, Katelynn Sharma, Ashley Cannaday, Daniel Brooks, and Di Xu. In particular, I am very grateful for the support that Dirk Fabian and SPIE provided me. The SPIE scholarship was given to me in the middle of my PhD program, when it was very much needed to replace my dead computer and laptop. The scholarship was used effectively to purchase a laptop, which has been used extensively for my research over the past 3 years or so, with which I have written my thesis as well! The funding and support to participate in committees and SPIE conferences have also been very beneficial in expanding my network and contributing to the professional optics community.

Both University of Rochester Communications and UR Ventures have allowed for unexpectedly successful media coverage and patent applications. Thank you Larry Arbeiter, David Barnstone, Leonor Sierra, Adam Fenster, Matt Mann from UR Communications. Also, thank you Scott Caitlyn, Reid Cunningham, Patrick

Emmerling, Johnny Fahner-Vihtelic, Curtis Broadbent, and the firms and lawyers associated with out patents.

Finally, I am deeply indebted to my family. My parents have taught me true spiritual principles, and the value of education and hard work. With my mother having been a pharmacist and my father a professor, after receiving his PhD in Instructional Science and Technology, they set excellent examples for me. They both continued to encourage and support me in my PhD endeavor and struggles. My sisters Pearl and Sarah, brothers Jacob and Michael, have been true life-long friends and examples for me in my life. They, and their families, have brought much joy to myself and my own family.

In particular, I would be remiss not to thank my mother-in-law, Wolsook Yoo. She has come to take care of Sora, our children, and myself, each time we had a child, or whenever Sora was sick and needed her care. My mother-in-law would spend a month to several months, each visit, and tirelessly cleaned and organized our house, cooked and took care of our children and Sora, with love. When Sora and the children visited Korea, my mother-in-law again would care for them without end. Thanks to her, I was able to focus on my studies and research for many months.

My PhD would not have been possible without the loving patience of my own family - my wife Sora and my children Elly and Clayton. Through countless hours in the lab and office, and years at school, my wife and children sacrificed probably the most for me to achieve my PhD. Although I tried to take care of my family through house chores and family errands, they had to endure a lot of time without me at home. Whenever I had to work long hours or come home late, Sora was always supportive. All I had to tell her was that it was for research or school, and she gladly let me work long hours and late nights without complaining. Completing a PhD is very difficult for both the student and his/her family, so Sora's sacrifice, support, and advice were crucial for my success. I love you Sora,

and adore you Elly and Clayton. I hope to spend more time with you now, so we can build memories that make up more than the past six years. My children, wife, and extended family have brought the most happiness, love and joy in my life, indescribable with words alone. I cherish the special relationship I have with them here and beyond.

Abstract

This thesis presents mainly two methodologies for achieving practical invisibility cloaking. Thus, using commercial technologies, devices that are good approximations to an ideal cloak can be achieved - a cloak that is omnidirectional, broadband, operational for the visible spectrum, three-dimensional (3D), and phase-matching for the light field, among other attributes. We first describe 'paraxial cloaking,' where cloaking is considered as an imaging system. The small-angle ('paraxial') formalism provides a first-order design requirement for any 'perfect' cloaking device. A ray optics four-lens cloak (called the "Rochester Cloak") is experimentally demonstrated, followed by theoretical work to match the phase for the entire visible spectrum. To extend our broadband, paraxial cloak to larger viewing angles, we then discretize space, angle, spectrum, and phase to approximate an ideal, omnidirectional cloak. Such 'discretized cloaking' is experimentally demonstrated as a digital cloak, where commercially available digital image capture and display technologies are used. In particular, we demonstrate an active cloak that uses lenticular lenslet arrays, similar to integral imaging for 3D displays. The 'digital integral cloak' we demonstrate is dynamic, but requires a time delay for image capture and processing, and is two-dimensional (2D) without phase-matching. Continuing improvements in commercial digital technology and computational power will minimize the resolution limitations of a digital cloak and enhance its processing speed. Thus, a wearable cloak can then be practically realized in the future.

Contributors and Funding Sources

This work was supervised by a dissertation committee consisting of Professor John C. Howell (advisor) of the Department of Physics and Astronomy and the Institute of Optics, Professors Carlos R. Stroud, Jr. and Nick Vamivakas of the Institute of Optics, Professor Andrew N. Jordan of the Department of Physics and Astronomy, and Professor Allan Greenleaf (defense chair) of the Department of Mathematics.

My PhD program has been funded by many sources. A DARPA DSO (Defense Advanced Research Projects Agency, Defense Sciences Office) grant (W31P4Q-12-1-0015) funded cross-phase modulation (XPM), while partially funding invisibility cloaking research. A grant (W911 NF-12-1-0263) from ARO (Army Research Office) was used to also partially fund invisibility cloaking research. The Robert L. and Mary L. Sproull Fellowship from the University of Rochester funded the majority of two years of my PhD program, with the Institute of Optics supporting the balance for my first year. Some funding from Northrop Grumman also provided support for digital integral cloaking efforts. NSF fully funded my second and third years as a PhD student with the IGERT Fellowship, which included travel for Ghana and tuition for a Master of Science degree in Technical Entrepreneurship and Management (T.E.A.M.). Professor Minhaeng Cho provided lodging during my summer IGERT internship in Seoul, Korea. I received two scholarships from SPIE (The International Society for Optics and Photonics)- An Optics and Photonics Education Scholarship in 2013, and a 2015 SPIE Student Chapter Officer

Travel Grant for the Optics + Photonics conference in San Diego, CA. As part of the Future Leaders Committee, I will also receive support from SPIE for conference visits in California for 2016- Photonics West, Optics + Photonics. Additional conference travel grants include that from University of Rochester Graduate Student Association for SPIE Photonics West (San Francisco, CA; February, 2015), and an APS (American Physical Society) student travel grant for their DAMOP meeting (Columbus, OH; June, 2015).

We were very fortunate to receive some media coverage with the "Rochester Cloak," which in turn brought additional travel support and invited talks. Professor Howell received many invitations internationally, but here I will list the support I directly received in particular. The New Jersey Chamber of Commerce provided travel to demonstrate the Rochester Cloak at the NJ 350th Anniversary Innovation Gala (Somerset, NJ; October, 2014). The Korean Ministry of Knowledge Economy provided support for an invited talk at Tech+ 2014 (Seoul, Korea; November, 2014), as did Arirang TV for an hour interview on "Heart to Heart" (Seoul, Korea; aired December, 2014). Edmund Optics provided the majority of the travel funds for SPIE Photonics West (San Francisco, CA; February, 2015), where I presented at a technical conference in addition to the Edmund Optics exhibitor booth. In addition, Edmund Optics delivered complimentary optics to build various versions of the Rochester Cloak, which totaled about $5,000. AAPT (American Association of Physics Teachers) provided travel funding to the BFY (Beyond the First Year) II conference, where I ran a workshop on using the Rochester Cloak for undergraduate lab courses (College Park, MD; July, 2015). In June, 2015, I attended the invitation-only Science Foo Camp ("SciFoo") at Google, sponsored by Google, O'Reilly Media, Nature Publishing Group, and Digital Science (Mountainview, CA).

Finally, Professor John Howell's university account was used to generously fund any remaining stipend and equipment. I thank Professor Howell for the

challenging task of finding funding for myself and our group. His and others' financial support have enabled me to not only continue my PhD program, but allow for wider dissemination of our research to the public and scientific community than otherwise possible. Thank you all.

I will now describe the various projects on which I worked while at the University of Rochester, and describe my contributions and that of others for each research projects. In the Howell lab, I worked on various experimental projects. One of my first projects was to help David Starling and Bethany Little build an interferometer using large mirrors, to enhance a previous weak value amplification measurement by the group. I have worked mostly in the atomic physics side of the lab, where we used Rubidium (Rb) atomic vapor cells to perform interesting quantum optical experiments. For example, using a heated Rb cell, I worked with Praveen Vudyasetu, Steven Bloch, David Starling, and Bethany Little to build an atomic prism with 50 MHz resolution over about 1.4 GHz bandwidth [1]. Later, Bethany Little's experiment was transferred to me, where a crossed laser beam generated periodic index modulation in a Rb cell, creating a 'photonic crystal' with dynamic reflectivity control. With Dr. Curtis Broadbent, Julian Martinez, and Chris Mullarkey, I worked on utilizing two-photon absorption of two laser beams in a hot Rb vapor cell, to produce cross-phase modulation (XPM) for long distance quantum communication. To further enhance the observed XPM, Julian and I built a low-finesse optical cavity around the Rb cell as well. To successfully set up a confocal cavity, sharing of knowledge, feedback, and equipment from Dr. Andrey Okishev of the Laboratory for Laser Energetics at the university was extremely valuable. Separately, I experimented with using the optical Kerr effect from the spatial profile of a Gaussian beam, to exploit Gouy phase shifts to increase XPM. As part of the IGERT program, I had a chance to intern with Professor Minhaeng Cho (Korea University) in the summer of 2012, working on a theoretical correction to 'superchiral' fields [2]. Later, Professor Cho asked Dr.

Hanju Rhee and I to join him on a mini-review for chiroptical amplifications. Dr. David Starling and Professor John Howell joined us to show how these enhancements of small chiral signals are similar to weak value amplifications [3].

Lastly, I spent the latter portion of his PhD program, from fall semester of 2013, to develop the theory and experimental demonstrations for realizing practical invisibility cloaking. As this thesis is a summary of our invisibility cloaking research, I will detail the individual contributions for each of the projects herein. Professor John Howell had the inspiration for the first cloaking project, after reading a temporal cloaking paper. His first ideas for cloaking were unidirectional ray optics cloaks, which he built three versions with his sons, in particular with his oldest son Benjamin. One cloak used a glass tank filled with water, another used Fresnel lenses, and the other used mirrors. All of these cloaks could hide centimeter to meter size objects, but only for one viewing angle. Their work was initially published on the arXiv in June, 2013, and generated a large interest from the public after an MIT Technology Review article. I was later asked to run some simulations of these cloaking systems using CODE V, as I was the only Optics student in the group. With these simulations and some revisions, the final paper was published in Applied Optics [4].

In the winter of 2013, we then set out to derive an invisibility cloak that would work for multiple viewing angles, and specifically for a continuous range of angles. Again, Professor Howell conceived the initial idea for a multidirectional cloak with two lenses and three mirrors. I then used CODE V to simulate the rays traversing the system to see if it worked. Realizing that there was potential, I then tried to optimize the system for cloaking. I quickly realized we needed to develop even a basic theory to describe cloaking, in order to know what metrics to use for optimization. I then considered cloaking as an imaging problem, which was a small but I think novel and significant approach, compared to what was done before with scientific cloaking. As an initial step in this direction, I went back to

the first-order equations, which Professor Julie Bentley regularly emphasized as the first steps for lens designing in her course. I applied geometric optics, specifically 'paraxial' (small-angle) ray optics propagation using ABCD 'ray transfer' matrices. This required defining what a cloaking device should be, which I did generally as well as to first-order. This allowed me to optimize our initial design and discover to my excitement that I could exactly match the required cloaking ABCD matrix. I tried building the original design after some optimization, but then we realized it would only work for two-dimensions (2D) with off-the-shelf optics. I was eager to demonstrate this 2D version and publish the theory, but Professor Howell had higher standards which proved to be prescient. He suggested we investigate whether simple lenses could be used for cloaking, even if the center-axis may not be cloaked. He took the initiative to look into 3 lenses, and quickly showed how it could cloak to some degree. Inspired by Professor Howell's persistence and kindness, I tackled the problem of finding the simplest possible cloaking device for three-dimensions (3D), with renewed confidence. I then solved for systems with 1 to 4 lenses, and showed that at least 4 lenses are required, if using only lenses, to build an ideal cloak. I applied the paraxial theory to simulations in CODE V for various lenses, and built a few iterations of both a 3 lens 'cloak' and a 4 lens cloak. The 3 lens version worked decently without achromats, but the 4 lens version required achromatic doublets to generate reasonable images of the background. After I set up and aligned the experimental demonstrations, Professor Howell and I made the experimental measurements. I wrote the final paper with revisions from Professor Howell [5]. In my opinion, the paraxial ray optics cloaking work successfully combined and utilized the talents and skills of both Professor Howell and myself. It was a synergistic outcome, where the project would have remained incomplete and unsolved without either one of us working together. Shortly after the publication of our "paraxial ray optics cloaking" paper [5], Professor Howell came up with an idea to use mirrors for cloaking the

center-axis region of the Rochester Cloak. This is described in Section 2.3.3.

I would like to also acknowledge the helpful geometric optics discussions with Aaron Bauer, Robert Gray, and Kyle Fuerschbach who helped me refine the theory and simulations for our paraxial ray optics cloaking work. In particular, Aaron has consistently been open to helping me with optics, designing, and metrology questions throughout my stay in Rochester. Greg Howland gave the idea for taking a long-exposure photo of our setup with a laser beam passing through it. The wide coverage by the media was possible through the first-rated materials (photos, videos, articles, and connections) provided by University of Communications (University of Rochester), led by Larry Arbeiter. Media coverage began shortly after we posted our paper in the arXiv in September, 2014, first by Alan Boyle of NBC News. The 4 lens cloak was named the "Rochester Cloak" by David Barnstone, of University Communications, who wrote the press release for our paper and a Do-It-Yourself (DIY) procedure that has been used by many in the public. In addition, Leonor Sierra and Matthew Mann planned and produced the viral videos about the Rochester Cloak. Adam Fenster's iconic photographs of the Rochester Cloak cloaking my hand or eye were immediately picked up by Reuters. The Reuters article by Caurie Putnam was published on a Friday night in September, 2014, and seemed to have been the cause for the Rochester Cloak trending over Facebook for that weekend, followed by international and local news coverage and invitations.

Scientific cloaking, in particular Transformation Optics cloaking, require the full phase and amplitude to match. I had been thinking about how to connect our paraxial ray optics cloaking to transformation optics but wasn't exactly sure how to extend ray optics cloaking to match the full-field phase. While working on Gaussian beam propagation for using Gouy phase for cross-phase modulation, I went through the derivation of paraxial beam propagation carefully and in detail. I then realized that the correct absolute phase of field propagation through

an optical system was the missing piece for connecting ray optics to 'full-field' (matching phase + amplitude) cloaking. After sharing this with Professor Howell, I derived the theory to match the phase for a paraxial ray optics cloak. I then used Mathematica to calculate the required index of refraction dispersion. I even attempted (unsuccessfully) at making a Mach-Zehnder interferometer to test phase-matching using our original Rochester Cloak and a Soleil-Babinet compensator. Since the required material to match the phase was not easy to obtain, I wrote the theoretical paper without any experimental demonstration, under Professor Howell's supervision [6]. Professor Allan Greenleaf, a mathematician who is himself a well-known expert in cloaking, helped me understand some background on Calderons inverse problem and uniqueness theorems for the paper. Professor James Fienup provided discussions and feedback on field propagation.

Shortly after publishing our paraxial ray optics cloaking paper, Professor Howell had several ideas on how to create large field-of-view (FOV) cloaks using active equipment. One was the same as demonstrated in the movie, "Mission: Impossible Ghost Protocol," where an eye-tracker is used to provide multidirectional cloaking for one observer. We tried various approximations to this but have not published our implementations. Other ideas of Professor Howell included using lenticular lenses to propagate rays for cloaking. This would allow multiple observers, or observation from multiple locations, for the cloak. We later found out that our method used was called 'Integral Imaging' when used for 3D displays. Professor Howell demonstrated such a cloak using Mathematica to process interlaced images of a 2D plane object. To increase resolution of the images, he also demonstrated a static cloak where a lenticular lens sheet was overlayed on an interlaced image that was printed with a high density printer. Soon after Professor Howell announced he had ideas for large FOV cloaks, but without disclosing how they worked, I independently derived my own version. This came up as I was contemplating ways to make a wearable cloak, in answer to a question posed by a journalist from

Nautilus magazine. I realized that discretizing space will allow a wearable cloak to be made, which I later generalized to 'discretized cloaking' for arbitrary shapes. Such cloaks can work for all viewing angles (omnidirectional), albeit in discrete steps. When I proposed this to Professor Howell, I also suggested that a processor to compute the proper ray propagations could be used, which with sensors can allow for creating a cloak that can change shapes dynamically. My idea for discretizing a cloak was to use detectors and emitters on curved surfaces, which I later improved to be more like a set of pin-hole cameras. I found out that such structures were very similar to what Lippman suggested for his original 'Integral Photography' around 1908-1911. We began implementing Professor Howell's idea using cylindrical lenticular lenses on digital display monitors/screens. I initially demonstrated a version that used a Pan-Tilt-Zoom (PTZ) camera to rotate and capture images, but this was not quite what we needed for cloaking. Professor Howell suggested using a camera mounted on a mechanical slider, to scan horizontally across the objects in the background. This has been the preferred choice of capturing images for our 2D 'digital integral cloak,' for which I demonstrated a dynamic version in collaboration with Professor Howell [7]. Professor Howell provided some of the initial ideas, funding, and I developed the theory, algorithm, coding, and demonstration. Again, Leonor Sierra, Matthew Mann, and Adam Fenster from University Communications have provided the press release and plans, videos, and photos, respectively for the media.

Table of Contents

List of Tables

List of Figures

List of Symbols

2D	Two-Dimension(al)
3D	Three-Dimension(al)
FOV	Field-Of-View
LPI	Lens Per Inch
NA	Numerical Aperture
OPL	Optical Path Length
PPI	Pixels Per Inch
RGB	Red, Green, Blue

1 Introduction

Optical spatial cloaking has captured the imagination of both the popular culture and scientific communities in our attempts to make invisible what is visible [8]. Characters that have devices or powers that allow them to be invisible, or magicians who use techniques and setups to make objects or humans disappear can be easily found in fictional literature, history, and in modern day. Aside from satisfying human curiosity, there are many practical applications for invisibility cloaking. These include making objects or space undetectable from observation for stealth purposes, allowing waves (acoustic, oceanic, seismic) to move around a region without disturbing it, or to make objects unseen for aesthetic or design purposes. Another side of invisibility cloaking includes making objects or regions visible, which may have been obstructed or obscured. For example, cargo that a truck may be carrying can be cloaked to allow the driver to see through and behind it, a surgeon could cloak his/her hand to see the surgical area unhindered, or walls can be turned into windows to save insulation costs.

1.1 Scientific Cloaking Background

Much scientific progress has been made recently in invisibility cloaking since the seminal works of Leonhardt [9] and Pendry, Schurig, and Smith [10]. They pro-

vided a theoretical framework to create a curved space for electromagnetic fields, by carefully constructing materials using coordinate transformations. This field has been called 'transformation optics,' since coordinate transformations were used to design the necessary material properties that morphed space for light [11, 12]. Transformation optics requires artificial electric and/or magnetic materials (called 'metamaterials'). However, experimental realization of these ideas has been difficult, due to the need for its narrow-band spectrum, infinite phase velocity (or negative index to compensate this), and anisotropy in the theory. Perhaps most importantly, creating the required spatial distribution of metamaterials, their anisotropy, and causality, limit the spectrum to single frequencies, or to a narrow bandwidth, and is particularly difficult to manufacture for visible frequencies [8, 11].

Nonetheless, inspired by transformation optics, there have been tremendous advances in cloaking. These include two-dimensional microwave cloaks [13, 14], cloaking from scattering cancellation [15, 16], and even cloaking in time [17, 18] or from seismic waves [19]. A few groups have been able to cloak millimeter- to centimeter-sized objects as well, using birefringent materials [20, 21]. In these developments to implement practical cloaks, Zhang has observed a shift from traditional metamaterials, to polymers, and to natural materials, suggesting that traditional optics can help to develop market-ready cloaking technologies [12].

In fact, to overcome the metamaterial requirements and to extend cloaking to a broadband, visible regime for large objects, researchers have recently looked to ray optics for cloaking [4, 22, 23]. In these cloaks, the amplitude and direction of light fields are considered, as opposed to the full preservation of fields (amplitude and phase) of transformation optics. These designs have been able to cloak centimeter- [22] to meter-sized [4] objects with commonly available optics. Yet, these schemes work only for unidirectionally incident light, or for discrete angles only, as they are not designed for continuously multidirectional cloaking, and they can have

non-unity magnifications [4, 22, 23]. For off-axis, non-zero angles, the background images show distortion and positional shifts. This may not be clear when the background is close to the cloaking device [22], but becomes particularly evident when they are far apart. In addition, as can be seen in Fig. 1 of Reference [4], rays that propagate through these cloaks, but go through the center at non-zero angles, can actually enter the cloaking region, effectively uncloaking the space.

Invisibility efforts by scientists have focused on building a broadband, omnidirectional cloaking device. Such a cloak that works in macroscopic dimensions, for the entire visible spectrum, with the full-field of light may be considered an 'ideal' cloaking device [24]. Much of the scientific work on cloaking has retained the omnidirectionality and full-field (amplitude and phase of light waves) nature of transformation optics [24]. With this, to make forays into large bandwidths in the visible spectrum, researchers have built reflecting 'carpet' cloaks that hide objects under a surface [25–29], proposed non-Euclidean geometry mapping [30], and suggested strongly diamagnetic superconductors [31].

Simultaneously, researchers have investigated the fundamental limits on bandwidths for these omnidirectional cloaks. It is generally agreed that causality requires such cloaking of a non-zero volume, either passive or active [32], to be only possible for single frequencies [33]. Chen et al. showed that zero scattering cross-section of a cloaked object (for an omnidirectional transformation optics cloak in two-dimensions (2D)) cannot be attained by neighboring frequencies of the target frequency, no matter how narrow the bandwidth [34]. They then derived an upper bound for the bandwidth that was proportional to the scattering cross-section radius. Hashemi et al. have also provided a theoretical bound for transformation optics cloaks, even if perfectly manufactured, which shows increased imperfections for increasing bandwidth [35]. Derived from causality, their "diameter-bandwidth product" limit states that the effective bandwidth is inversely proportional to the cloaked object diameter. They suspect a similar sensitivity to

'carpet cloaks' as well. Similarly, Monticone and Alù showed that any linear, passive, non-diamagnetic cloak must increase the overall scattering, compared to an uncloaked object, when integrated over all wavelengths [36]. Even if scattering is suppressed in a finite bandwidth, this will need to be "paid back" in the rest of the spectrum. On the other hand, Leonhardt and Tyc's broadband solution is a three-dimensional (3D), anisotropic cloak [30]. Their "price to pay for practical invisibility" is relaxing the full-field requirement to allow time delays. So broad bandwidth and omnidirectionality appear to be the main competing elements for ideal invisibility cloaking, as both seem unachievable simultaneously [6, 37]. Thus, to demonstrate cloaking, researchers have relaxed, and continue to relax, these or other ideal characteristics. Some of these efforts have yielded a unidirectional phase-matching cloak [14], and a cylindrical cloak for light through a diffusive medium [38].

1.2 Our Approach to Cloaking

In light of the broadband difficulties imposed by omnidirectional field cloaking, Hashemi et al. suggested that a precise understanding of when the cloaking problem can become easy, would be valuable [35]. What they considered in their conclusion was restricting the incident waves and/or observation, by limiting the angles and/or phase requirements. They considered knowing what cloak was the "weakest" relaxed, yet still practical for large objects, to be valuable, due to the difficulties of transformation optics cloaks. Our ray optics cloaking demonstration, to be discussed in Chapter 2, relaxed both of these parameters, and showed that only four lenses were needed for 3D, stand-alone cloaking for small ranges of angles [5]. This paraxial cloak was the simplest design we found that used only isotropic, off-the-shelf optics, designed for the entire visible spectrum.

Despite the advances in cloaking, a 3D multidirectional cloak had been elusive

prior to our work [5]. As shown by Wolf and Habashy [39] and Nachman [40], no isotropic cloaking scheme can hide an object from *all* viewing angles. Their works answered a question that stemmed from Devaney [41], who elegantly showed how to mathematically construct potentials with zero scattering fields, hence invisible. However, Devaney's result was for a finite number of discrete directions, and not for a continuous range of angles.

Our approach has been to begin with broadband cloaking for the entire visible spectrum, but within the paraxial approximation, then to expand the cloaked size and angles [42]. This is typically the method used in optical engineering, as increasing the field-of-view (angles) and/or numerical aperture (refractive index multiplied by the solid angle of the accepted light) can be challenging [43]. So in this paper, we use the definition for "cloak" that is to "hide," since the cloaked object is not necessarily covered in all directions as if by a garment. In addition, what may be considered new for the field of cloaking was that we considered it as an imaging problem, rather than a design for materials to control electromagnetic fields.

1.3 Clarification of Cloaking Terminology

1.3.1 Ideal Cloak

An 'ideal' invisibility cloak can be considered to be broadband, omnidirectional, 3D, macroscopic, operational in the visible spectrum, and with matching of phase for the full-field of light [8, 24].

1.3.2 Defining "Cloak"

We first clarify what we mean by a "cloak" in this thesis. Rather than the commonly used definition of a wearable clothing, we use the other definition of "cloak,"

which is to "hide." In this regard, our use of "cloaking" includes a broad meaning of "invisibility."

1.4 Outline of thesis

The outline of this thesis is briefly discussed. Chapter 1 provided an introduction to possible merits and history of invisibility cloaking, as well as background research found in the scientific literature. Chapter 2 then simplifies cloaking to its first order approximation- a 'paraxial' propagation of rays, to gain insights for how a 'perfect' cloak would behave in this limit. Chapter 3 extends the formalism of Chapter 2 to the "full-field" by matching the phase for a paraxial cloak. Chapter 4 provides a new, perhaps practical, approach to achieving omnidirectional cloaks by considering discretization of space. Lastly, the Conclusion summarizes and provides some insights into our attempts to achieve practical invisibility cloaking.

2 Paraxial Ray Optics Cloaking [5]

Despite much interest and progress in optical spatial cloaking, a three-dimensional (3D), transmitting, continuously multidirectional cloak in the visible regime had not yet been demonstrated prior to our work, to our knowledge. In this chapter, we experimentally demonstrate such a cloak using ray optics, albeit with some edge effects. Our device requires no new materials, uses isotropic off-the-shelf optics, scales easily to cloak arbitrarily large objects, and is as broadband as the choice of optical material, all of which have been challenges for current cloaking schemes. In addition, we provide a concise formalism that quantifies and produces perfect optical cloaks in the small-angle ('paraxial') limit.

2.1 Introduction

In this chapter, we demonstrate a ray optics cloak that is designed for continuously multidirectional angles in 3D (See Fig. 2.1). This is the first such device, to our knowledge, for transmitting rays in the visible regime. It also uses off-the-shelf isotropic optics, scales easily to arbitrarily large sizes, has unity magnification, and is as broadband as the optical material used. Thus, many of the difficulties encountered in invisibility cloaking schemes so far are solved, albeit with edge

effects that are present. We also provide a concise and effective formalism, using

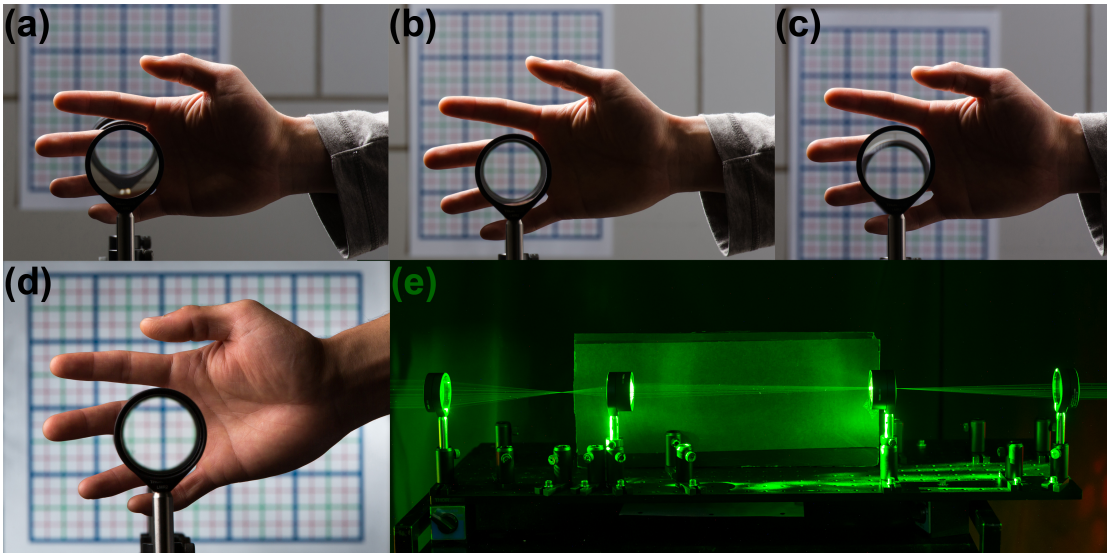

Figure 2.1: Example of a practical paraxial cloak. (a)-(c) A hand is cloaked for varying directions, while the background image is transmitted properly (See Reference [5] Media 1 and Media 2 for videos). **(d)** On-axis view of the ray optics cloaking device. **(e)** Setup using practical, easy to obtain optics, for demonstrating paraxial cloaking principles. (Photos by J. Adam Fenster, videos by Matthew Mann / University of Rochester)

ray optics, to describe all perfect optical cloaks in the small-angle ('paraxial') limit. We apply our formalism to general optical systems up to four lenses, and show what systems can be considered 'perfect' paraxial cloaks for rays.

2.2 Theoretical formalism

To begin, we use a slightly different philosophy than transformation optics. Rather than starting with the bending or reshaping of the space for fields, we first consider replacing the cloaking space entirely. If the cloaking device can be replaced in a simple manner, then engineering every field to move around the cloaked space may be unnecessary, or automatic. This can be accomplished by considering the cloaking device as an optical system that images the background. Our scope is

limited to ray optics, so we do not attempt to preserve the complete phase of the fields.

2.2.1 Exploring the meaning of a "cloak"

Let's suppose we have a black box that is to hide an object in its space. Let's first discuss what a 'perfect,' or 'ideal,' cloaking box would do to light rays as seen by an observer. An obvious first requirement is that any cloaking system must have a non-zero volume to hide an object. In addition to this, we may initially try to make a box such that light does not 'see' it. Thus, we would attempt to remove the space of the box. If this is done, then light rays entering the box should exit the box exactly as it entered. This is called an "identity transformation." Just like particles are described by their positions and momenta, light rays can also be described by their positions and angles of direction. So for a box that is an identity transformation, the positions and angles of the light rays will not change (See Figure 2.2 (a)).

What is the physical effect of removing the box volume? The exiting rays, as seen by an observer, will be closer, by the length of the box (See Figure 2.2 (b)). Thus, an object behind the device will appear to be closer than its actual location. The mirror device in Figure 9 of our paper [4] is a box that is almost like an identity transformation, but it *adds* distance instead, making the object behind it to appear *farther* away.

The identity transformation is a good candidate for a cloaking box. It is not quite how a cloak should work, however. If we did have a perfectly cloaking box, then it should make objects appear exactly where they are. In fact, a perfect cloak should act the same way as if it was filled with the surrounding medium. So to cloak in air, the black box should act like it *was* air (See Figure 2.2 (c)). This is then a necessary condition for defining a *'perfect cloak'* for ray optics- it

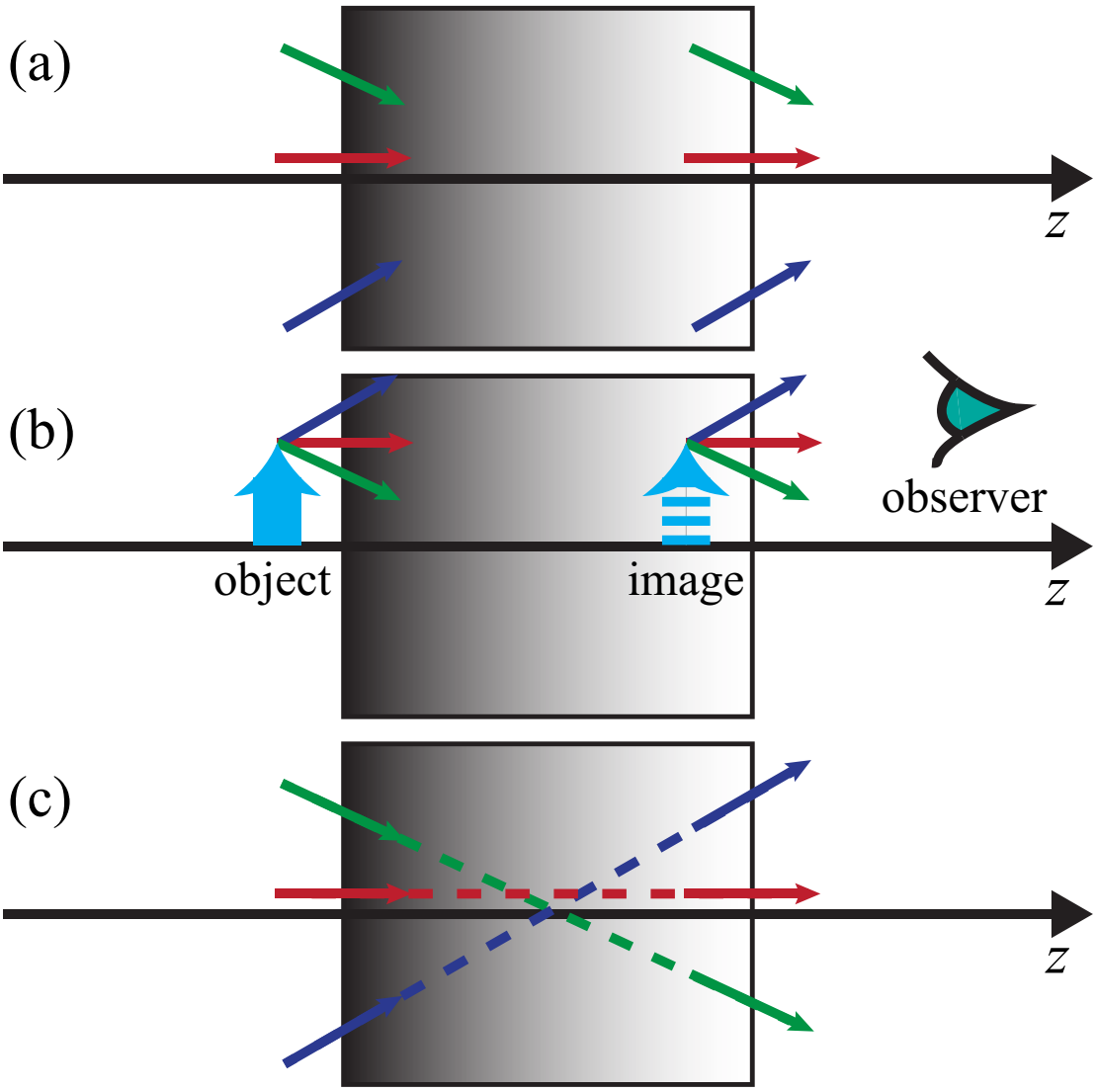

Figure 2.2: Possible candidates for ray optics cloaking. **(a)** A black box that is an identity transformation. Three rays of light enter the box from the left. They exit (to the right) with the same positions and directions. **(b)** How an observer views an identity transformation box. An object behind the box will appear to be closer than its real position, by the length of the box. **(c)** A black box that is a 'perfect' cloak. Rays propagate through the box as if the box was filled with the surrounding medium.

behaves as if its space was replaced by the surrounding medium, for all light rays entering it.

2.2.2 Defining a 'perfect' cloak

We summarize the conditions for defining a 'perfect,' or 'ideal,' cloaking device. The obvious first requirement is that a 'perfect' cloak must have a non-zero volume to hide an object. Second, such a cloak should act the same way as if it was not there. This is equivalent to the device being replaced completely by the ambient medium. These two conditions then are sufficient and necessary for defining a *'perfect cloak'* in general. For such, both the cloaked object and the cloaking device are invisible [9, 13].

We now discuss what a perfect cloak would do to light rays in the ray optics picture. According to our definition, such a device should behave as if its space was replaced by the surrounding medium. Then, the ray angles exiting the device would not change, but the ray positions do shift (See Fig. 2.3(a)). The image of an object behind the device, as seen by an observer, would be identical to the object itself. This implies that the image location, size, shape, and color should be exactly that of the actual object. A perfect ray optics cloak would generate images with unity magnification, zero transverse and longitudinal shifts, and no aberrations, i.e., *no* changes, compared to the actual object, for *all* ray positions and directions.

2.2.3 Quantifying a perfect paraxial cloak

So far, our definition of a 'perfect' cloak was applicable generally. We will now develop a formalism using geometric optics, to quantify this definition in the paraxial approximation. To first-order approximation, called the "paraxial approximation," light rays are assumed to deviate minimally from the center axis of

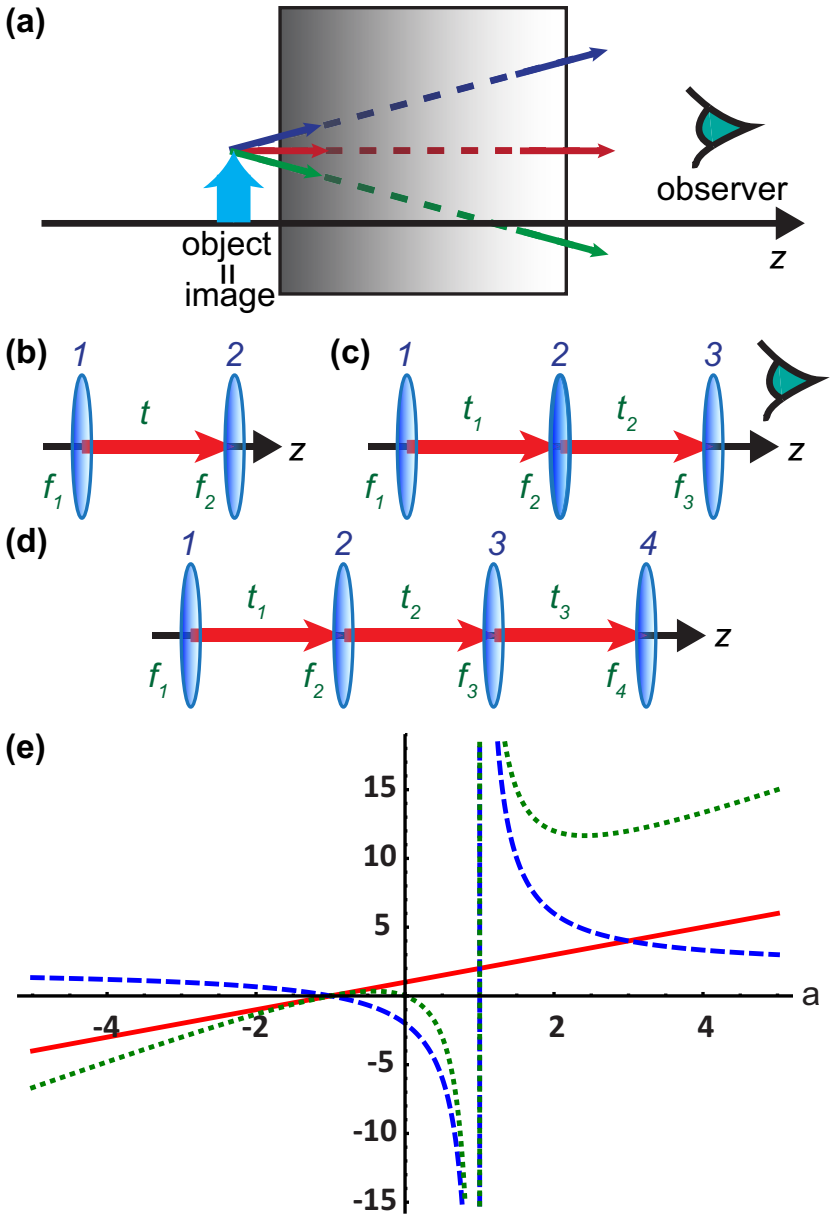

Figure 2.3: Investigating 'perfect' paraxial cloaking with rays. **(a)** A 'perfect' ray optics cloaking box. Rays exit the box as if the box was filled with the surrounding medium. Non-zero volume inside hides an object. Angles do not change, but the positions shift proportionally to the ray angles and box length. The image seen by the observer should match the object exactly. **(b)-(d)** Diagrams for a two lens **(b)**, three lens **(c)**, or four lens **(d)** system. f's are the focal lengths, t's are the distances between the elements. **(e)** All possible four lens, symmetric, perfect paraxial cloaks for rays. Plot of t_1/f_2 (solid), t_2/f_2 (dashed), and L/f_2 (dotted) as a function of $\mathsf{a} \equiv f_1/f_2$. Assumed symmetric left and right halves ($f_1 = f_4$, $f_2 = f_3$, and $t_1 = t_3$). L is the total length of the system. The physical feasibility and presence of a non-empty cloaking region must be checked separately.

the system. Hence, it is a small-angle approximation. In this regime, also known as "Gaussian optics" [44], propagation of light rays through an optical system can be described by 'ABCD' matrices (see Fig. A.1 in Appendix A.1) [45, 46]. Because a perfect cloaking device simply replicates the ambient medium throughout its volume, its ABCD matrix is just a 'translation matrix':

$$\begin{bmatrix} A & B \\ C & D \end{bmatrix}_{\text{perfect cloak}} = \begin{bmatrix} 1 & L/n \\ 0 & 1 \end{bmatrix}. \tag{2.1}$$

L is the length of the cloaking system, and n is the index of refraction of the surrounding medium (For a nonuniform ambient medium, see Equation (A.5) in Appendix A.2).

Equation (2.1) is at the heart of this work. Since any paraxial system can be written with ABCD matrices, if an optical system meets Equation (2.1) and has a cloaking region, then it *is* a perfect paraxial cloak. Any 'perfect' cloak should also be perfect in first-order, so Equation (2.1) is a necessary condition for all such cloaks. Note that this does not violate the findings by Wolf and Habashy [39] and Nachman [40] since this is a paraxial approximation, and hence does not work for large angles. However, we show this to be a surprisingly effective condition, despite its simplicity.

Because ABCD matrices have a determinant of 1, Equation (2.1) gives only three conditions to be satisfied: $B = L/n$, $C = 0$, and *either* $A = 1$ *or* $D = 1$. Note that a perfect cloaking system is "afocal" ($C = 0$), meaning the optical system has no net focusing power. So an object at infinity will be imaged to infinity. This is helpful for the design process, since an afocal condition can be easily checked.

It is worth distinguishing a 'perfect' paraxial cloak (Equation (2.1)) from a 'perfect' cloak. In the paraxial regime, ray optics is used, there are no aberrations by definition, and sags or edges of optics are ignored because of the small-angle

limit [46, 47]. However, real optics are not paraxial only, so a perfect paraxial cloak will have aberrations (non-ideal images), and unwanted rays may be visible near the edges (what we term as 'edge effects'). On the other hand, a 'perfect' cloak would hide an object entirely from the full field (amplitude and phase), so no changes to the field can be observed, including any aberrations. These distinctions do go away for small-angle, nearly on-axis rays, and large optics.

2.2.4 Designing a perfect paraxial cloak with rays

It is not obvious that an optical system can satisfy Equation (2.1), despite containing a cloaking region. The discussion and conditions for a 'perfect cloak' may have little meaning unless a physical solution actually does exist. We will now carefully build general optical systems, to see whether a perfect paraxial cloak can be designed with rays. We attempt to find the simplest nontrivial solution, so we will only consider rotationally symmetric systems with thin lenses, and in free space with $n = 1$.(Our initial multidirectional design was not rotationally symmetric in 3D. This is presented in Appendix C.1.)

The ABCD matrix for one thin lens is given by

$$\begin{bmatrix} A & B \\ C & D \end{bmatrix}_{\text{thin lens}} = \begin{bmatrix} 1 & 0 \\ -1/f & 1 \end{bmatrix}, \tag{2.2}$$

where f is the focal length of the lens. We can easily see that Equation (2.1) will only be satisfied if $f = \pm\infty$, i.e. the lens has no optical power (it's flat). This has no cloaking region and no optical effect.

For the following, we will use f's to denote the focal lengths, and t's to denote the distances between the optical elements (Fig. 2.3(b)-(d)). The ABCD matrix

for a two lens system (Fig. 2.3(b)) is

$$\begin{bmatrix} 1 & 0 \\ -1/f_2 & 1 \end{bmatrix} \cdot \begin{bmatrix} 1 & t \\ 0 & 1 \end{bmatrix} \cdot \begin{bmatrix} 1 & 0 \\ -1/f_1 & 1 \end{bmatrix} = \begin{bmatrix} 1 - t/f_1 & t \\ -(f_1 + f_2 - t)/(f_1 f_2) & 1 - t/f2 \end{bmatrix}. \tag{2.3}$$

Equation (2.1) will only be satisfied if $f_1 = f_2 = \pm\infty$. This is a system that is essentially made of empty space only, quite literally, again with no cloaking region nor optical effect.

A three lens system (Fig. 2.3(c)) has the following ABCD matrix:

$$\begin{bmatrix} 1 & 0 \\ -1/f_3 & 1 \end{bmatrix} \cdot \begin{bmatrix} 1 & t_2 \\ 0 & 1 \end{bmatrix} \cdot \begin{bmatrix} 1 & 0 \\ -1/f_2 & 1 \end{bmatrix} \cdot \begin{bmatrix} 1 & t_1 \\ 0 & 1 \end{bmatrix} \cdot \begin{bmatrix} 1 & 0 \\ -1/f_1 & 1 \end{bmatrix}. \tag{2.4}$$

We can solve for f_2 by setting $C = 0$:

$$f_2 = -\frac{(f_1 - t_1)(f_3 - t_2)}{f_1 + f_3 - t_1 - t_2}. \tag{2.5}$$

Using Equation (2.5), the ABCD matrix becomes

$$\begin{bmatrix} \frac{f_3(f_1 - t_1)}{f_1(f_3 - t_2)} & t_1 + t_2 + t_1 t_2 \frac{(f_1 + f_3 - t_1 - t_2)}{(f_1 - t_1)(f_3 - t_2)} \\ 0 & \frac{f_1(f_3 - t_2)}{f_3(f_1 - t_1)} \end{bmatrix}. \tag{2.6}$$

Requiring $B = t_1 + t_2$ then gives

$$t_1 t_2 \frac{(f_1 + f_3 - t_1 - t_2)}{(f_1 - t_1)(f_3 - t_2)} = 0. \tag{2.7}$$

However, this is only true if $t_1 = 0$, or $t_2 = 0$, or if $(f_1 + f_3 - t_1 - t_2) = 0$. The first two cases give the two lens system which we already showed cannot be a perfect cloak. The last case makes $f_2 \to \infty$, which also turns this system into a two lens system.

Although a three lens system cannot be a perfect cloak, it can asymptotically approach a paraxial one. For simplicity, let us consider the case with symmetric halves ($f_1 = f_3, t_1 = t_2$). Then, Equation (2.5) becomes

$$f_2 = (t_1 - f_1)/2, \tag{2.8}$$

and Equation (2.7) becomes

$$2t_1^2/(f_1 - t_1) = 0. \tag{2.9}$$

So for $f_1 \gg t_1$, both Equations (2.8) and (2.9) can be satisfied in this limit. We will demonstrate the practicality of this case later.

Lastly, we consider a four lens system (Fig. 2.3(d)). We desire to undo any changes that the first half of our system makes, as a possible strategy to make the system behave as if absent. This can be done by making the second half symmetric to the first half ($f_1 = f_4$, $f_2 = f_3$, $t_1 = t_3$). We then require $A = 1$ and $C = 0$ for such a four lens ABCD matrix. Both conditions are conveniently satisfied by

$$t_1 = f_1 + f_2. \tag{2.10}$$

With Equation (2.10), the ABCD matrix becomes

$$\begin{bmatrix} 1 & f_1(-2t_1^2 + f_1(2t_1 + t_2))/(f_1 - t_1)^2 \\ 0 & 1 \end{bmatrix}. \tag{2.11}$$

We can now set $B = (2t_1 + t_2)$, and solve for t_2:

$$t_2 = 2f_2(f_1 + f_2)/(f_1 - f_2). \tag{2.12}$$

We have finally found an exact solution for Equation (2.1). At least four lenses are required for a perfect paraxial cloak, for a rotationally symmetric lens-only system. With Equations (2.10) and (2.12), the total length is

$$L = 2t_1 + t_2 = 2f_1(f_1 + f_2)/(f_1 - f_2). \tag{2.13}$$

We plotted t_1, t_2, and L (Equations (2.10), (2.12), and (2.13)) in Fig. 2.3(e). The figure describes all possible symmetric, four lens, perfect paraxial cloaks using rays. For now, we note only a few points of interest. We can see that when

$f_1 \to -f_2$, the system approaches a one lens system ($t_1 = t_2 = L = 0$). The two extrema for L, seen in Fig. 2.3(e), occur when

$$f_1 = (1 \pm \sqrt{2}) f_2. \tag{2.14}$$

Although these solutions satisfy Equation (2.1) mathematically, checks must be made to ensure they contain a finite cloaking region and are physically feasible.

2.3 Experiments and simulations

We now demonstrate two cloaks using the paraxial cloaking formalism that was developed. Recall that our formalism was for rotationally symmetric systems. Hence, to show continuous multidirectionality in 3D, we need only demonstrate the cloaking effect by varying angles along one transverse direction. Viewing angles along all other transverse directions, spanning a 3D range of incident angles, are the same due to rotational symmetry.

2.3.1 Three lens cloak

The cloaking region for our lens designs depend on what incident angles, or "field-of-view," are allowed. To view the size of the cloaking space, we provide ray-trace simulations using CODE V. We first simulate a three lens cloak with symmetric left and right halves (Fig. 2.4(a),(b)). Recall that this system approaches a perfect paraxial cloak as its length goes to zero. Details of both the three lens and four lens setups are provided in Appendix B.1. The size of the ray bundle entering the system ("entrance pupil") was set to the first lens diameter in our experimental setup (75 mm). The field-of-view is $-3.5°$ to $3.5°$. The cloaking region is between the lenses and is the ring-shaped region where no rays pass. Fig. 2.4(a) compares the final image rays to the original rays near the first lens. For a perfect cloak,

these rays would overlap exactly. We can see that the angles are similar, and the transverse shifts are not too large.

We used plano-convex and plano-concave lenses for the three lens cloak. For the experimental demonstration (Fig. 2.4(c)-(g)), the object (wall) was approximately 2 m from the closest lens in the back. The camera was 5.3 m away from the front lens, but optically zoomed in by 21x (the maximum magnification of the camera). The images were taken from on-axis (0°), 0.55°, 0.83°, and 1.11°, by increasing the height of the camera. A ruler was placed near the center diverging lenses. We can see that the middle of the ruler is cloaked. Also, the lines of the wall match the background wall, as expected for a good cloak.

2.3.2 'Perfect' paraxial four lens cloak, a 'Rochester Cloak'

We now simulate a four lens 'perfect' paraxial cloak for our experimental setup, that has symmetric left and right halves. Real lens systems produce aberrations that can blur and distort the observed image. So we used 'achromatic doublets' that combine two lenses as one, to correct for chromatic (color) and other aberrations. We corrected Equations (2.10) and (2.12) to include the lens thicknesses, and calculated t_1, t_2, and t_3 ($t_1 = t_3$). The simulations in Fig. 2.5 use only these calculated paraxial values without any additional optimization. The cloaking region is an elongated cylinder between the lenses where the rays do not pass.

Finally, we demonstrate the ease of scalability for our designs, to fit any cloaking size. We only need to scale all radii of curvature, lengths, and entrance pupil by the same factor. In Fig. 2.5(d), we simply doubled all of these parameters to obtain double the cloaking space in each dimension.

In constructing our four lens cloak, we used achromatic doublets to reduce the aberrations of the images. Photographs of this paraxial cloak are shown in Fig. 2.6. The grids on the wall were 1.9 m from the closest lens to the back. The

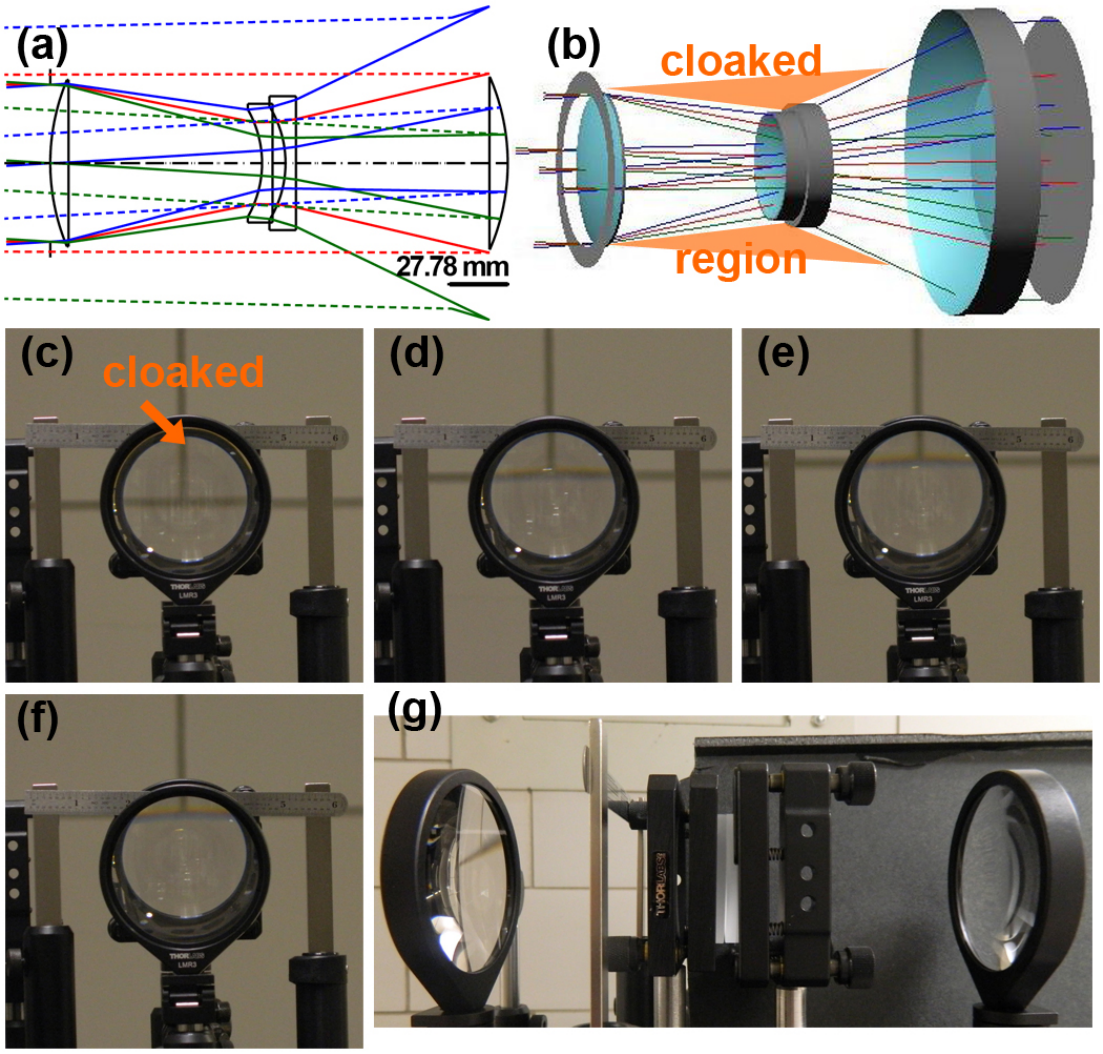

Figure 2.4: A symmetric three lens cloak. Two diverging lenses are combined into one diverging lens, and placed in the center of two converging lenses. **(a)** Simulation in CODE V. Entrance pupil is 75 mm, and field-of-view is $-3.5°$ to $3.5°$. Object is placed at infinity. Ray bundles propagate from left to right, through the lenses, then are traced back to the first lens. This allows comparison of the image (dashed) rays, as seen by an observer on the right, with the original (solid) rays. We see that the angles are similar, and the transverse shifts are not large. **(b)** 3D rendering of **(a)**. The cloaking region is a 3D triangular-ring between the first and last lenses (shaded area). **(c-g)** Experimental demonstration of the three lens cloak. The lines seen through the lenses match those on the background wall. The inner portion of the ruler is cloaked. Images at various camera-viewing angles: **(c)** On-axis ($0°$), **(d)** $0.55°$, **(e)** $0.83°$, **(f)** $1.11°$. **(g)** Side profile of experimental setup.

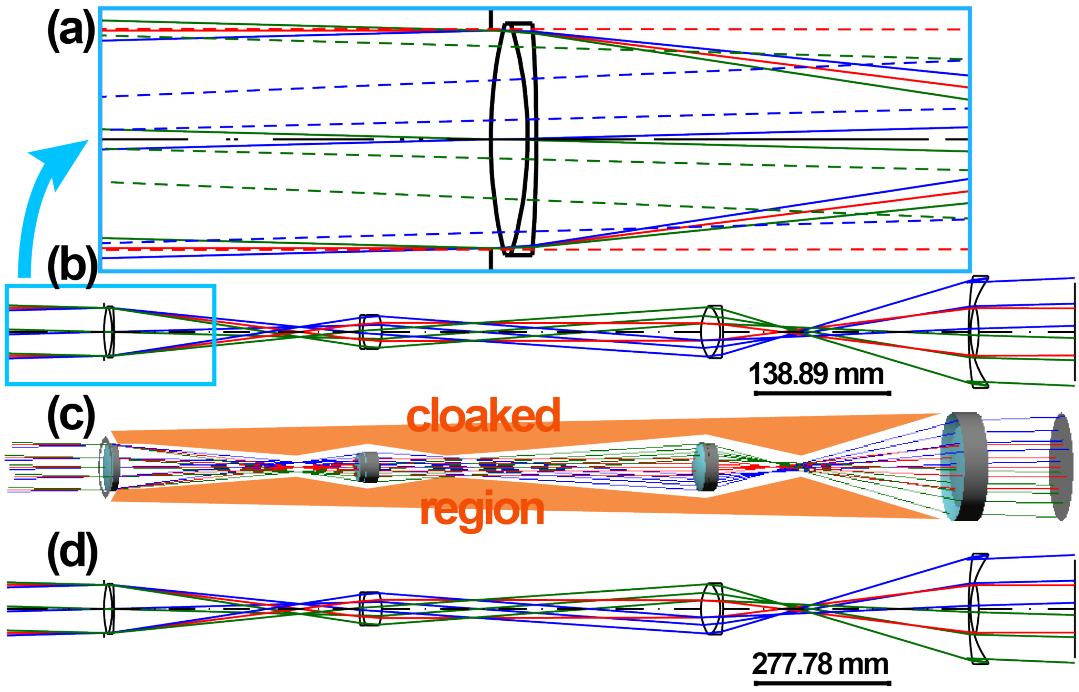

Figure 2.5: CODE V simulation of a symmetric, perfect paraxial cloak, with four lenses using rays. Four achromatic doublets are placed with separations determined from Equation (2.1). Entrance pupil is 50 mm, with $-1.5°$ to $1.5°$ field-of-view. Simulations are shown with *no* separate optimization. Object is placed at infinity. **(a)** Zoomed-in region of **(b)** with image rays (dashed; traced back to the first lens) added to compare with the original rays (solid). We see that the angles are nearly identical, and the transverse shifts are small. **(b)** Full simulation using off-the-shelf optics. **(c)** 3D rendering. The cloaking region (shaded) is a cylindrical region between the first and last lenses. **(d)** Scaling of **(b)** by a factor of 2. The cloaking size is doubled in each dimension by doubling the optical curvatures, lengths and entrance pupil. Only the length scales distinguish **(d)** from **(b)**.

camera was 3.1 m away from the front lens, but optically zoomed in by 21x. The images were taken from $-0.65°$, on-axis ($0°$), at $0.47°$, and $0.95°$ viewing angles, by changing the height of the camera. A ruler was placed behind the second doublet from the front. The middle of the ruler is cloaked near the center-axis of the device. In particular, the grids on the wall are clear for all colors, have minimal distortion, and match the sizes and shifts of the background grids for all the angles, demonstrating the quality of this multidirectional cloak.

University Communications, from University of Rochester, named the four lens version shown in this section as the "Rochester Cloak." [48] Since then, the media and public have used that name for describing our paraxial four lens cloak. As different lenses can be used, we have generally defined the "Rochester Cloak" as the four lens symmetric solution for a ray optics cloak. Hence, the "Rochester Cloak" solves the following equations in the paraxial, thin lens approximation (Refer to Figure 2.3(d)):

$$f_1 = f_4, \tag{2.15a}$$

$$f_2 = f_3, \tag{2.15b}$$

$$t_1 = t_3 = f_1 + f_2, \tag{2.15c}$$

$$t_2 = 2f_2(f_1 + f_2)/(f_1 - f_2). \tag{2.15d}$$

2.3.3 "Rochester Cloak" version 2: Center-axis cloaked

In the original version of the "Rochester Cloak," the cloaking region required the center of the optical system to not be obstructed (See Figure 2.5(c)). Also the cloaking region depended on the incident ray angles. This was intentional so as to provide the simplest nontrivial solutions that demonstrated perfect paraxial cloaking for rays. Shortly after demonstrating the initial ray optics cloaks [5], we demonstrated a four lens, symmetric version, that could cloak the center-axis and surrounding region. This was achieved simply by adding two pairs of mirrors

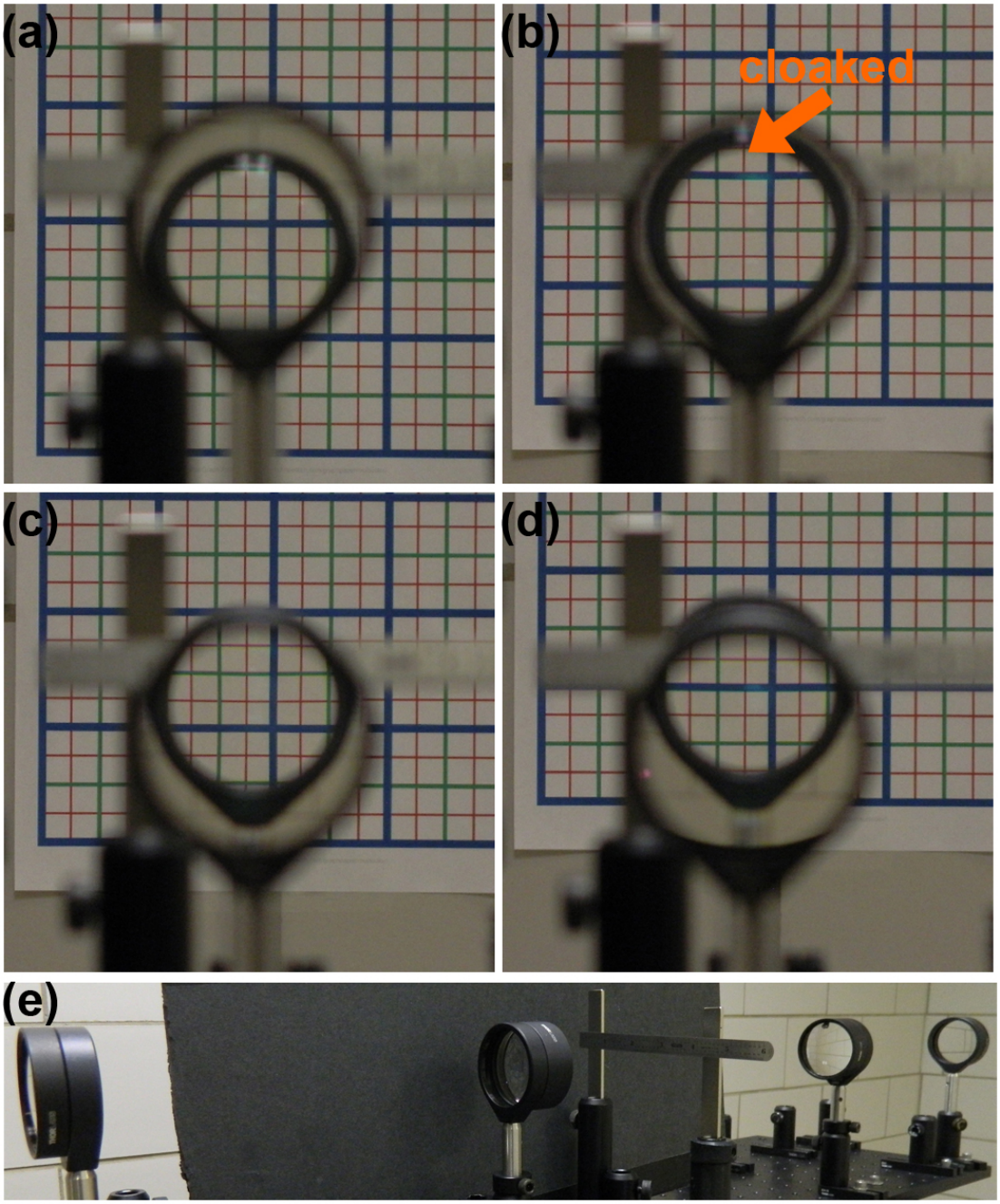

Figure 2.6: Experimental demonstration of a 'perfect' paraxial cloak with four lenses. Camera was focused on the wall. The grids on the wall can be seen clearly, and match the background for all colors and viewing angles. The middle of the ruler is cloaked inside the lens system for all angles shown. Images at various camera-viewing angles: **(a)** $-0.65°$, **(b)** on-axis ($0°$), **(c)** $0.47°$, **(d)** $0.95°$. **(e)** Side profile of experimental setup. See Reference [5] Media 3 and Media 4 for videos). (Videos by Matthew Mann / University of Rochester)

to divert light around the center-axis (See Figure 2.7). The extra room for the mirrors was obtained by using larger diameter (3 inch) lenses for the outermost lenses, compared to the original version (2 inch diameters). Because of the larger diameter lenses, the designed field-of-view and cloaking diameter were about 2x and 1.5x, respectively, larger than those of the original 2 inch diameter Rochester Cloak. However, due to alignment of the mirrors, this was reduced somewhat in actual implementation. Details of the setup can be found in Appendix B.1.3.

2.4 Limitations

It is important to state the limitations of our designs here, so that future work can improve on these. The broadband capability of our designs is only limited by the coating and material used. This can be quite large, spanning the whole visible spectrum and beyond. However, to maintain clear images for an extended spectrum, well-designed achromats and coatings, combined with other lens design techniques are necessary to correct for aberrations. Here, a study of a particular "NonLens" problem, which satisfies Equation (2.1) but without requiring the presence of a cloaking volume, may be useful [49]. Though the NonLens solutions were for a particularly constrained system, the third-order ('Seidel') aberration corrections can be applicable for cloaking designs.

Another challenge is to minimize the visibility of unwanted rays, near the edges, in the paraxial designs. These edge effects become apparent in our cloaks and in unidirectional ray optics cloaks, when the incident angles are non-zero (with respect to the center axis of symmetry). The paraxial formalism does not correct for these, since edges are considered to be 'infinitely' far away from the center-axis, and hence no longer 'paraxial.' So a paraxial cloak may be visible near the edges, although the paraxially valid region inside remains invisible for both the cloaked object and the cloaking device. Though difficult to eliminate, the edge

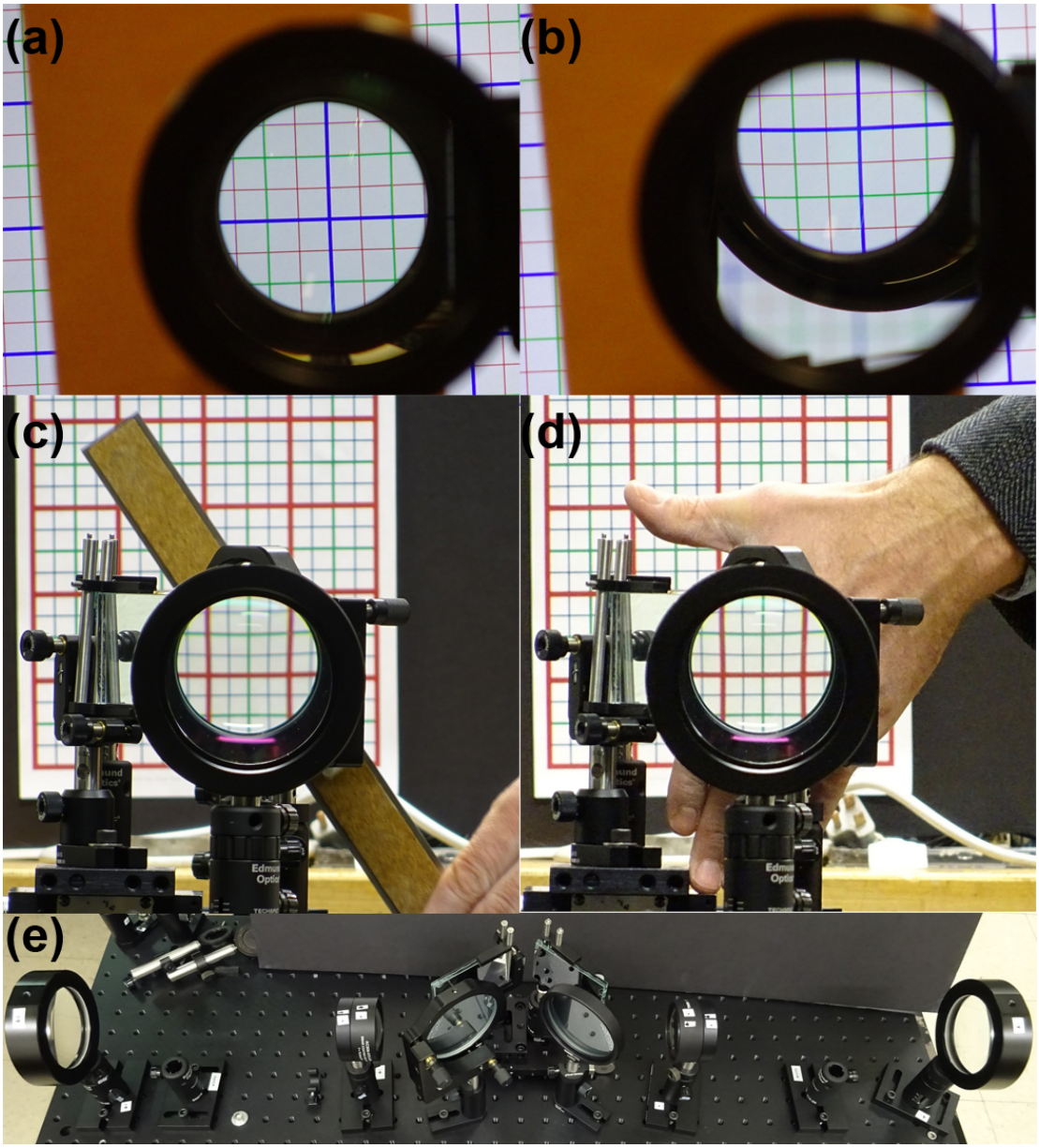

Figure 2.7: Rochester Cloak v.2: Center-axis cloaked. **(a)-(d)** Demonstration of the center region being cloaked. **(e)** Top profile of the setup.

effects can be improved. One method is to use the correct size for each lens or optical element, so as to match the optical design of the cloaks (See Fig. 2.5). This was not necessarily the case for the cloaks demonstrated here. Other strategies include reducing the total length of the system, using large optics, placing the cloaking device far away from observation, and using a thin outer shell to block stray light.

Perhaps the most difficult design issue is increasing the incident angles, or field-of-view. The paraxial equations we presented are valid for angles θ that satisfy $\tan\theta \approx \sin\theta \approx \theta$. This is true for $\theta = 10^\circ - 15^\circ$, while even θ up to 30° is considered to be valid for paraxial propagation [45]. Due to the choice of lenses, our cloaks were limited to 3 - 5 degrees. However, we expect lens design techniques to be able to generate cloaks with much larger viewing angles, since ours relied on little, if any, such optimizations. To achieve larger field-of-view, balancing between lens radii of curvature and lens separation distances is needed. However, this is not necessarily easy, particularly when image quality must also be maintained. Optical engineering will be necessary to create cloaking devices that work for viewing angles beyond the paraxial regime, have high quality imaging, and allow for increased commercial utility. Nonetheless, a small field-of-view can still be practical in cloaking satellites orbiting the earth, or for viewing distances that are far away.

2.5 Conclusion

In summary, we have defined what a perfect cloak should do in ray optics. We then provided a sufficient and necessary algebraic condition for a perfect cloak in the first-order, or paraxial, approximation. We finally derived a device that fits this definition, and experimentally demonstrated several cloaks for continuous ranges of directions. In addition to hiding an object, these cloaking devices can also make

an object behind a barrier visible, or deflect light rays. Transformation optics and quasiconformal mapping are general formalisms used for cloaking fields. Here we provided another formalism that can effectively describe ray optics invisibility.

3 Paraxial Full-field Cloaking [6]

In this chapter, we complete the 'paraxial' (small-angle) ray optics cloaking formalism presented in the previous chapter 2 [5], by extending it to the full-field of light. Omnidirectionality is then the only relaxed parameter of what may be considered an ideal, broadband, field cloak. We show that an isotropic plate of uniform thickness, with appropriately designed refractive index and dispersion, can match the phase over the whole visible spectrum. Our results support the fundamental limits on cloaking for broadband vs. omnidirectionality, and provide insights into when anisotropy may be required.

3.1 Introduction

The task to build a broadband cloak over the visible spectrum becomes simplified when the complete preservation of phase is no longer required. This is the case for ray optics cloaking, which matches field amplitude and direction only. On the other hand, transformation optics preserves the full-field, which includes both the amplitude and phase of light. In addition to the demonstration of cloaks that work for the whole visible spectrum, ray optics cloaks have been able to hide macroscopic objects from non-coherent observation [4, 22]. The initial ray optics cloaks worked for unidirection only, or multiple discrete directions. Our

work described in Chapter 2 extended ray optics cloaking to a continuous range of directions.

In this chapter, we remove the ray optics requirement from Chapter 2, to complete a paraxial cloaking theory that works for the full-field (matched amplitude *and* phase). Such paraxial full-field cloaking satisfies all but the omnidirectionality condition of an 'ideal' cloaking device. This lays a groundwork for connecting ray optics cloaking with transformation optics to first-order, and may help with understanding some of the difficulties experienced in full-field cloaking. We show how thin plates or metamaterials can be utilized for paraxial field cloaking, with the possibility of being realized using current manufacturing technologies.

3.2 Full-field Paraxial Cloaking- Theory

We first discuss the propagation of a monochromatic field through an optical system described by an 'ABCD' matrix. Since an arbitrary field of light can be written as a linear superposition of such monochromatic fields, we do not lose any generality, other than that of the paraxial approximation. This then implies that our theory is broadband.

The "paraxial approximation" is a first-order approximation, with respect to the angle of the rays of light [47]. This allows linear equations to describe the propagation of positions and directions of light, enabling 'ray transfer,' or 'ABCD,' matrices to be used (See Appendix A.1. Rays are assumed to deviate minimally from the center axis of the system, so it is a small-angle approximation. Theoretically, it works for ray angles up to around $\pm 15°$, or more [45].

Duan et al. provided phase matching with a unidirectional cloaking system based off of geometric optics [50]. They provided a heuristic reason why rays that pass through the edge of their optical system may match the phase of rays that pass through the center instead, for their particular setup with split lenses. They

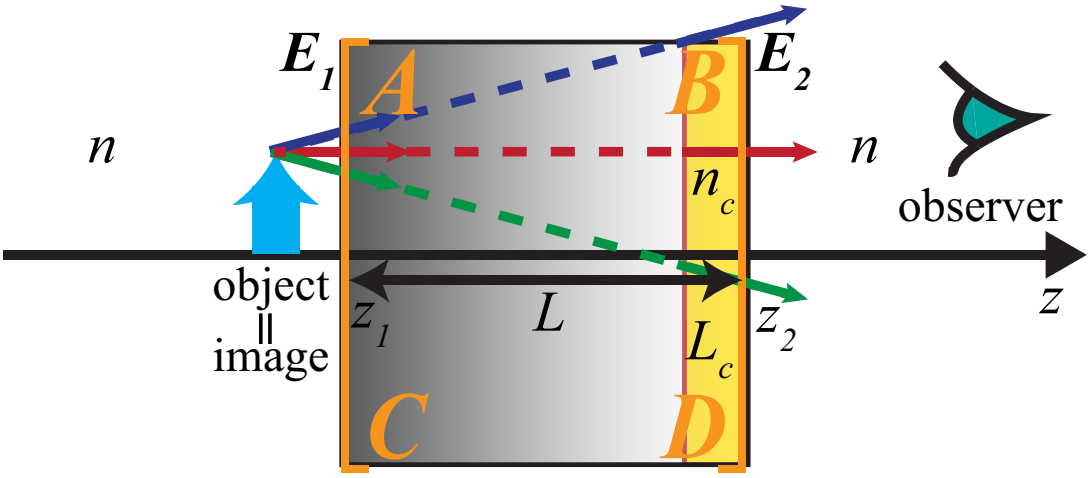

Figure 3.1: Ideal ('perfect') paraxial cloak. The image from a cloaking device is the same as the object. Propagation of light rays can be described by an 'ABCD' matrix. n is the index of refraction of the ambient medium. L is the longitudinal length of the device along the center **z**-axis. E_1, E_2 are the input and output fields, respectively, at $z = z_1$ and z_2. Phase matching is achieved with a flat plate with index n_c and length L_c.

then simulated phase-matched cloaking for discretely separated wavelengths of micro-waves to mm-waves. Here we analytically show phase matching for general paraxial optical systems, including continuously multidirectional cloaks. It is based on the formula given by Siegman and others, for propagation of any paraxial field through a generalized paraxial optical system [45]. The resulting formula is proved using Fermat's principle and Huygens' integral, by accounting for the optical path lengths of all rays. Details are shown in Appendix A.3.

We assume rotational symmetry about the propagation axis **z**, and no limiting apertures. For a complex field $\tilde{E}_1$ incident at $z = z_1$, the propagated field at $z = z_2$ (See Fig. 3.1) is

$$\tilde{E}_2(x_2, y_2) = \frac{ie^{-ik_0 L_0}}{B\lambda_0} \iint_{-\infty}^{\infty} \tilde{E}_1(x_1, y_1) \exp\left\{ -i\frac{\pi}{B\lambda_0} \right.$$
$$\left. \left[A\left(x_1^2 + y_1^2\right) - 2\left(x_1 x_2 + y_1 y_2\right) + D\left(x_2^2 + y_2^2\right)\right] \right\} \mathrm{d}x_1 \mathrm{d}y_1. \qquad (3.1)$$

Here, λ_0 and $k_0 (= \omega/c = 2\pi/\lambda_0)$ are the wavelength and wavevector in free space,

or vacuum. $\tilde{E}_1, \tilde{E}_2$ are the complex, spatial amplitudes of the input and output field distributions, respectively (E_1, E_2 in Fig. 3.1 are their real parts, but without the $e^{+i\omega t}$ harmonic time dependence). x, y are the two-dimensional, transverse, spatial coordinates. A, B, C, D are the coefficients of the ABCD matrix, and L_0 is the on-axis optical path length (OPL):

$$L_0 = \sum_i n_i L_i, \tag{3.2}$$

where n_i is the index of refraction, and L_i is the physical thickness along the longitudinal ($\mathbf{z}$) axis, for each ith optical element.

Eq. (3.1) is a useful result. It allows us to account for the full phase of light rays through a general optical system described by an ABCD matrix. It shows that if two optical systems have the same ABCD matrix, then only the on-axis phases, L_0's, need to match to result in the same propagated fields, at least for the paraxial regime. For full-field cloaking, we just need to ensure that the propagated field matches that of a 'perfect' cloaking device.

In Chapter 2 we stated that a 'perfect' cloaking device (of length L) simply replicates the ambient medium throughout its volume. So its ABCD matrix is given by

$$\begin{bmatrix} A & B \\ C & D \end{bmatrix}_{\text{perfect cloak}} = \begin{bmatrix} 1 & L/n \\ 0 & 1 \end{bmatrix}. \tag{3.3}$$

Then, for a 'perfect' full field cloak, the propagated full field should be:

$$\tilde{E}_2^{\text{perfect cloak}}(x_2, y_2) = \frac{ine^{-ik_0 nL}}{L\lambda_0} \iint_{-\infty}^{\infty} \tilde{E}_1(x_1, y_1) \times$$
$$\exp\left\{-i\frac{n\pi}{L\lambda_0}\left[\left(x_1^2 + y_1^2\right) - 2\left(x_1 x_2 + y_1 y_2\right) + \left(x_2^2 + y_2^2\right)\right]\right\} \mathrm{d}x_1 \mathrm{d}y_1. \tag{3.4}$$

3.3 Ray Optics Cloaking to Full-field Cloaking

In deriving Equation (3.4), we equated a perfect cloaking system to its ambient medium, entirely. However, for practical applications, a cloaking system is composed of optical elements, rather than made of the ambient medium itself, so $L_0 \neq nL$. Recall that Equation (3.3) can be satisfied with just ray optics cloaking, as was demonstrated in Chapter 2. Then, by comparing Equation (3.1) and Equation (3.4), we see that an optical system satisfying Equation (3.3), or a ray optics cloak, can match a perfect full-field cloak, if the following phase-matching condition is met:

$$e^{-ik_0 L_0} = e^{-ik_0 nL}. \tag{3.5}$$

Eq. (3.5) provides the recipe for *absolute phase matching*. However, phases that are congruent modulo 2π are effectively the same value, i.e., every 2π addition to a phase gives the same value for the field. This then gives the *phase-matching to integer multiples of* 2π condition for full-field cloaking:

$$k_0 L_0 \equiv k_0 nL \pmod{2\pi}, \text{or} \tag{3.6a}$$

$$L_0 \equiv nL \pmod{\lambda_0}. \tag{3.6b}$$

The significance of the phase-matching conditions given in Equation (3.5), or Equations (3.6), is that these allow for full phase-matching, hence 'perfect' full-field cloaking, for *any* incoming fields within the paraxial approximation. The phase-matching condition only needs to be satisfied once for the given optical system, and then all ray directions and positions, or any field distribution ($\tilde{E}_1$) will exit the system as if they traversed ambient space only. Note that a ray optics cloak will usually be phase-matched with a full-field cloak, by integer multiples of

2π, for multiple, but discretely separated, wavelengths automatically. However, we can do better and match it for a continuous, broad bandwidth with appropriate dispersion control.

To apply Equations (3.6) to a broadband, full-field cloak, we explicitly include the wavelength dependence (dispersion of the index of refraction):

$$L_0(\lambda_0) = \sum_i n_i(\lambda_0) L_i \equiv n(\lambda_0) L \pmod{\lambda_0}. \tag{3.7}$$

Using

$$L \equiv \sum_i L_i, \tag{3.8}$$

Equation (3.7) becomes

$$\sum_i n_i(\lambda_0) L_i \equiv n(\lambda_0) \sum_i L_i \pmod{\lambda_0}, \tag{3.9a}$$

or, there exists an integer m ($\exists m \in \mathbb{Z}$), such that

$$\sum_i \left[n_i(\lambda_0) - n(\lambda_0) \right] L_i = m\lambda_0. \tag{3.9b}$$

Equation (3.9b) shows that only the segments that are *not* composed of the ambient medium, i.e., $n_i(\lambda_0) \neq n(\lambda_0)$, affect our phase-matching requirement, as expected.

We now summarize the conditions that are required for 'perfect' full-field cloaking in the paraxial regime:

1. A non-zero volume for cloaking/hiding an object must be present.
2. The optical system must have an ABCD matrix of a 'perfect' cloak (Equation (3.3)).
3. The full-field phase-matching condition should be met (Equations (3.9)).

The first two conditions are met by ray optics cloaking. The last condition ties ray optics to full-field cloaking.

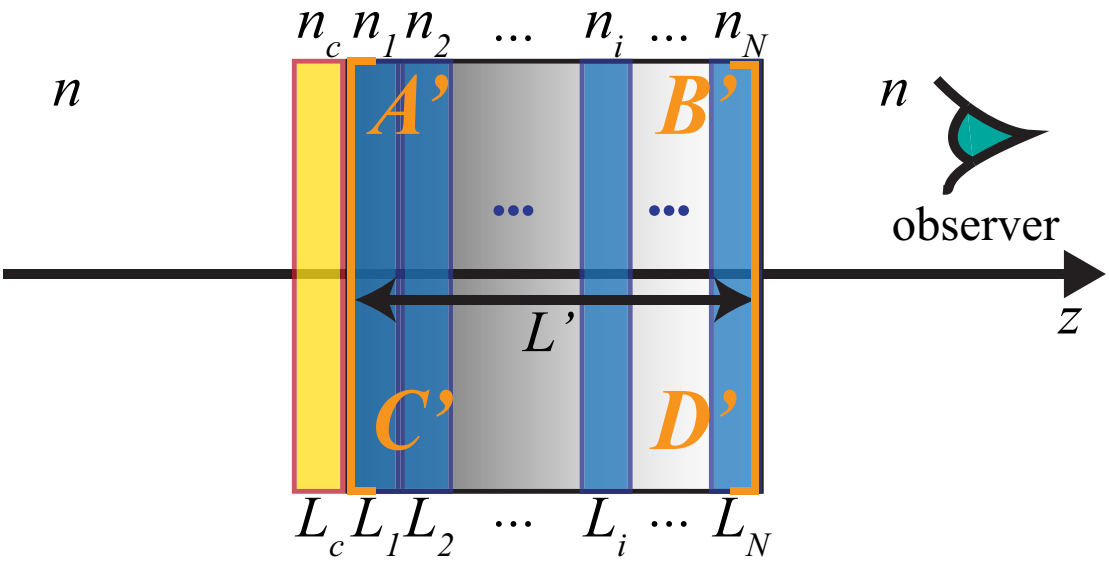

Figure 3.2: Example of paraxial full-field cloaking. A thin, flat plate (labeled with subscript 'c') is placed immediately before (or after) the original ray optics cloaking system. This allows full-field phase-matching (Equations (3.9)) for a 'perfect' full-field cloaking system. The original system (of length L') is described by the ray transfer matrix coefficients A', B', C', D'. n's represent the refractive indices of the material for the given space. L's are the physical lengths of each optical element, along the **z**-axis

3.4 Building a Full-field Cloaking System

A cloaking system that satisfies Equation (3.3) will usually satisfy Equations (3.9) for multiple, but discretely separated, wavelengths. The key is then to match the phase for a broad range of frequencies. We suggest one method, which is to use a thin, flat plate for phase-correction (See Fig. 3.2). The flat plate can be placed anywhere before, after, or within, the original cloaking system, as long as it is placed between the observer and the background object(s) to be imaged.

We first provide an intuitive reasoning for this method. Recall that a cloaking system is 'afocal' ($C = 0$ in Equation (3.3)). So, at a given plane in z, all fields at different transverse positions should have the same phase. For example, when

the field exits the system at $z = z_2$, the phase of $\tilde{E}_2(x_2, y_2)$ should be independent of (x_2, y_2). Otherwise, the plane at a given $z = z_2$ can have a focusing/diverging effect [51], which makes it 'focal' instead. This then implies that a flat plate can correct the phase for the entire field, since it changes the phase in the same manner for all transverse positions. We now show this explicitly.

A thin, flat plate is optically equivalent to a thin lens with infinite focal length. Then its ABCD matrix is given by [46]:

$$\lim_{f\to\infty} \begin{bmatrix} 1 & 0 \\ -1/f & 1 \end{bmatrix} = \begin{bmatrix} 1 & 0 \\ 0 & 1 \end{bmatrix}, \tag{3.10}$$

or in other words, the identity matrix. So it will not affect the final ABCD matrix of the complete optical system. (We quantify what is considered "thin" in Appendix A.4. In particular, a plate is "thin" when $|L_c/L'| \ll 1$ and $|L_c/L'| \ll |n_c/n|$ as given in Equations (A.14).) Specifically, if a system already satisfies Equation (3.3), then adding a thin, flat plate will still satisfy Equation (3.3).

The only condition left to satisfy for full-field cloaking is Equations (3.9). Let the original cloaking system be described by the matrix with coefficients A', B', C', D'. We assume it already satisfies Equation (3.3) and contains a non-zero cloakable volume. Let N be the number of optical elements in the $A'B'C'D'$ system, with $L' = \sum_{i=1}^{N} L_i$ being the total length of the original cloaking system. n is still the ambient refractive index. n_i, L_i are the index of refraction and physical longitudinal length, respectively, for the i^{th} optical element; n_c, L_c are likewise for the correcting thin plate. (See Fig. 3.2.)

Let's now include the phase-correcting flat plate and rewrite the phase-matching condition:

$$n_c(\lambda_0)L_c + \sum_{i=1}^{N} n_i(\lambda_0)L_i \equiv n(\lambda_0)\,(L_c + L') \pmod{\lambda_0}, \tag{3.11a}$$

or, $\exists m \in \mathbb{Z}$, such that

$$[n_c(\lambda_0) - n(\lambda_0)]\, L_c + \sum_{i=1}^{N} [n_i(\lambda_0) - n(\lambda_0)]\, L_i = m\lambda_0. \tag{3.11b}$$

From Equation (3.11b) we can see that if the dispersion relation of $n_c(\lambda_0)$ balances that of the optical elements $n_i(\lambda_0)$, so that the combined 'effective' dispersion is linear with respect to the wavelength, the phase will be matched.

One phase-matching method that can work is to use negative index ($n_c < 0$) to correct the full-field phase, since usually $n_i > n$ in Equation (3.11a). In similar manner, from Equation (3.11b), it can be possible to compensate the phase with even a positive index, provided it is less than the index of the ambient medium: $0 < n_c < n$. For most optical materials, $n_i > 1$, and they have *normal dispersion* (decreasing index of refraction for increasing wavelength; or refractive index increases with frequency). So for these cases, *anomalous dispersion* (increasing index of refraction for increasing wavelength) may be necessary, in particular for $n_c > n$ values.

Note that for a given thin plate (with fixed $n_c(\lambda_0)$ and L_c), if an integer $m = m'$ works for one wavelength $\lambda_0 = \lambda'$, then there are possibly other wavelengths $(\lambda_0 = \lambda'_{\pm 1}, \lambda'_{\pm 2}, \cdots)$ that correspond to the integers $m = m' \pm 1, m' \pm 2, \cdots$, so that Equation (3.11b) is satisfied. A precaution must be given, since these countably infinite wavelength solutions may or may not exist, as they are dependent on the explicit dispersion relations of n, n_i, n_c. However, this does show how any given cloaking system (with or without a phase-correcting plate) may have discrete but infinite number of wavelengths/frequencies for which the full-field phases match, as mentioned previously.

We can rearrange Equation (3.11b) to write the dispersion relation of n_c for our phase-correcting plate:

$$n_c(\lambda_0, m, L_c) = n(\lambda_0) + \frac{1}{L_c}\left\{ m\lambda_0 + \sum_{i=1}^{N} [n(\lambda_0) - n_i(\lambda_0)]\, L_i \right\}. \tag{3.12}$$

We emphasize that any integer $m(\in \mathbb{Z})$ will satisfy Equation (3.12), so there are infinite, but discrete, n_c's that will match the full-field phase required. Physically realizable values of $n_c(\lambda_0)$ should then be selected. We have included this m dependence, along with the L_c dependence, explicitly in $n_c(\lambda_0, m, L_c)$ above.

3.5 Application to a Symmetric Four Lens Cloak

We now have all the tools for creating a paraxial full-field cloaking system. We can apply these conditions to evaluate the material requirements for the phase-correcting plate. Let us use the symmetric, paraxial four lens cloak that was demonstrated in Chapter 2. This ray optics cloaking device satisfied Equation (3.3) and had a non-zero volume for cloaking an object. We then only need to match the full-field phase condition using Equation (3.12).

For simplicity, we assume that the cloaking system is placed in air, with $n = n_{\text{air}} = 1$ for all wavelengths, and we also ignore any coatings. The lens coatings can be modeled as additional thin plates as needed. With these, Equation (3.12) becomes

$$n_c(\lambda_0, m, L_c) = 1 + \frac{1}{L_c}\left\{ m\lambda_0 + \sum_{i=1}^{N} \left[1 - n_i(\lambda_0)\right] L_i \right\}. \tag{3.13}$$

The dispersion relation n_i and the length L_i ("thickness") for each optical component are given in Appendix B.2.

Let's point out some of the characteristics of the phase-correcting plate in Equation (3.13). First, as mentioned previously, only the actual optical elements (those different than the ambient medium) play a role for phase-matching. Second, the integer m is the slope of an added linear phase, with respect to the wavelength. So increasing $|m|$ increases the amount of change in n_c over the spectrum, and increases the shift of the plot as well. Third, L_c has an opposite effect to that

of m. It also affects how strongly the on-axis pathlengths of the optical elements affect the phase.

We consider the visible spectrum ($\lambda_0 \in [400\text{ nm}, 700\text{ nm}]$ for our discussion). Fig. 3.3(a) shows the dispersion of the total on-axis optical pathlength ($\sum_i n_i L_i$) for only the non-air elements, which we would like to compensate. There are infinitely many combinations of L_c and m that are possible for $n_c(\lambda_0, m, L_c)$. Ultimately, the choice of which to use should depend on physically realizable n_c's. As mentioned earlier, some methods to correct phase include using negative index ($n_c < 0$), the use of positive but less than ambient index ($0 < n_c < n = 1$), or using index greater than that of the ambient medium ($n_c > n = 1$). A few solutions for these cases, that phase-correct the four lens ray optics cloak in Chapter 2, with refractive indices that may be physically realizable, are shown in Fig. 3.3(b). Thicker compensating flat plates can reduce the required dispersion range, but this also affects the imaging quality, so we have purposely limited the thickness here somewhat.

Many of the solutions for positive refractive indices require anomalous dispersion, as shown in Fig. 3.3(b). For the purposes of cloaking, such dispersion for broadband spectrum with low losses is needed to imitate ambient space properly. This is similar to the finite bandwidth cloak made of anisotropic layers, as suggested by Kildishev et al., which required strong anomalous dispersion combined with loss compensation [52]. Costa and Silveirinha have suggested using nanowire metamaterial to provide such anomalous dispersion, and they numerically calculated their index of refraction to be near $2.9 \sim 3.1$ for the entire visible spectrum [53]. They can achieve these low loss, broadband, anomalous dispersion properties by utilizing the collective, spatial properties of metamaterials. This allows the high loss and narrow band properties of typical transparent materials, imposed by the Kramers-Kronig relations, to be overcome [54]. In addition, Theisen and Brown have experimentally demonstrated anomalous dispersion for

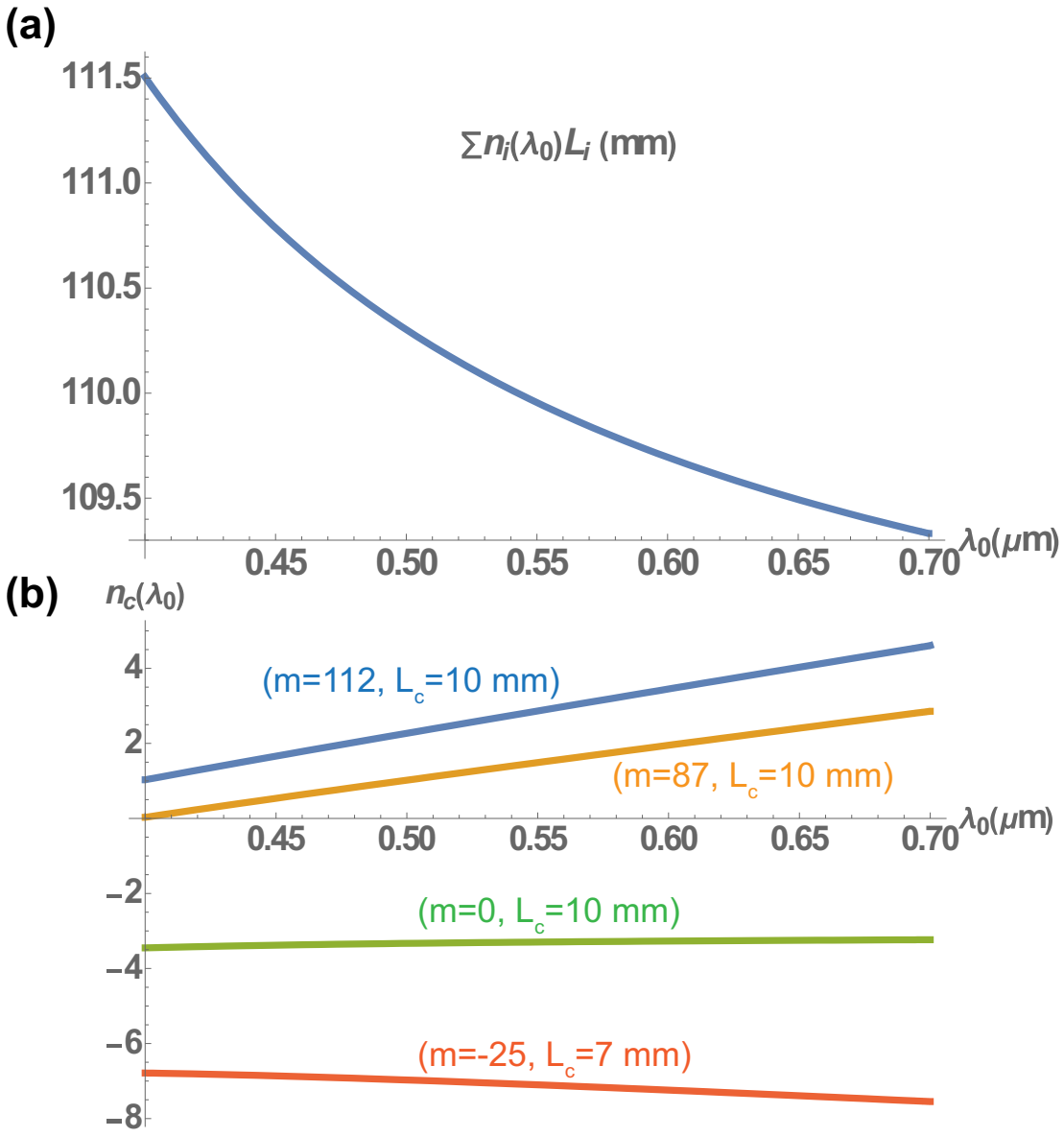

Figure 3.3: Dispersion of phase-correcting plate for a four lens symmetric cloak. **(a)** On-axis optical pathlength total ($\sum_i n_i L_i$) (in mm) for only the non-air elements of the ray optics four lens cloak in Chapter 2 (Ref. [5]). **(b)** Various thin, flat, phase-correcting plates to compensate for the pathlength shown in **(a)**. The dispersion relation of the refractive indices for these plates are shown for various values of m and L_c (mm), using Equation (3.13) (ambient air).

$0.5 \sim 1$ μm wavelengths, with Gallium implanted Silicon pads [55]. These have refractive indices near 2 or 4, with variations of about 1 over the spectrum, depending on the doping level.

Negative-index metamaterials are good candidates for phase-correction as well [56]. The utilization of metamaterials may have been expected, since we expanded ray optics cloaking to the field cloaking aspect of transformation optics. Much progress is being made, both theoretically and experimentally, for creating negative index materials for broadband optical frequencies [57]. Some refractive index values demonstrated experimentally include between -3 and 0 for microwave frequencies in 2D [58], n = 0.63 at 1,200 nm to n = -1.23 at 1,775 nm in a low loss, 3D bulk material [59], and n = 1 to -7.5 for 1.1-2.4 μm wavelengths [60].

3.6 Methods for Improvement

For proper cloaking, the background image must be transmitted clearly with minimal 'aberrations' that distort the image. To do this, and to move beyond the paraxial angles, optical engineering using real ray tracing will be necessary. Lens design optimizations can account for thick optical elements and account for the thickness of the phase-correcting plates. Although $L_c = 7 - 10$ mm used in Fig. 3.3(b) can still be considered "thin" (Appendix A.4), this will affect the system design so that lens design optimization will be required for good background imaging. One option is to include the thin plate material and optically design the entire lens system together. Costa and Silveirinha applied their nanowire metamaterial to designing achromats [53], so it is possible to incorporate anomalous dispersion in the lenses themselves to allow thick L_c values and aberration corrections simultaneously. In addition, negative index materials may also improve the image quality of the system, as using a negative index lens can create 'perfect' imaging [61].

Broadband matching can be a challenge that will likely require iterations for finding optimal solutions for both the ABCD matrix and for the phase-matching conditions. For real optics, ABCD matrices themselves can be frequency-dependent. For example, real lenses are thick, and hence their ABCD matrices will contain the indices of refraction for the material used, which have dispersion. So to accurately match phase, the ABCD system itself must be included to match the dispersion accurately, and iterations may be necessary. In addition, to match the phase for broadband frequencies, we considered phases separated by a fixed multiple of 2π to be equivalent to matching the absolute phase. However, it might be possible that this scheme gives net propagation delays from the cloak, which could then be observed by a time-resolving detection scheme such as a high resolution LIDAR. Lastly, we note that exploring various ambient media (various values of n) that are different than air, may allow readily available phase-correcting schemes, too.

3.7 Concluding Thoughts

By relaxing only omnidirectionality for an 'ideal' cloak, we have shown how to match the phase for the whole visible spectrum. The phase-matching plate may require negative index metamaterials or anomalous dispersion, which are broadband and low loss, but current research has shown much progress in this regard. We had shown that building a 3D, broadband, macroscopic cloak, for the visible spectrum, can be fairly "easy" for ray optics in the small angle limit [5]. Extending this to the full-field seems to not be too challenging with recently developed materials. As with typical lens designs, we expect that extending such cloaks to large angles may be difficult, though possible. However, making it work for all angles appears to likely be fundamentally limited. Realizing omnidirectionality from a paraxial full-field cloak has not been achieved to our knowledge, as this coincides with achieving broadband with transformation optics cloaks. By show-

ing paraxial cloaking that is broadband to be practical, but without a similar ease for omnidirectional and broadband cloaks, our work supports recent work showing a trade-off between broadband and scattering cross-section. This is because small scattering cross-section implies large angles, and zero cross-section gives omnidirectionality.

It is interesting that paraxial full-field cloaking does not require anisotropy, though being 3D, macroscopic, and broadband. Anisotropy seems to be a requirement when creating an omnidirectional cloak, from a paraxial cloak, not necessarily a property of 3D or field cloaks alone [9, 10, 30, 62]. Although our cloak is broadband, Greenleaf et al. have shown that the cloaked material itself has eigenfrequencies that need to be avoided for proper cloaking [63, 64]. As a side, most, if not all, cloaks to date, can be detected by measuring a pulse incident on the cloak [24, 30]. This is the same for our cloak presented here, unless absolute phase is matched with negative index materials. Finally, an open question seems to be whether an isotropic, 3D, omnidirectional, broadband cloak can be achieved for ray optics. This is possible for anisotropic materials [30], but an isotropic, 3D, omnidirectional, full-field cloak is not possible [39, 40]. However, accepting time delays might allow some freedom, as shown here where ray optics allowed relaxing of the material requirements.

In summary, we have given the phase of fields propagating through a cloaking system described by ray optics, along with a formalism to match the phase. A thin plate can be used to match the full-field phase. Low loss, broadband, anomalous dispersion or negative index metamaterials can be used for constructing such thin plates for the paraxial regime.

4 Digital Integral Cloaking [7]

We propose 'digital cloaking' as a method for practical cloaking, where space, angle, spectrum, and phase are discretized. At the sacrifice of spatial resolution, a good approximation to an 'ideal' cloak can be achieved- a cloak that is omnidirectional, broadband, operational for the visible spectrum, three-dimensional (3D), and phase-matching for the light field, among other attributes. Experimentally, we demonstrate a two-dimensional (2D), planar, ray optics version of our proposed digital cloak by using lenticular lenses, similar to 'integral imaging' for 3D displays. With the continuing improvement in commercial digital technology, the resolution limitations of a digital cloak will be minimized, and a wearable cloak can be developed in the future.

4.1 Introduction

In this chapter we propose 'digital cloaking' that is practical to build, and which utilizes commercially available technologies that are improving independent of any cloaking efforts. This is done by discretizing space, angle, spectrum, and phase, as an approximation to ideal cloaking. Since detectors, including imaging systems such as our eyes, are limited in resolution (spatially and temporally), digital cloaking can appear to be omnidirectional for a broad spectrum when observed.

In fact, discretization of space is inherent in nature with atoms and molecules making up matter. Even metamaterial cloaking relies on discrete structures that are sub-wavelength in scale, to generate an averaging effect for the operational wavelength(s) [8]. Della Giovampaola and Engheta went further and proposed digitizing metamaterials, by using just two types of 'metamaterial bits' to make exotic lenses and designs [65]. For our digital cloak, we simply propose the discretization to be larger than atomic or wavelength scales, on the order of resolution limits of the observer, be it biological or a machine/device. For human visual acuity, resolution finer than about 30 arcseconds is sufficient [66].

The digital cloak we demonstrate is an 'active' device that requires external power input. However, passive discretized cloaking is also possible (see Appendix D for this, along with a lensless version and a 25 inch version of digital cloaking). Active cloaks have been proposed before, where the incoming signals are known a priori, or detected quickly, so that outgoing signals from antennas cancel the incoming wave(s) [67]. Other active cloaks, which compensate for absorption and increase bandwidth, include using active metamaterial surfaces for dominant scattering cancellation, or using electronic circuits for acoustic cloaks [37]. These rely on custom-engineered material, whereas our digital cloaks can use commercially available technology. We believe this will be an advantage for scaling and implementation.

4.2 Discretized / Digital Cloaking

Recall that invisibility cloaking makes the cloaked object appear transparent, as if the light fields exited the cloaked space *without* anything in it. It is a form of illusion, where light bends around the cloaked space, but re-forms afterwards to appear as if it had never bent. This allows both the cloaked object and the cloaking device to not only be hidden, but appear transparent [5, 9].

Let's begin with an ideal cloak (broadband, omnidirectional, 3D, phase-matching, etc.). We first make a 'ray optics' approximation, where the full phase of the electromagnetic field of light is not necessarily matched (We later show how to remove this approximation). For imaging, whether by camera or by the human eye, the phase is typically not detectable, which is why ray tracing is usually sufficient for designing imaging devices. Ray optics cloaking can be considered a discretization of spectrum and phase for a given ray, since its phase (modulo 2π) will match for one or more discrete frequencies, or discrete phase values can be matched for a given frequency. Ray optics alone significantly reduces the complexities of cloaking such that isotropic, off-the-shelf materials can be used to build macroscopic cloaks for small angles [5].

Figure 4.1(a) shows some rays that enter and exit an ideal, spherically symmetric cloak. We assume rotational symmetry (about $\mathbf{z}$), so only the cross-section of the spherical cloak is shown. For simplicity, only rays with one angle are shown, but due to spherical symmetry this implies that the cloak will work for all angles (omnidirectional). The dashed arrows show how the rays should *appear* to have traveled inside the cloak, which is to exit as if each ray propagated through the cloak in a straight line. In reality, the rays within the cloak should curve *around* an object or space that is intended to be invisible.

Building an omnidirectional cloak has been elusive to demonstrate, even for ray optics. For practical usage, since detectors including the human eye have finite resolution, the appearance for omnidirectionality can be achieved by discretizing space and momentum (or angle). We call this method of cloaking, '*discretized cloaking*.' A rotationally symmetric example is shown in Figure 4.1(b), where each discretization in space is called a 'pixel.' Each spatial 'pixel' can contain separate 'subpixels' that detect and/or display discrete ray angles. Additional 'subpixels' may also be necessary for other ray characteristics. Discretized cloaking allows digital imaging and display technologies to be placed on the surface of

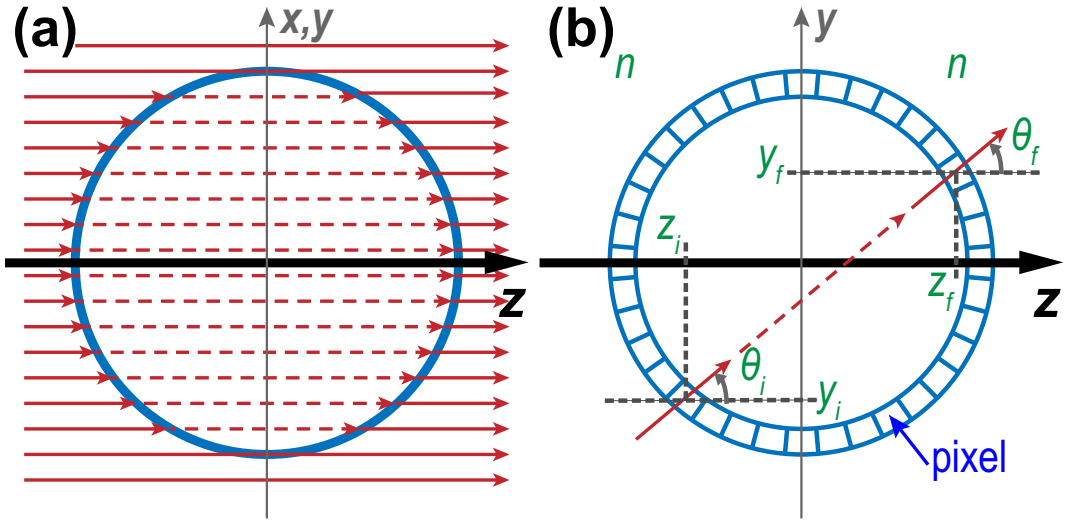

Figure 4.1: (a) Ideal, spherically symmetric cloak. Example rays (solid arrows) that enter and exit the cloak (circle in 2D, sphere in 3D). Dashed arrows show how the rays *appear* to have traveled inside the cloak (where objects are invisible). **(b) Discretized, symmetric cloak.** Solid arrows depict a ray of light entering and exiting. The surface of the cloak is discretized, so that each 'pixel' in space can both detect and emit discrete ray positions and angles. A 'digital cloak' uses digital detection and display technologies for these discrete 'pixels.'

the cloak. Utilizing such digital technology for cloaking is what we call '*digital cloaking*.' Strictly speaking, digital cloaking may discretize the spectrum of frequencies further than just the ray optics approximation. For example, some digital displays might only show red, green, and blue (RGB), so additional subpixels for discrete color may be required.

Implementing a discretized cloak or a digital cloak requires propagating the rays from input to output correctly. This can be done using the 'paraxial cloaking' matrix (Equation (1) of Ref. [5]), since the final ABCD matrix is still valid outside of the 'paraxial' (small-angle) regime. This is also shown in Figure 4.1(b), where given a transverse position y_i, angle θ_i, and longitudinal position z_i of the input ray, the output ray is given by (with same variable names but with subfix '$_f$'):

$$\begin{bmatrix} y_f \\ n\tan\theta_f \end{bmatrix}_{z=z_f} = \begin{bmatrix} 1 & (z_f - z_i)/n \\ 0 & 1 \end{bmatrix} \begin{bmatrix} y_i \\ n\tan\theta_i \end{bmatrix}_{z=z_i}. \tag{4.1}$$

We have assumed rotational symmetry about the center axis ($\mathbf{z}$) and that the ambient medium has refractive index n. Note that each ray has its own longitudinal distance $L = (z_f - z_i)$ that is dependent on its input and output planes for the cloak. To be direct, we have used the 'real' angle θ instead of the 'paraxial angle' $u(= \tan\theta)$. Although Figure 4.1(b) shows a cloak that is circular in 2D, or spherical in 3D, arbitrarily shaped discretized cloaks are possible. For cloaks with general shapes, Equation (4.1) can be applied for each 2D plane containing the $\mathbf{z}$-axis.

4.3 Demonstration of an 'Integral Cloak'

We now present and demonstrate a method for digital cloaking. As described previously, the key to digital cloaking and discretized cloaking is to detect and reproduce proper ray positions and angles. One way to achieve this is to utilize

'ShackHartmann' wavefront sensors, or 'fly's eye' lens arrays. These allow the position and momentum of rays to be captured by using arrays of small lenses, which can spatially separate rays of different angles (See Figure 4.2(a)). Remarkably, Lippmann had proposed photography using this concept in 1908, and attempted to demonstrate this 'integral photography' with limited technology [68]. Resolution, depth of field, and limited viewing angles are typically drawbacks for 'integral' 3D displays, but improvements are being made [69]. In particular, with current commercial efforts to increase the pixel density of displays, we anticipate resolution to improve continually. For cloaking, we can use lens arrays on a display panel to generate the desired ray output pattern according to Equation (4.1).

Micro-lenslet arrays have been suggested previously for transformation optics by the Courtial group [70]. They use two pairs of lenslet arrays in a confocal setting (both focal planes overlapping), as a 'window' that can refract light passing through. They have suggested using these pairs of arrays as the building blocks for a passive cloaking device, where the object inside appears shrunk. So far, they have simulated such effects only [71].

We term '*integral cloaking*' to be cloaking that uses integral imaging techniques. An example implementation is shown in Figure 4.2(b), where for simplicity, two parallel plates are used together with lenslet arrays. Each plate and lens combination has two functions- to capture light rays and to display cloaking light rays. This can be done by placing both detector pixels and display pixels next to, or nearby each other, for example. The displayed light rays (output) use the incident rays from the other plate (input) according to Equation (4.1).

Figure 4.2(b) is symmetric, where an observer can be in front of either side. However, for purposes of demonstration, we will capture rays with one plate and display rays with the other, only. With parallel plates, $L = (z_f - z_i)$ is constant in Equation (4.1) for all rays. To simplify the required equipment, we limit our cloak to 2D, where observers are at a fixed height, and move only in the plane horizontal

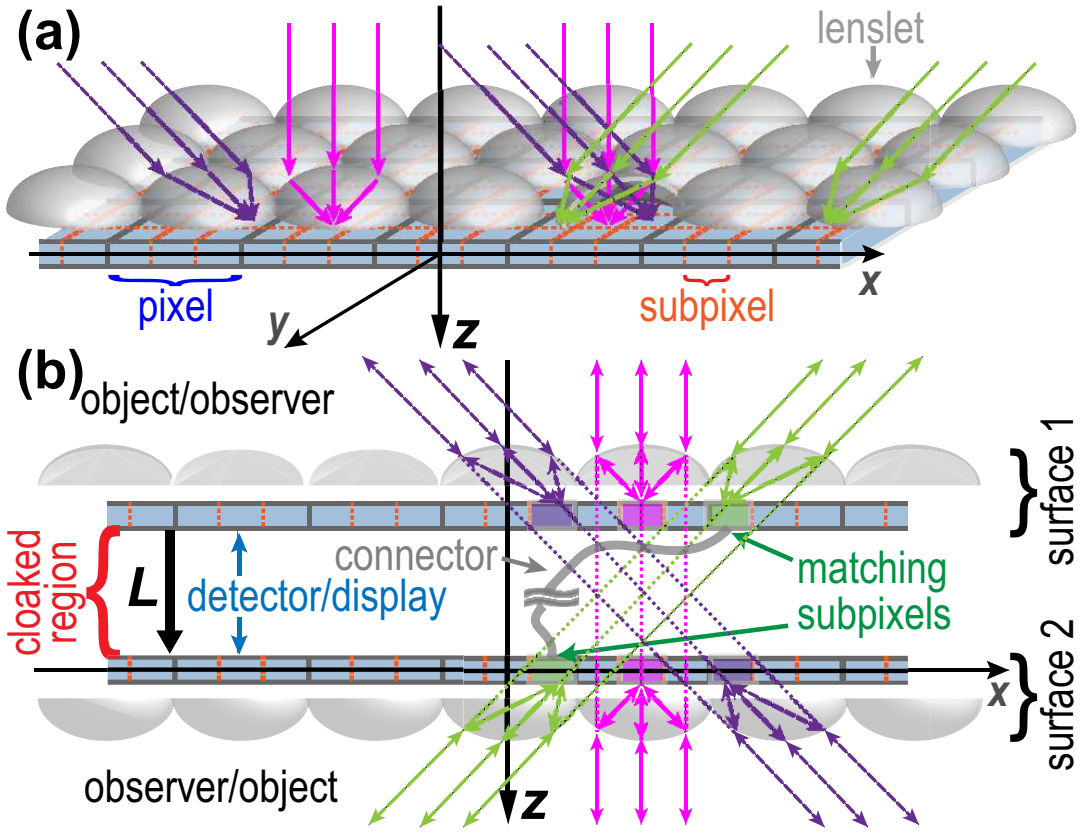

Figure 4.2: (a) 'Fly's eye' lens array principle. Rays (arrows), on a single **x**-**z** plane are shown. Each lenslet focuses these rays into its corresponding 'pixel,' placed at the focusing plane below. Different incident angles are then spatially separated into different 'subpixels.' **(b) An 'integral cloak.'** Cross-section of two parallel, 2D plates and their lenslet arrays. Each 'surface' (lens array + plate) captures light rays and displays rays for cloaking. Displayed rays are output as if the rays entered one side and exited the other with nothing in between (dotted lines). Each matching subpixel pair is connected with a 'connector' (wiring and/or computer).

to the floor (**x-z** plane in Figure 4.2(b)). Since both eyes of an observer typically lie on the same horizontal plane, stereoscopic depth can still be perceived with the 2D version. Integral cloaking in the vertical plane follows the same principles, just rotated, so that in algorithm and in theory, 2D cloaking extends to 3D in a relatively straightforward manner.

Figures 4.3(a) and 4.3(b) show the setup for our 2D integral cloak. The input plane (input camera sensor on slider) and display screen were separated by $L = 13$ cm. The background objects consisted of four sets of colored blocks, the total depth of the object space (from the input plane) being 90 cm (see Appendix D for details of the setup). Rays from the input camera are processed by a computer that uses Equation (4.1) ($y \to x$) to determine the output rays for each display pixel.

For the image capture (input) plane, we used a digital camera (Sony DSC-RX10), mounted on a mechanical slider that scans horizontally at a fixed speed (see Visualization 4.1; a shorter scan distance than Visualization 4.1 sufficed for our setup). Visualization 4.2 shows the actual scan used for generating our cloaked image, but sped up and reduced in size. For 2D, a scanning camera was not only easier to obtain than a combination of lenslet and detector arrays (like 'surface 1' of Figure 4.2(b)), but it had improved performance. This is because a continuous scan gave a horizontal spatial resolution of 0.106 mm in camera positions. This was about 10 times better than the horizontal spatial resolution of our final system (1.34 mm), which was set by the output lenslet array. (Calculation details in Appendix D.) In addition, commercial cameras are highly aberration-corrected, whereas lenslet arrays usually have little, if any, corrections; this causes the latter to have blurred images, both for input and output.

The benefits of our horizontal scanning method come at the cost of a delay in time. For our setup (Figure 4.3), the input scan required 29 seconds, and the computational processing required 22 seconds on the laptop that ran our code.

We required additional time to test and transfer data, but with proper hardware interfacing, this can be automated with little delay. Both scan and processing times increase with the dimensions of the cloakable volume. For example, the horizontal scan distance required is $(Ws + 2L\tan(FOV_l/2))$. Here, W_s is the active screen width of the output display, and FOV_l is the field-of-view (FOV) of the output lenslet array. Subjective quality requirements of the cloak can dictate the speed as well. A 3D version would require raster scanning over a 2D (**x**-**y**) plane, which can be difficult and time-consuming, if using a single camera. Thus, for real-time or 3D digital cloaking, using a 2D array of detectors combined with a fly's eye lenslet array (Figure 4.2(b)) for the input surface would be the practical, though likely costly, approach.

We now describe the display (output) plane of our cloak. For the output display, we used a 20 cm (diagonal) LCD monitor (Apple iPad mini 4). Our output lenslet array was a 2D cylindrical lenslet array (20 lens-per-inch array from Micro Lens Technology). Both display monitor and lenslet array were commercially available. For a 3D integral cloak, a fly's eye lens array should replace the cylindrical lenslet array. By slanting the cylindrical lenses, we utilized the 3 RGB subpixels to gain 3 times the horizontal angular resolution (in number of 'views'), at the sacrifice of vertical resolution [69]. Our output system generated 51.5 discrete 'views' over 29° of viewing angles (field-of-view), horizontally. This 29° was the field-of-view of the lenslet array (FOV_l), and limited the cone of angles for both the output and input of our cloaking system, since the input camera field-of-view was larger (∼60°). Each 'view' corresponds to a discrete ray angle/momentum that is displayed for our system. This determined the output angular resolution of our cloaking system, giving 0.56° between neighboring views. Note that this output 'angular resolution' of the digital integral cloak is how much an observer must move to see a change in image (corresponding to the subsequent 'view'). So smaller angular resolution values provide more continuous viewing, and allow

farther observation distances, than larger values.

Figures 4.3(c)-(f) show a horizontal (**x**) demonstration of this 2D integral cloak. An "observer" camera at a fixed height (y) near the center of the cloak, and fixed distance z from the cloak, was placed on a slider to scan horizontally (x). This camera was 260 cm from the display screen (cloak). Figures 4.3(c)-(f) show 10.8° of the total 13.4° viewing range of Visualization 4.3. The objects behind the cloak match in horizontal alignment, size (magnification), and parallax motion for varying object depths (from the cloak). As expected for real 3D scenery, the objects that are farther from the screen move across the cloaking screen quicker than those closer to the screen. (Visualization 4.4 shows just the cloak recorded.)

The vertical magnification was matched for a particular observer distance and object depth combination, since this was a 2D cloak that used cylindrical lenses. In our case, from the observation distances we used, as in Figures 4.3(c)-(f), the vertical sizes of objects near the farthest blocks (dark green) and red blocks were roughly matched. However, if spherical fly's eye lenslet arrays are used for a full 3D integral cloak, the vertical alignment and magnification will match for all object and observer distances, in theory.

Figures 4.4(a)-(d) show a longitudinal (**z**) demonstration of our integral cloak, by varying observation distances away from the cloaking screen. The horizontal field-of-view occupied by the cloaking screen, from the observer camera, were 2.53°, 2.93°, 3.38°, 4.59°, for Figures 4.4(a)-(d), respectively (Assumptions in Appendix D). This is the range of angles ('views') of the light rays that the observer camera captures. As an observer moves closer to the cloak (towards Figure 4.4(d) from Figure 4.4(a)), a larger range of angles is seen. This corresponds to a larger spatial amount of the background scene being shown by the cloak (horizontally). For a cloaking system, which should appear as if absent (transparent), this is as expected.

Finally, we characterize our digital integral cloak with additional quality met-

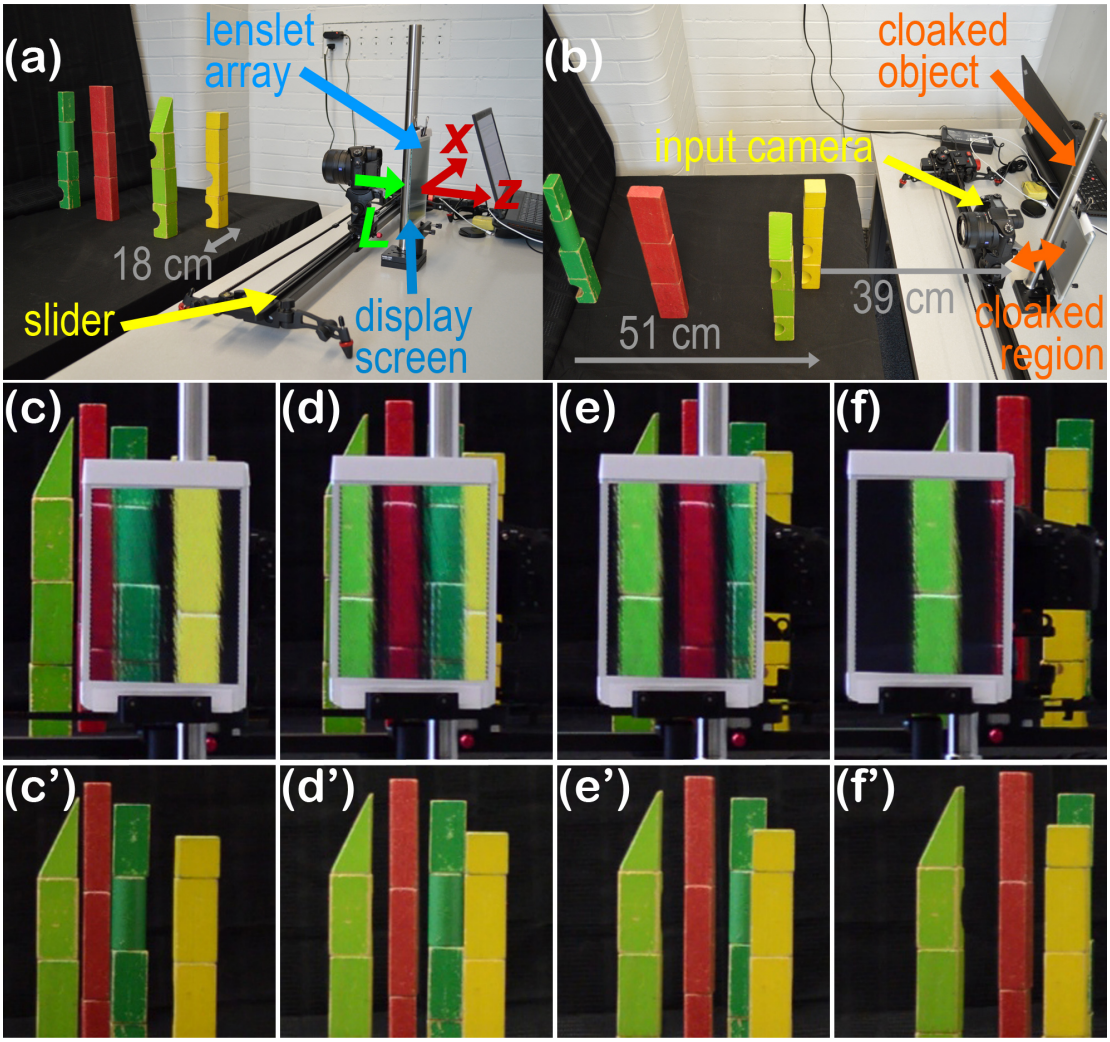

Figure 4.3: (a)-(b) 2D integral cloak setup. The input camera on a slider (input plane) scans horizontally to gather input rays. The lenslet array on the display screen (output plane) together emit rays according to Equation (4.1). The space between the input and output planes (separated by L) is the cloaked region. **(c)-(f) *With* the integral cloak.** Screen shots by an "observer" camera that moved horizontally (from Visualization 4.3). Viewing angles from screen center to observer camera: **(c)** $-4.1°$, **(d)** $0.0°$, **(e)** $2.0°$, **(f)** $6.7°$. **(c')-(f') *Without* the integral cloak.** The cloaking screen, in **(c)-(f)**, horizontally matches **(c')-(f')** respectively, in size, alignment, and parallax motion.

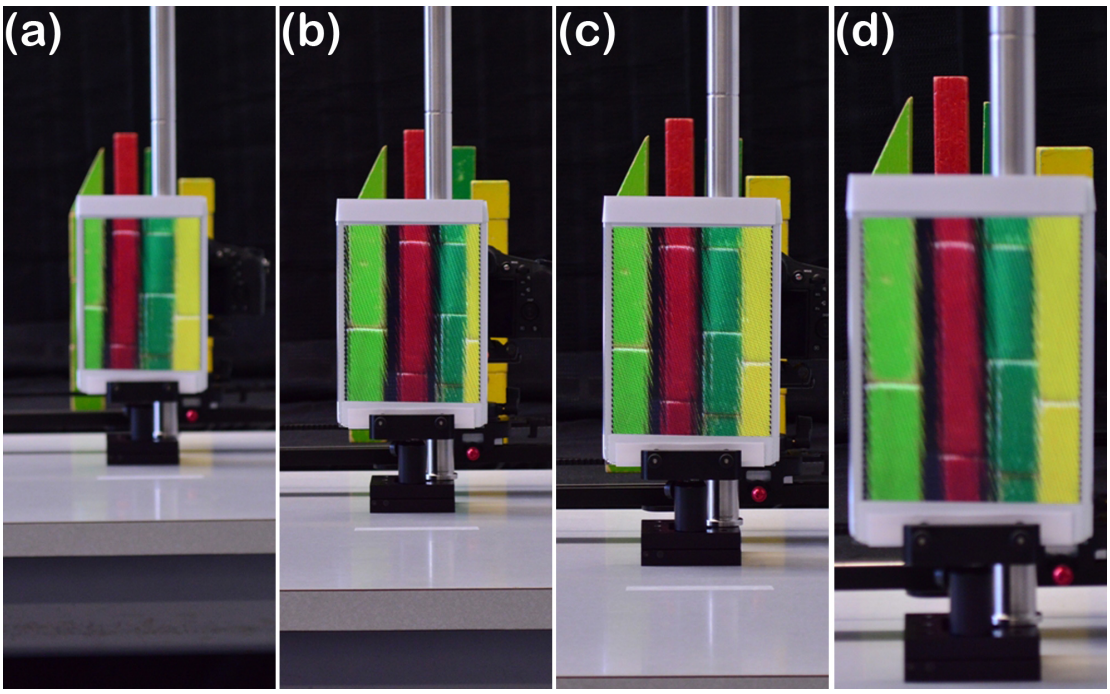

Figure 4.4: (a)-(d) Integral cloak longitudinal (z) demonstration. Observer (camera) at different distances in front of the display screen of the cloak: 272 cm, 235 cm, 203 cm, and 150 cm, for (a)-(d), respectively. As expected, the cloak displays more of the background objects, spatially, for closer observation.

rics. Detailed characterization calculations and additional quality factors are provided in Appendix D. Since ours was a 2D demonstration, we limited our analysis to the horizontal ($\mathbf{x}$) and longitudinal ($\mathbf{z}$) dimensions. The horizontal input angular resolution for our system was 0.031°, which corresponds to the uncertainty in the input ray angles. (Recall the output angular resolution was 0.56°.) To provide sufficient depth-of-field, we stopped-down our input camera to f-number = f/10. The resulting input aperture diameter was then 0.88 mm. This corresponds to the range of transverse spatial positions, of the objects, that are captured for each detector pixel of the input camera. Comparatively, the output aperture was 1.34 mm.

As shown in Visualization 4.2 and Appendix D, our demonstrated depth-of-field was over 60 cm, such that all the objects we demonstrated for the cloak (Figures 4.3 and 4.4) were at least in good focus when collected for input. The input camera was not the limiting factor here, as we could achieve several meters depth-of-field, but the display (output) surface limited the resolution to display object depths clearly. The spatial sensitivity of our slanted lenslet array to be misaligned on the display is such that a 0.026 mm change in position will shift the 'view' seen. The angular sensitivity of the lenslet array alignment with respect to the display screen pixels was $(8.8 \times 10^{-3})°$.

4.4 Discussion

Our digital cloak demonstration was dynamic, so that a changing background could be displayed properly, after a finite lag time for scanning and processing. Work to make a real-time cloak is underway. A static cloak for an observer with fixed z-position can also be obtained relatively simply by recording with a camera *from* the planned observer locations. For large observation distances, a finite number of camera images can be used (one image for each 'view') for reasonable

results. The ray processing becomes simplified, with each 'view'/angle using a single camera location corresponding to that given view.

The phase of the light fields can be matched by including properly engineered materials for a fixed-shape cloak, or spatial light modulator arrays for a cloak with dynamic shapes. If we assume each subpixel corresponds to a single ray position, angle, frequency, it is straightforward to trace an input subpixel to its output subpixel (Equation (4.1)). To good approximation, each pair is then a unidirectional propagation from input subpixel to output subpixel (dotted lines in Figure 4.2(b)), with respect to a new **z**-axis. This allows the paraxial full-field cloaking theory to be used for each subpixel pair, to calculate the phase and dispersion necessary for phase-matching of light fields [6]. These assumptions and approximations become increasingly accurate as the cloak pixel size decreases.

Lastly, with increased computational power and refined resolution, digital cloaking can be adapted to be wearable. Sensors can be used to determine the position and orientation for each pixel (or subpixel), with a processor calculating the correct ray propagation (Equation (4.1)) and output pixel (or subpixel). This will allow wearable cloaks, or suits, that are dynamic in shape, to be manufactured.

In conclusion, to approximate an ideal cloak for practical observation, we have proposed discretized cloaking. In particular, we have demonstrated a 2D digital integral cloak, by using commercially available technologies- A camera to capture the input rays, and a monitor + cylindrical lenslet array for the output rays. Our demonstration had 0.56° angular resolution over 29° field-of-view, and spatial resolution of 1.34 mm, limited by the output system. The principles for generating a 3D integral cloak follow easily. Although our demonstration was for ray optics cloaking, we have suggested other designs, including methods to match the phase of the light fields. Digital cloaking has good potential for wide implementation as a wearable cloak, since the digital technology required continue to improve commercially.

5 Conclusion

In this thesis, we explored practical methods for invisibility cloaking that works broadband in the visible regime, which has been a challenge for metamaterial cloaks. This was achieved by restricting the viewing angles to small angles, and considering cloaking as an imaging problem. This allowed us to formulate a paraxial formalism for cloaking. Initially the theory was for ray optics only, for which we demonstrated a 4 lens-only cloak (called the 'Rochester Cloak') that satisfied the 'perfect' cloaking ABCD matrix (Equation (2.1)). We then extended the theory to match the full phase of the electromagnetic field, by using Huygens' integral for propagating fields. We could then show that a thin, flat plate, with specific index and dispersion properties, could match the phase for a ray optics cloak over a broad range of frequencies. This completed the formalism for describing invisibility cloaking in the paraxial limit ('paraxial cloaking').

Optical engineering, to expand the field-of-view and numerical aperture of a ray optics cloak, is a promising route to build cloaks that are more useful than a paraxial cloak. We have begun exploring such improvements. In the mean time, building a truly omnidirectional cloak, even from ray optics principles, has yet to be demonstrated experimentally. In addition, whether an isotropic, 3D, omnidirectional, broadband cloak can be achieved for ray optics, seems to still be an open question, even theoretically. Some consensus is being met, however,

where the growing literature suggests that broadband appears to be impossible for an omnidirectional, ideal cloak that matches phase, which our work so far seems to agree.

An ideal cloak that is both omnidirectional and broadband can be achieved if we remember that invisibility cloaking is inherently an illusion shown to the unsuspecting observer. Light from behind the cloak simply needs to get around a cloaked space, and 'reconvene' in front of the cloak, as if it had traveled in a straight path through the cloak. All observers, even machines, have resolution limits for detecting light. We can then use this to our advantage, by discretizing space and angle at below the resolution limit of the observer. The length and angular scales depend on the distance from the observer, too, so that a large, low-resolution cloak could be used for far-away observation.

Using this concept of discretization, we provided a new methodology to achieve practical, 3D, broadband, omnidirectional, macroscopic, and phase-matched cloaking ('discretized cloaking'). We then demonstrated a 2D, ray optics version, using commercially available digital technology and integral imaging techniques ('digital integral cloaking'). We believe this will open avenues to bring practical invisibility to the public, as the basic technology required is already widely available and improving quickly due to consumer demand. The principles to achieve a dynamic, wearable cloak have already been provided in this thesis.

In the end, after trying multiple methods to achieve cloaking, it appears that our original "Rochester Cloak" was quite close to 'perfect' in the paraxial regime. The ability of this paraxial cloak to display background images clearly and undistorted, while matching the background motion for moving observers or different observers, has been a standard to achieve for other cloaking designs. In addition, this rudimentary cloak is truly passive, where no extra lighting control is necessary, and an observer can focus at different depths over a large depth-of-field. It acts quite nicely as if it was not present, while still hiding an object effectively.

Of course the limitation being paraxial is a large drawback for making it widely useful, but the image quality remains one of the best, if not the best, out of the currently available multidirectional cloaks we know. And so we come full circle.

Bibliography

[1] D. J. Starling, S. M. Bloch, P. K. Vudyasetu, J. S. Choi, B. Little, and J. C. Howell, "Double Lorentzian atomic prism," Physical Review A **86**, 023826 (2012).

[2] J. S. Choi and M. Cho, "Limitations of a superchiral field," Physical Review A **86**, 063834 (2012).

[3] H. Rhee, J. S. Choi, D. J. Starling, J. C. Howell, and M. Cho, "Amplifications in chiroptical spectroscopy, optical enantioselectivity, and weak value measurement," Chemical Science **4**, 4107 (2013).

[4] J. C. Howell, J. B. Howell, and J. S. Choi, "Amplitude-only, passive, broadband, optical spatial cloaking of very large objects," Applied Optics **53**, 1958 (2014).

[5] J. S. Choi and J. C. Howell, "Paraxial ray optics cloaking," Optics Express **22**, 29465 (2014).

[6] J. S. Choi and J. C. Howell, "Paraxial full-field cloaking," Optics Express **23**, 15857 (2015).

[7] J. S. Choi and J. C. Howell, "Digital integral cloaking," Optica **3** (2016), (accepted).

[8] G. Gbur, "Invisibility Physics: Past, Present, and Future," Progress in Optics **58**, 65 (2013).

[9] U. Leonhardt, "Optical Conformal Mapping," Science **312**, 1777 (2006).

[10] J. B. Pendry, D. Schurig, and D. R. Smith, "Controlling Electromagnetic Fields," Science **312**, 1780 (2006).

[11] M. McCall, "Transformation optics and cloaking," Contemporary Physics **54**, 273 (2013).

[12] B. Zhang, "Electrodynamics of transformation-based invisibility cloaking," Light-Science and Applications **1**, e32 (2012).

[13] D. Schurig, J. J. Mock, B. J. Justice, S. A. Cummer, J. B. Pendry, A. F. Starr, and D. R. Smith, "Metamaterial electromagnetic cloak at microwave frequencies," Science **314**, 977 (2006).

[14] N. Landy and D. R. Smith, "A full-parameter unidirectional metamaterial cloak for microwaves," Nature Materials **12**, 25 (2013).

[15] J. C. Soric, P. Y. Chen, A. Kerkhoff, D. Rainwater, K. Melin, and A. Alu, "Demonstration of an ultralow profile cloak for scattering suppression of a finite-length rod in free space," New Journal of Physics **15**, 033037 (2013).

[16] D. Rainwater, A. Kerkhoff, K. Melin, J. C. Soric, G. Moreno, and A. Alu, "Experimental verification of three-dimensional plasmonic cloaking in free-space," New Journal of Physics **14**, 013054 (2012).

[17] M. Fridman, A. Farsi, Y. Okawachi, and A. L. Gaeta, "Demonstration of temporal cloaking," Nature **481**, 62 (2012).

[18] J. M. Lukens, D. E. Leaird, and A. M. Weiner, "A temporal cloak at telecommunication data rate," Nature **498**, 205 (2013).

[19] S. Brule, E. H. Javelaud, S. Enoch, and S. Guenneau, "Experiments on Seismic Metamaterials: Molding Surface Waves," Physical Review Letters **112**, 133901 (2014).

[20] B. L. Zhang, Y. A. Luo, X. G. Liu, and G. Barbastathis, "Macroscopic Invisibility Cloak for Visible Light," Physical Review Letters **106**, 033901 (2011).

[21] X. Z. Chen, Y. Luo, J. J. Zhang, K. Jiang, J. B. Pendry, and S. A. Zhang, "Macroscopic invisibility cloaking of visible light," Nature Communications **2**, 176 (2011).

[22] H. Chen, B. Zheng, L. Shen, H. Wang, X. Zhang, N. I. Zheludev, and B. Zhang, "Ray-optics cloaking devices for large objects in incoherent natural light," Nature Communications **4**, 2652 (2013).

[23] T. R. Zhai, X. B. Ren, R. K. Zhao, J. Zhou, and D. H. Liu, "An effective broadband optical 'cloak' without metamaterials," Laser Physics Letters **10**, 066002 (2013).

[24] R. Fleury and A. Alu, "Cloaking and Invisibility: A Review," Progress in Electromagnetics Research-PIER **147**, 171 (2014).

[25] J. S. Li and J. B. Pendry, "Hiding under the Carpet: A New Strategy for Cloaking," Physical Review Letters **101**, 203901 (2008).

[26] J. Valentine, J. Li, T. Zentgraf, G. Bartal, and X. Zhang, "An optical cloak made of dielectrics," Nature Materials **8**, 568 (2009).

[27] R. Liu, C. Ji, J. J. Mock, J. Y. Chin, T. J. Cui, and D. R. Smith, "Broadband Ground-Plane Cloak," Science **323**, 366 (2009).

[28] T. Ergin, N. Stenger, P. Brenner, J. B. Pendry, and M. Wegener, "Three-Dimensional Invisibility Cloak at Optical Wavelengths," Science **328**, 337 (2010).

[29] J. Fischer, T. Ergin, and M. Wegener, "Three-dimensional polarization-independent visible-frequency carpet invisibility cloak," Optics Letters **36**, 2059 (2011).

[30] U. Leonhardt and T. Tyc, "Broadband Invisibility by Non-Euclidean Cloaking," Science **323**, 110 (2009).

[31] F. Monticone and A. Alu, "Physical bounds on electromagnetic invisibility and the potential of superconducting cloaks," Photonics and Nanostructures-Fundamentals and Applications **12**, 330 (2014).

[32] Q. Ma, Z. L. Mei, S. K. Zhu, T. Y. Jin, and T. J. Cui, "Experiments on Active Cloaking and Illusion for Laplace Equation," Physical Review Letters **111**, 173901 (2013).

[33] D. A. B. Miller, "On perfect cloaking," Optics Express **14**, 12457 (2006).

[34] H. Chen, Z. Liang, P. Yao, X. Jiang, H. Ma, and C. T. Chan, "Extending the bandwidth of electromagnetic cloaks," Physical Review B **76**, 241104 (2007).

[35] H. Hashemi, C.-W. Qiu, A. P. McCauley, J. D. Joannopoulos, and S. G. Johnson, "Diameter-bandwidth product limitation of isolated-object cloaking," Physical Review A **86**, 013804 (2012).

[36] F. Monticone and A. Alu, "Do Cloaked Objects Really Scatter Less?" Physical Review X **3**, 041005 (2013).

[37] R. Fleury, F. Monticone, and A. Alu, "Invisibility and Cloaking: Origins, Present, and Future Perspectives," Physical Review Applied **4**, 037001 (2015).

[38] R. Schittny, M. Kadic, T. Bueckmann, and M. Wegener, "Invisibility cloaking in a diffusive light scattering medium," Science **345**, 427 (2014).

[39] E. Wolf and T. Habashy, "Invisible bodies and uniqueness of the inverse scattering problem," Journal of Modern Optics **40**, 785 (1993).

[40] A. I. Nachman, "Reconstructions from boundary measurements," Annals of Mathematics **128**, 531 (1988).

[41] A. J. Devaney, "Nonuniqueness in inverse scattering problem," Journal of Mathematical Physics **19**, 1526 (1978).

[42] C. Discovery Channel, "Daily planet," Bell Media (March 18, 2015), two 4 lens cloaks are presented: One is the original "Rochester Cloak." The other has almost double the field-of-view, 1.5 times the cloaked diameter, and a cloaking region that no longer needs the center unobstructed.

[43] W. Smith, *Modern Lens Design*, 2nd ed. (McGraw-Hill, 2005).

[44] M. Born and E. Wolf, *Principles of optics: Electromagnetic theory of propagation, interference and diffraction of light*, 7th ed. (Cambridge University Press, New York, 2010).

[45] A. E. Siegman, *Lasers* (University Science Books, Sausalito, CA, 1986).

[46] M. Bass, *Handbook of optics*, 3rd ed., Geometrical and physical optics, polarized light, components and instruments, Vol. 1 (McGraw-Hill, New York, 2010).

[47] J. E. Greivenkamp, *Field guide to geometrical optics*, Vol. FG01 (SPIE, Bellingham, WA, USA, 2004).

[48] D. Barnstone, "cloaking device uses ordinary lenses to hide objects across range of angles," University of Rochester (2014).

[49] P. P. Clark and C. Londono, in *1990 Intl Lens Design Conf*, Vol. 1354 (Proc. SPIE, 1991) pp. 555–569.

[50] R. Duan, E. Semouchkina, and R. Pandey, "Geometric optics-based multi-band cloaking of large objects with the wave phase and amplitude preservation," Optics Express **22**, 27193 (2014).

[51] J. W. Goodman, *Introduction to Fourier optics*, 3rd ed. (Roberts and Co., Englewood, CO, 2005).

[52] A. V. Kildishev, W. Cai, U. K. Chettiar, and V. M. Shalaev, "Transformation optics: approaching broadband electromagnetic cloaking," New Journal of Physics **10**, 115029 (2008).

[53] J. T. Costa and M. G. Silveirinha, "Achromatic lens based on a nanowire material with anomalous dispersion," Optics Express **20**, 13915 (2012).

[54] M. G. Silveirinha, "Anomalous Refraction of Light Colors by a Metamaterial Prism," Physical Review Letters **102**, 193903 (2009).

[55] M. J. Theisen and T. G. Brown, in *Frontiers in Optics 2012/Laser Science XXVIII*, OSA Technical Digest (online) (Optical Society of America) p. FTu4A.3.

[56] V. G. Veselago, "The electrodynamics of substances with simultaneously negative values of epsilon and mu," Soviet Physics Uspekhi-Ussr **10**, 509 (1968).

[57] C. M. Soukoulis and M. Wegener, "Past achievements and future challenges in the development of three-dimensional photonic metamaterials," Nature Photonics **5**, 523 (2011).

[58] R. A. Shelby, D. R. Smith, and S. Schultz, "Experimental verification of a negative index of refraction," Science **292**, 77 (2001).

[59] J. Valentine, S. Zhang, T. Zentgraf, E. Ulin-Avila, D. A. Genov, G. Bartal, and X. Zhang, "Three-dimensional optical metamaterial with a negative refractive index," Nature **455**, 376 (2008).

[60] D. Chanda, K. Shigeta, S. Gupta, T. Cain, A. Carlson, A. Mihi, A. J. Baca, G. R. Bogart, P. Braun, and J. A. Rogers, "Large-area flexible 3D optical negative index metamaterial formed by nanotransfer printing," Nature Nanotechnology **6**, 402 (2011).

[61] J. B. Pendry, "Negative refraction makes a perfect lens," Physical Review Letters **85**, 3966 (2000).

[62] A. Greenleaf, M. Lassas, and G. Uhlmann, "Anisotropic conductivities that cannot be detected by EIT," Physiological Measurement **24**, 413 (2003).

[63] A. Greenleaf, Y. Kurylev, M. Lassas, and G. Uhlmann, "Full-wave invisibility of active devices at all frequencies," Communications in Mathematical Physics **275**, 749 (2007).

[64] A. Greenleaf, Y. Kurylev, M. Lassas, and G. Uhlmann, "Isotropic transformation optics: approximate acoustic and quantum cloaking," New Journal of Physics **10**, 115024 (2008).

[65] C. Della Giovampaola and N. Engheta, "Digital metamaterials," Nature Materials **13**, 1115 (2014).

[66] M. Bass, J. M. Enoch, and V. Lakshminarayanan, *Vision and vision optics*, 3rd ed., Handbook of optics, Vol. 3 (McGraw-Hill, New York, 2010).

[67] F. G. Vasquez, G. W. Milton, and D. Onofrei, "Active Exterior Cloaking for the 2D Laplace and Helmholtz Equations," Physical Review Letters **103**, 073901 (2009).

[68] G. Lippmann, "Epreuves reversibles. Photographies integrales," C. R. Acad. Sci. **146**, 446 (1908).

[69] J. Geng, "Three-dimensional display technologies," Advances in Optics and Photonics **5**, 456 (2013).

[70] A. C. Hamilton and J. Courtial, "Generalized refraction using lenslet arrays," Journal of Optics A: Pure and Applied Optics **11**, 065502 (2009).

[71] S. Oxburgh, C. D. White, G. Antoniou, E. Orife, and J. Courtial (Proc. of SPIE, 2014) p. 91931E.

[72] D. Buralli, *OPT 441- Geometrical Optics* (The Institute of Optics, University of Rochester, Rochester, NY, U.S.A., 2010).

[73] A. Nussbaum, *Optical system design* (Prentice Hall PTR, Upper Saddle River, NJ, 1998).

[74] A. Nussbaum, "Teaching of advanced geometric optics," Applied Optics **17**, 2128 (1978).

[75] J. R. Fienup, "Optics 461: Physical optics 1," The Institute of Optics (2010), course lecture notes.

[76] S. A. Collins, "Lens-system diffraction integral written in terms of matrix optics," Journal of the Optical Society of America **60**, 1168 (1970).

[77] J. Bentley, "Optics 444- lens design," The Institute of Optics (2012), course lecture notes.

[78] Schott, *Optical Glass- Data Sheets*, Report (Schott North America, Inc., 2013).

[79] M. N. Polyanskiy, "Refractive index database," http://refractiveindex.info (2015).

[80] "Integral Photography," Scientific American **105**, 164 (1911).

A Appendix: Additional Background

A.1 ABCD matrix background

We borrow well-known linear equations from the field of geometric optics [46]. We will assume rotational symmetry for the system. To first approximation, called the "paraxial approximation," light rays are assumed to deviate minimally from the axis of rotational symmetry for the system (z in Fig. A.1). We can then see that in the paraxial approximation, ray angles are small.

All light rays can then be described by its transverse position y and the paraxial angle u, much like a particle can be described by its position and momentum. Here,

$$u \equiv \tan\theta \approx \theta, \tag{A.1}$$

where θ is the exact, real angle of the ray from the z-axis.

Because of the linearity of optics in the paraxial approximation, the propagation of light rays through an optical system can be described by matrices. Utilization of matrices for ray optics has a rich history, with equations that originated from Newton and Gauss [73, 74]. These matrices are called 'ray transfer'

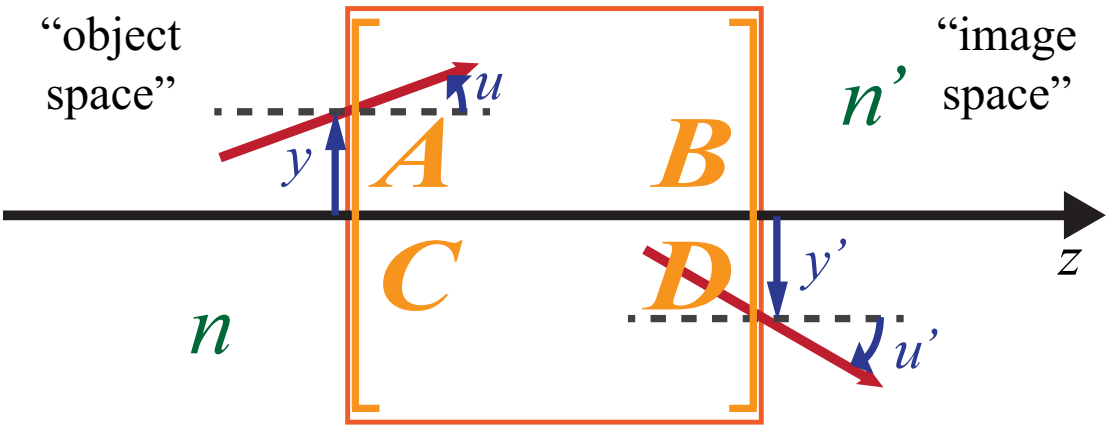

Figure A.1: Light rays and the ‘ABCD’ matrix. Ray optics picture in the paraxial approximation. We assume a rotationally symmetric system (about the z-axis), with light traveling from left to right. The optical system (box in the center) can be described by an ‘ABCD’ matrix. This matrix maps the initial position (y) and paraxial angle (u) to those exiting the system (y', u'). The “object space” is the space before the ABCD system, with index of refraction n. Likewise, the “image space” is the space after the system, with index of refraction n'. In this diagram, $y > 0$, $u > 0$, $y' < 0$, and $u' < 0$, for our sign convention [72].

matrices, or ‘ABCD’ matrices, and are used as follows:

$$\begin{bmatrix} y' \\ n'u' \end{bmatrix} = \begin{bmatrix} A & B \\ C & D \end{bmatrix} \begin{bmatrix} y \\ nu \end{bmatrix}, \tag{A.2}$$

where n is the index of refraction, y is the transverse position, and u is the paraxial angle, immediately before the ABCD matrix. n', y', and u' are those for after the matrix (See Fig. A.1). For example, the ABCD matrix for a space of length t, with index of refraction n_t, is the ‘translation matrix’ (or ‘transfer matrix’):

$$M_t = \begin{bmatrix} 1 & t/n_t \\ 0 & 1 \end{bmatrix}. \tag{A.3}$$

A.2 ABCD matrix for a cloak

So what does the ABCD matrix for a perfect cloaking system look like? It is precisely the translation matrix M_t in Equation (A.3), where $t = L$ is the length

of the system, and $n_t = n = n'$. This is because a perfect cloaking device simply replicates the surrounding medium throughout its volume. We then see that

$$\begin{bmatrix} y' \\ nu' \end{bmatrix} = \begin{bmatrix} 1 & L/n \\ 0 & 1 \end{bmatrix} \begin{bmatrix} y \\ nu \end{bmatrix} = \begin{bmatrix} y + Lu \\ nu \end{bmatrix}. \tag{A.4}$$

As expected, the angle remains the same, i.e. $u' = u$, and the position shifts by the angle multiplied by the length, i.e. $y' = y + Lu$.

So far we assumed the ambient medium of the cloaking device to be uniform. Suppose this was not the case. In the paraxial approximation, we can then assume the changes happen along z only, since transverse deviations are small. Thus we can write $n \to n(z)$ to account for the nonuniform medium. Let's assume there are N segments along z within the device, such that $n(z) \equiv n_i$ is constant for the region $z \in [z_{i-1}, z_i)$. Here, $z = z_0$ at the beginning of the device, and $z = z_N = (z_0 + L)$ at the end of the device (of length L). Then, the ABCD matrix for a perfect cloak can be written as

$$\prod_{i=1}^{N} \begin{bmatrix} 1 & (z_i - z_{i-1})/n_i \\ 0 & 1 \end{bmatrix} = \tag{A.5}$$
$$\begin{bmatrix} 1 & (z_N - z_{N-1})/n_N \\ 0 & 1 \end{bmatrix} \cdots \begin{bmatrix} 1 & (z_2 - z_1)/n_2 \\ 0 & 1 \end{bmatrix} \cdot \begin{bmatrix} 1 & (z_1 - z_0)/n_1 \\ 0 & 1 \end{bmatrix}.$$

A.3 Propagation of a Field using Huygens' Integral

We first clarify our notation for writing light as an electromagnetic field. Such a physical field can be written mathematically as a real vector:

$$\mathbf{E}(\mathbf{r}, t) = \frac{1}{2} \left[\tilde{\mathbf{E}}(\mathbf{r}) e^{+i\omega t} + \tilde{\mathbf{E}}^*(\mathbf{r}) e^{-i\omega t} \right] = \mathrm{Re} \left\{ \tilde{\mathbf{E}}(\mathbf{r}) e^{+i\omega t} \right\}, \tag{A.6}$$

where ω is the angular frequency, $\mathbf{r}$ is the position, and t is the time. Note the use of tildes($\tilde{}$) to denote the complex field. $\tilde{E}(\mathbf{r})$ is the complex, spatial amplitude of the field distribution, without the $e^{+i\omega t}$ harmonic time dependence (HTD).

Field propagation based off of Huygens' principle of wavelet propagation, is effective and widely used in diffraction theory and Fourier optics [51]. We first assume that the field is in a spatially uniform ambient medium with index of refraction n, and that the optical system is described by an ABCD matrix, which is assumed to be rotationally symmetric for simplicity (See Fig. 3.1). Nonuniform medium or non-rotationally symmetric systems can be derived from here.

For one transverse dimension, Huygens' integral for free space propagation of a complex field $\tilde{E}_1$ is [45]:

$$\tilde{E}_2(x_2) \approx \sqrt{\frac{i}{L\lambda}} \int_{-\infty}^{\infty} \tilde{E}_1(x_1) \exp\left[-ik\rho(x_1, x_2)\right] \mathrm{d}x_1, \tag{A.7}$$

where x_1, x_2 are the transverse positions on the input plane $z = z_1$ and $z = z_2$, respectively. Equation (A.7) is derived from Huygens' principle, which is that the incident field for each point on a surface becomes a new source for a spherical wave, and then approximated for paraxial fields. The input field is $\tilde{E}_1$ and the output field is $\tilde{E}_2$. L is the on-axis propagation distance along the **z**-axis (See Fig. 3.1). $\rho(x_1, x_2)$ is the path length of an optical ray traveling from x_1 to x_2 in free space. For travel through a general optical medium, it is called the optical path length (OPL), or "*eikonal function*." The OPL is the phase traversed for a given field, and is given by

$$\rho(x_1, x_2) = \int_{\mathcal{C}} n(s) \mathrm{d}s, \tag{A.8}$$

where $n(s)$ is the index of refraction at the point s, along the traveled path $\mathcal{C}$ from (x_1, z_1) to (x_2, z_2).

For a general optical system that is described by an ABCD matrix, we can utilize Fermat's principle to determine the OPL function $\rho(x_1, x_2)$ in Equation (A.8).

Fermat's principle asserts that the OPL of an actual ray, between two points, is an extremum [44, 47]. This can be restated as "all rays connecting two conjugate points must have the same optical path length between these two points" [45]. *Conjugate points* are object-image points where all rays leaving the axis from the object point will be focused back to the axis at the image point.

Using Fermat's principle and making a paraxial approximation, the OPL for a general optical system is shown to be [45]:

$$\rho(x_1, x_2) \approx L_0 + \frac{1}{2B}\left(Ax_1^2 - 2x_1x_2 + Dx_2^2\right). \tag{A.9}$$

A, B, C, D are the coefficients of the ABCD matrix. $L_0 = \sum_i n_i L_i$ is the OPL for a ray traveling exactly on-axis for the given system, where each ith optical element has index of refraction n_i and physical thickness L_i along the longitudinal, center axis.

Combining Equation (A.7) and Equation (A.9), and extending to rotationally symmetric two-dimensions, we obtain Huygens' integral in the Fresnel (or, paraxial) approximation (Adapted from References [45, 75, 76]):

$$\tilde{E}_2(x_2, y_2) = \frac{ie^{-ik_0L_0}}{B\lambda_0}\iint_{-\infty}^{\infty}\tilde{E}_1(x_1, y_1)\exp\Big\{-i\frac{\pi}{B\lambda_0} \\ \left[A\left(x_1^2 + y_1^2\right) - 2\left(x_1x_2 + y_1y_2\right) + D\left(x_2^2 + y_2^2\right)\right]\Big\}\mathrm{d}x_1\mathrm{d}y_1. \tag{A.10}$$

λ_0 and k_0 are the wavelength and wavevector in free space. The input field $\tilde{E}_1$ spatially depends on the transverse dimensions (x_1, y_1), and the output field $\tilde{E}_2$ depends on (x_2, y_2).

As mentioned, Eq. (A.10) assumes the paraxial approximation, that the system is rotationally symmetric (use of a single ABCD matrix), and that there are no limiting apertures [75]. It describes a scalar, monochromatic wave propagating in the z-direction with spatial distribution over two transverse dimensions (x, y).

A.4 Thin, Flat Plate Approximation

Another way to see that a thin, flat plate does not affect the total ABCD matrix is to write out the ABCD matrix for a thick, flat plate. This can be done by noting that a thick, flat plate is just space made of the plate material. So,

$$\begin{bmatrix} A & B \\ C & D \end{bmatrix}_{\text{thick, flat plate}} = \begin{bmatrix} 1 & L_c/n_c \\ 0 & 1 \end{bmatrix}, \tag{A.11}$$

where L_c and n_c are the physical thickness (along $\mathbf{z}$) and refractive index of the material, for the phase-correcting flat plate, respectively. When $L_c \to 0$, or the plate is "thin," we obtain the identity matrix.

Though thin optical elements are useful for first-order calculations and designs, they are not correct models for real optical setups. In particular, the thin, flat plate we used to correct for the full-phase of a cloaking system will break down as the thickness of the plate increases. Equation (A.11) by itself might be difficult to use for determining when a plate is "thin" enough. To quantify this, we can look at the total the ABCD matrix, rather.

Let's assume we have a ray optics cloaking system described by $\begin{bmatrix} 1 & L'/n \\ 0 & 1 \end{bmatrix}$, where L' is its total longitudinal length and n is the ambient index of refraction. For simplicity, let's place a flat plate (Equation (A.11)) immediately before (or after) the original ray optics cloak. The complete ABCD matrix for the combined system is then

$$\begin{bmatrix} A & B \\ C & D \end{bmatrix}_{\text{combined}} = \begin{bmatrix} 1 & (L'/n + L_c/n_c) \\ 0 & 1 \end{bmatrix}. \tag{A.12}$$

To satisfy Equation (2.1) for the combined system, we then want

$$\frac{(L' + L_c)}{n} = \frac{L'}{n} + \frac{L_c}{n_c}. \tag{A.13}$$

Assuming $n_c \neq n$, since otherwise there would be no phase-correction by the plate, we can only approximately satisfy Equation (A.13). We can do this by making both sides of Equation (A.13) approach L'/n:

$$\left|\frac{L_c}{L'}\right| \ll 1, \quad \text{and} \tag{A.14a}$$

$$\left|\frac{L_c}{L'}\right| \ll \left|\frac{n_c}{n}\right|. \tag{A.14b}$$

When the two conditions of Equations (A.14) are satisfied by the flat plate, we can consider the phase-correcting plate to be "thin" for our purposes. Such a thin plate will not change the ABCD matrix from the original cloaking system that satisfied Equation (2.1).

To be careful, we see that a thick, flat plate may affect the 'B' coefficient inside and outside of the integral given in Equation (3.1). Ray directions and transverse positions are not affected much by small variations in the ABCD coefficients, but small changes in phase may be significant. So the dependence on B inside the integral could be problematic, but if the plate is thin so that it satisfies Equations (A.14), then this contribution becomes negligible as well. This is because B will be dominated by L'/n. This then shows that a thin, flat plate will only affect the phase of the exponential outside of the integral in Equation (3.1), and the rest of the field will match Equation (3.4) very closely. This then concludes why we can match the phase condition given in Equation (3.5) or Equations (3.9) by including such a thin plate.

B Appendix: Methods

B.1 Ray Optics Cloaking Methods

It is important to point out that the ABCD matrix equations in Appendix A assumed that all the lenses are infinitely thin. In reality, lenses have thicknesses, and this can make a difference in obtaining the correct solutions for Equation (2.1). So to set up our simulations, we took a step further to include the lens thicknesses and materials.

B.1.1 Three lens symmetric cloak

For the first and last lenses (1 and 3) we used 200 mm focal length, BK7, 75 mm diameter lenses (Edmund Optics stock #45-371: Plano-convex lens 75.0 mm dia. x 200.0 mm FL, uncoated). For the center lens, we used two -100 mm focal length, BK7, 50 mm diameter lenses, back-to-back, to create a lens with focal length ≈ -50 mm (Edmund Optics stock #45-036: Plano-concave lens 50.0 mm dia. x -100 FL, uncoated). All lenses were catalogue optics from Edmund Optics. From Equation (2.8), we obtain $t_1 = t_2 \approx 100$ mm. Including the lens thicknesses and the material indices of refraction, we optimized t_1 slightly so that the afocal condition $C = 0$ was closely achieved. Diameter of last lens needs to be > 150 mm

for all rays to pass (no "vignetting"). For the CODE V simulation, the apertures were not restricted to the actual lens sizes. The aperture stop was the first surface. Aperture diameter sizes (for no vignetting) of the first and second diverging lenses in the center are 54 mm and 61 mm, respectively. Total length of the system is 219 mm.

Proper alignment is important for the cloaking effect. We analyzed the sensitivity of the system due to perhaps the easiest misalignment to occur- changes in the lens separation, i.e. t_1 and t_2 for the three lens case. The magnification calculations were for finite object and image "conjugates," a distance of 2 m from the first surface, and 5.3 m from the last surface, respectively. As stated previously, $t_1 = t_2$ with the ideal value being $\approx$ 100 mm. With a $\pm$1% change in t_1, the magnitude of the effective focal length (for infinite conjugates) decreased by a factor of $\approx$ 40, and the magnification changed by $\approx$ 10% from 1.0. For a $\pm$10% change in t_1, the magnitude of the effective focal length (for infinite conjugates) decreased by a factor of $\approx$ 400, and the magnification changed by a factor of $\approx$ -20 and 0.5.

Using CODE V, aberrations were calculated for the simulation given in Fig. 2.4(a), but for an object distance of 2 m from the first surface, and an image distance of 5.3 m from the last surface. For the nominal wavelength (587.6 nm), the total surface contributions (in mm) for the third-order 'structural' aberrations (σ coefficients for the transverse ray errors [72, 77]) were 4.3, -12.4, 8.4, -1.0, -4.3 for spherical aberration, coma, astigmatism, Petzval, and distortion, respectively. The CODE V generated axial and lateral colors were 7.7 mm and -2.9 mm, respectively, with a total distortion of 1.4% for the -3.5° field angle. Most of the aberrations occurred at the last (third) lens. These aberrations are expected, since only t_1 was numerically optimized (and t_2 matched to t_1) to produce a nearly afocal system, while no aberration corrections were made.

B.1.2 Four lens symmetric cloak

For the first and last lenses (1 and 4), we used 200 mm focal length, 50 mm diameter achromatic doublets composed of BK7 and SF2 glasses (Thorlabs AC508-200-A-ML: f=200 mm, 2"OD achromatic doublet, SM2 threaded mount, AR coated 400 - 700 nm). For the center two lenses (2 and 3), we used 75 mm focal length, 50 mm diameter achromatic doublets composed of SF11 and BAF11 glasses (Thorlabs AC508-075-A-ML: f=75 mm, 2"OD achromatic doublet, SM2 threaded mount, AR coated 400 - 700 nm). All doublets were off-the-shelf catalogue optics from Thorlabs and had anti-reflection coating in the visible spectrum. For the CODE V simulations, the aperture sizes were not restricted, so as to ensure no vignetting. The aperture stop was the first surface. Diameters of the second, third, and last doublets need to be $>$ 33 mm, 51 mm, and 112 mm, respectively, for no vignetting. The thick lens distance separations were obtained by solving Equation (2.1). $t_1 = t_3 = 255.49$ mm, $t_2 = 332.17$ mm, and total length $L = 910.15 (= 332.17 + (255.49 + 10.5 + 23) * 2)$ mm.

Again, we analyzed the sensitivity of the system due to lens separation misalignments, i.e. t_1, t_2, and t_3 for the four lens cloak. Finite conjugates were also used for magnification, with an object distance of 2 m from the first surface, and an image distance of 3 m from the last surface. Since ours is a symmetric cloak, $t_1 = t_3$, which was maintained. Only one variable was changed at a time, either $t_1 = t_3$ or t_2, and not both, for this analysis. With a $\pm 1\%$ change in t_1, the magnitude of the effective focal length (for infinite conjugates) decreased by a factor of $\approx 5 \times 10^4 \sim 6 \times 10^4$, and the magnification changed by $\approx 30 - 40\%$ from 1.0. For a $\pm 10\%$ change in t_1, the magnitude of the effective focal length (for infinite conjugates) decreased by a factor of $\approx 3 \times 10^5 \sim 8 \times 10^5$, and the magnification changed by a factor of $\approx$ -0.8 and 0.2. No changes in these values were seen for $1\% \sim 10\%$ changes in t_2, since t_2 does not affect the on-axis fields at 0 degrees.

Aberrations were calculated for the simulation given in Fig. 2.5(b) using CODE V, but for an object distance of 2 m from the first surface, and an image distance of 3 m from the last surface. For the nominal wavelength (587.6 nm), the total surface contributions (in mm) for the third-order 'structural' aberrations (σ coefficients for the transverse ray errors [72, 77]) were 10.4, -8.6, 8.2, 0.4, -8.1 for spherical aberration, coma, astigmatism, Petzval, and distortion, respectively. The CODE V generated axial and lateral colors were 2.4 mm and -1.3 mm, respectively, with a total distortion of 7.7% for the $-1.5°$ field angle. Most of the aberrations occurred at the last two achromats. These aberrations are not surprising, given that no optimization was performed, other than the use of achromats.

B.1.3 Rochester Cloak version 2

For our particular demonstration of the four lens cloak that can hide the center-axis, we used (Refer to Figure 2.3(d)):

Lenses 1 & 4 Edmund Optics 75 mm outer diameter x 200 mm focal length, MgF2 coated, achromatic doublet lens (Stock number #45-417),

Lenses 2 & 3 These were the same as the original Rochester Cloak. Thorlabs AC508-075-A-ML: focal length = 75 mm, 2 inch outer diameter, achromatic doublet, SM2 threaded mount, AR coated for 400 - 700 nm.

The calculated distances between the lens surfaces, which solved Equation (2.1) for the thick lenses were: $t_1 = t_3 = 249.444$ mm, $t_2 = 333.391$ mm, and total length $L = 926.159$ mm.

We then used a combination of rectangular and circular mirror pairs that were placed between lenses 2 and 3, as shown in Figure 2.7(e). This was to deflect light around the middle region between lenses 2 and 3 so that the center-axis of that area could be cloaked. Some of the mounts for these mirrors are visible in

Figures 2.7(c)-(d). Ideally they should also be hidden behind lenses 1 and 4, and can be reduced with careful alignment or larger outermost lenses (lenses 1 and 4).

Another setup we tried used all Edmund Optics lenses:

Lenses 1 & 4 Edmund Optics 75 mm outer diameter x 200 mm focal length, MgF2 coated, achromatic doublet lens (Stock number #45-417),

Lenses 2 & 3 Edmund Optics 50 mm outer diameter x 75 mm focal length, MgF2 coated, achromatic doublet lens (Stock number #49-291).

We present the thick lens distances that were calculated for this setup, for those who would like to try this version as well: $t_1 = t_3 = 248.9$ mm, $t_2 = 333.9$ mm, and total length $L = 928.5 (= 333.9 + (248.9 + 23.94 + 24.5) * 2)$ mm.

B.2 Material Data for Symmetric, Paraxial Four Lens Cloak

Here we provide material data necessary for full-field phase-matching of the four lens "Rochester Cloak." Details of the lenses used can be found in Appendix B.1.2.

The index of refraction for the three Schott glasses follow the Sellmeier dispersion formula [44, 78]:

$$n^2(\lambda) = 1 + \frac{B_1\lambda^2}{\lambda^2 - C_1} + \frac{B_2\lambda^2}{\lambda^2 - C_2} + \frac{B_3\lambda^2}{\lambda^2 - C_3}. \tag{B.1}$$

The Sellmeier coefficients for the Schott glasses used are given in Table B.2.

The Hikari EBAF11 glass uses a different dispersion formula than the Sellmeier equation. Its coefficients and dispersion formula are given in Ref. [79], which were

Table B.1: Paraxial four lens cloak specifications. Information for each surface- Radius of curvature (mm), thickness (mm) and material type. Thicknesses denote on-axis distances to the right of the surface until the next surface. Material type left blank implies air.

Surface	**Radius**	**Thickness**	**Material**
Lens 1 (left)	109.86	8.500	Schott NBK7
Lens 1 (center)	-93.11	2.000	Schott SF2
Lens 1 (right)	-376.25	255.491	
Lens 2 (left)	247.70	3.000	Schott NSF11
Lens 2 (center)	41.69	20.000	Hikari EBAF11
Lens 2 (right)	-50.80	332.167	
Lens 3 (left)	50.80	20.000	Hikari EBAF11
Lens 3 (center)	-41.69	3.000	Schott NSF11
Lens 3 (right)	-247.70	255.491	
Lens 4 (left)	376.25	2.000	Schott SF2
Lens 4 (center)	93.11	8.500	Schott NBK7
Lens 4 (right)	-109.86		

Table B.2: Several Schott glass coefficients of the Sellmeier dispersion formula. C coefficients are in units of μm^2. Values from Ref. [78].

Glass	B_1	B_2	B_3
	C_1	C_2	C_3
NBK7	1.03961212	0.231792344	1.01046945
	0.00600069867	0.0200179144	103.560653
SF2	1.40301821	0.231767504	0.939056586
	0.0105795466	0.0493226978	112.405955
NSF11	1.73759695	0.313747346	1.89878101
	0.013188707	0.0623068142	155.23629

verified in CODE V (the optical simulation software used):

$$\begin{aligned} n^2(\lambda) =& 2.71954649 - 1.00472501 \times 10^{-2}\lambda^2 \\ &+ 2.00301385 \times 10^{-2}\lambda^{-2} + 4.65868302 \times 10^{-4}\lambda^{-4} \\ &- 7.51633336 \times 10^{-6}\lambda^{-6} + 1.77544989 \times 10^{-6}\lambda^{-8}, \end{aligned} \tag{B.2}$$

where λ is in μm.

C Appendix: Additional Optical Designs

C.1 Initial Multidirectional Ray Optics Cloak

C.1.1 Design

We provide a simple optical system that fulfills both requirements for a ray optics cloak in the paraxial regime- it contains a non-zero volume to hide an object, and satisfies Equation (2.1). Figure C.1 is such a solution. For the on-axis ray shown (thick arrows), this appears to be perhaps a trivial solution. However, it is not as straight-forward for all other possible ray directions and positions.

For simplicity, our system is in air, with the index of refraction of air (n_{air}) set to 1. The ABCD Matrix for the system is given as:

$$\begin{bmatrix} 1 & 0 \\ 1/f_5 & 1 \end{bmatrix}.\begin{bmatrix} 1 & -t_4 \\ 0 & 1 \end{bmatrix}.\begin{bmatrix} 1 & t_3 \\ 0 & 1 \end{bmatrix}.\begin{bmatrix} 1 & 0 \\ \frac{-2}{r_3} & 1 \end{bmatrix}.\begin{bmatrix} 1 & -t_2 \\ 0 & 1 \end{bmatrix}.\begin{bmatrix} 1 & t_1 \\ 0 & 1 \end{bmatrix}.\begin{bmatrix} 1 & 0 \\ -1/f_1 & 1 \end{bmatrix}, \tag{C.1}$$

where the t's are the longitudinal distances (along the $z-$axis) between each optical element, f's are the focal lengths, and r_3 is the radius of curvature of the center mirror (See Figure C.1). The four thick arrows follow the path of an on-axis ray. Note that this uses the thin lens approximation (lens thickness $\to 0$). Also, the $z-$axis follows the thick arrows, since this is the center axis of symmetry.

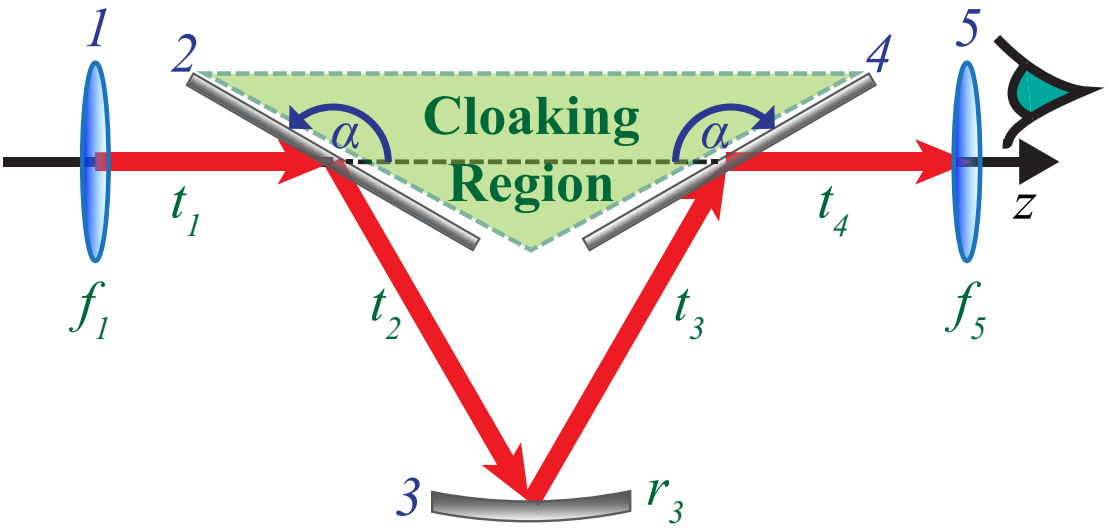

Figure C.1: Diagram of our initial ray optics cloaking device in air. t's are longitudinal distances (along the $z-$axis), f's are focal lengths, and r_3 is the radius of curvature of mirror 3. Elements 2 and 4 are flat mirrors. The four thick arrows follow the path of an on-axis ray with incident angle zero.

Care must be given for the signs of all the terms in Equation (C.1), so as to remain consistent. Otherwise, the correct solution space will not be found. We follow the convention found in Reference [72], where after odd number of reflections the propagation distance t and the index of refraction n change signs. With this convention, the space in which light exits (to the far-right) has index of refraction $n_5 = -n_{\text{air}} = -1$ and the y-axis also changes signs (by carefully considering propagation directions). In our space, a perfect cloaking system fulfills the following modified condition:

$$\begin{bmatrix} y' \\ -u' \end{bmatrix} = \begin{bmatrix} -1 & -L \\ 0 & -1 \end{bmatrix} \begin{bmatrix} y \\ u \end{bmatrix} = \begin{bmatrix} -(y+Lu) \\ -u \end{bmatrix}. \tag{C.2}$$

We desire to undo any changes that the first half of our system makes on the light rays. Doing so may make the rays retain the same direction, similar to a retro-reflector. This can be done by making the second half symmetric to the first half ($f_5 = -f_1$, $t_4 = -t_1$, $t_3 = -t_2$). We can then easily solve for f_1 such that

$A = -1$ for the ABCD matrix:

$$f_1 = t_1 - t_2. \tag{C.3}$$

Serendipitously, this is the same condition that sets $C = 0$. As noted before, $D = -1$ is automatically satisfied. Equation (C.3) shows that requiring our system to have symmetric halves is helpful. With f_1 set to Equation (C.3), the ABCD matrix for our device simplifies to:

$$\begin{bmatrix} -1 & 2(t_1 - t_2)(r_3 - t_1 + t_2)/r_3 \\ 0 & -1 \end{bmatrix}. \tag{C.4}$$

We can now solve for the radius of curvature of the center mirror, r_3, to satisfy the remaining condition: $B = -L$. With the geometry shown in Figure C.1,

$$L = 2\left(t_1 - t_2 \sin\left(2\alpha - 3\pi/2\right)\right). \tag{C.5}$$

Solving for r_3 we obtain our second condition:

$$r_3 = -\frac{(t_1 - t_2)^2}{-2t_1 + t_2 + t_2\cos(2\alpha)}. \tag{C.6}$$

It is interesting to point out that if $r_3 = f_1$, then $B = 0$. We see then that our optical system can either be an identity transformation *or* a cloaking system.

Only equations (C.3) and (C.6) need to be met for this optical system to be a perfect cloak, paraxially. For a lens with $f_1 = 200$ mm, mirror 2 tilt angle $\alpha = 150°$, and $t_2 = -40$ mm, we solved for t_1 and r_3. $t_1 = 160$ mm. We calculated $r_3 = 105.3$ mm from Equation (C.6). The net length of the system was then $L = 360$ mm. Using these values we directly traced the real rays (using Snell's Law directly; accurately simulates rays in a real lens, beyond the paraxial approximation) in CODE V, as shown in Figure C.2(a). For the simulation, we obtained t_1 by subtracting $|t_2|$ from the back focal length of the lens used, to properly account for the lens thickness (so $t_1 \approx 150$ mm). We see that the on-axis

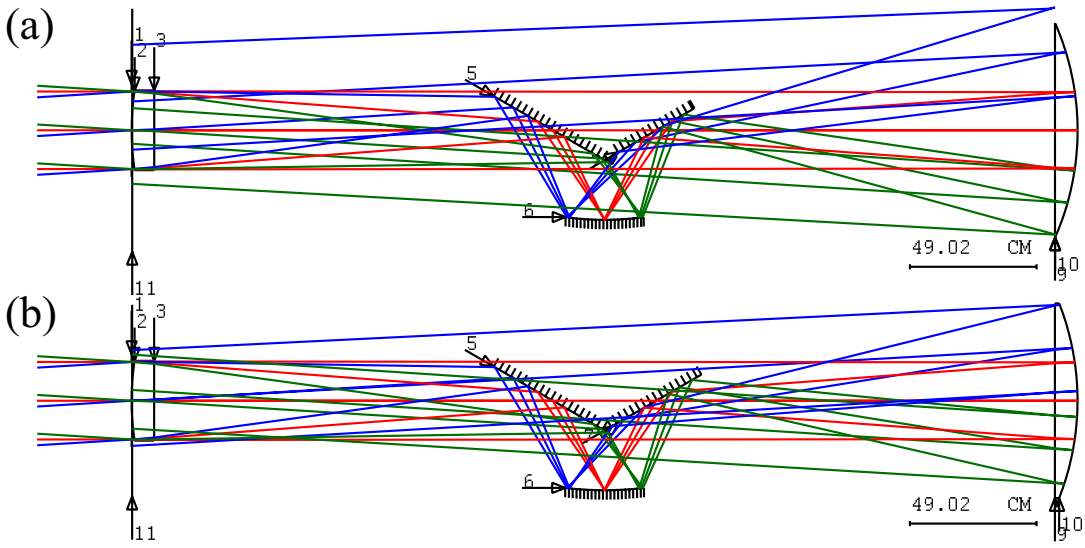

Figure C.2: Simulations for our initial cloaking design. (a) Cloaking Design 1. Entrance pupil is 30 mm, with field-of-view $-3.5°{\sim}3.5°$. Diameter of last lens needs to be > 95 mm for clearance (no "vignetting") of all entering rays. **(b)** Cloaking Design 2. Same as Design 1, but optimized for r_3 to reduce transverse shifts of off-axis rays. Entrance pupil and field of view are same, but minimum diameter for last lens has been reduced to 74 mm.

rays are perfectly undeviated, and the other field rays are only slightly shifted while maintaining their initial angles quite closely.

A quick optimization was run in CODE V to bring the center of the angled rays closer to where they should be located. We simply optimized r_3 only, the curvature of the center mirror, and obtained the improvement shown in Figure C.2(b). Though the size of the ray bundles entering the system ("entrance pupil") was the same, the required minimum diameter of the last lens was reduced by over 20 mm. The range of incident angles that our optical system can accept ("field-of-view") was $-3.5°\sim+3.5°$.

Both figures in Figure C.2 show some shifts in the positions of the off-axis rays. It is easy to conclude that this may be because we used the paraxial approximation. A careful look shows that the transverse shifts are different for different incident angles. This hints at the system no longer being rotationally symmetric. This is because the center mirror has a non-zero focusing power and a tilt, simultaneously.

C.1.2 Rotationally Symmetric Improvement

Typically, the ABCD ray tracing matrices assume rotational symmetry since only y is used, instead of both x and y. We can easily correct the breaking of rotational symmetry seen in Figure C.1. We simply replace the center mirror with a focusing lens and a flat mirror. Since we also want symmetric halves, we will use two lenses and a flat mirror. This is shown in Figure C.3.

The ABCD matrix for this new system is:

$$\begin{bmatrix} 1 & 0 \\ 1/f_5 & 1 \end{bmatrix} \cdot \begin{bmatrix} 1 & -t_4 \\ 0 & 1 \end{bmatrix} \cdot \begin{bmatrix} 1 & t_3' \\ 0 & 1 \end{bmatrix} \cdot \begin{bmatrix} 1 & 0 \\ -1/f_3' & 1 \end{bmatrix} \cdot \begin{bmatrix} 1 & t_3 \\ 0 & 1 \end{bmatrix} \cdot \begin{bmatrix} 1 & -t_2' \\ 0 & 1 \end{bmatrix} \cdot \begin{bmatrix} 1 & 0 \\ 1/f_2' & 1 \end{bmatrix} \cdot \begin{bmatrix} 1 & -t_2 \\ 0 & 1 \end{bmatrix} \cdot \begin{bmatrix} 1 & t_1 \\ 0 & 1 \end{bmatrix} \cdot \begin{bmatrix} 1 & 0 \\ -1/f_1 & 1 \end{bmatrix} \tag{C.7}$$

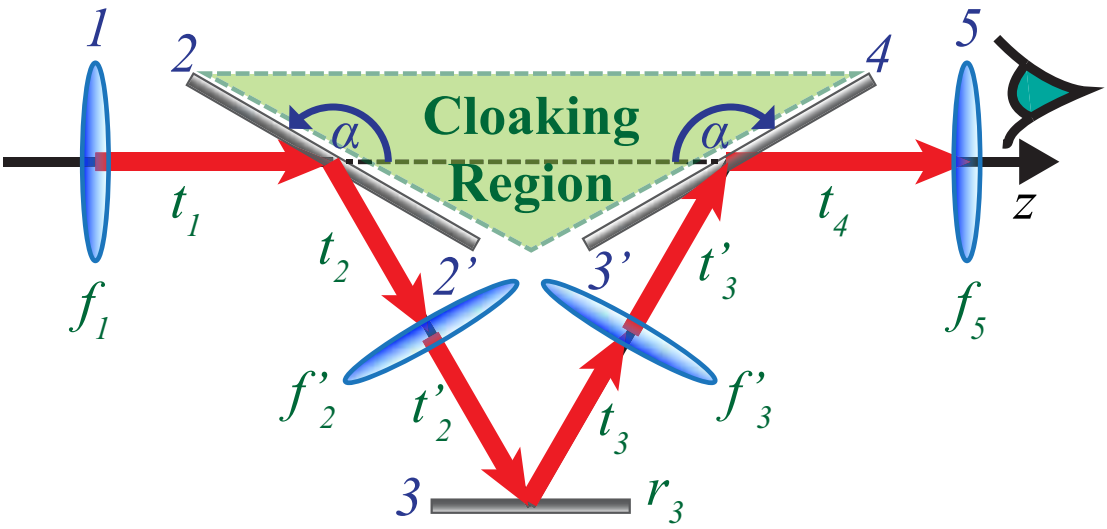

Figure C.3: Rotationally symmetric version of our initial cloak. Cloaking Design 3. Rotationally symmetric design of Figure C.1. t's are longitudinal distances and f's are focal lengths. Elements 2, 4 *and* 3 are flat mirrors. The thick arrows follow the path of an on-axis ray with zero incident angle.

This time we would like to fix f_1 to be the focal length of the lens to be used, and instead find a solution for t_1. This is because it is usually easier to purchase a ready-made lens and then adjust the spacing, rather than the other way around. Requiring $A = -1$ and $C = 0$, we obtain

$$t_1 = \left[f_1(f_2' - t_2') + f_2'(t_2 + t_2') - t_2 t_2'\right] / \left(f_2' - t_2'\right). \tag{C.8}$$

With t_1 set to Equation (C.8), the ABCD matrix for our device becomes:

$$\begin{bmatrix} -1 & \left(2f_1[f_2'^2 + f_1(f_2' - t_2')]\right) / f_2'^2 \\ 0 & -1 \end{bmatrix}. \tag{C.9}$$

Similar to the simple design before, we can solve for the the focal length of the lens $2'$, f_2'. We want $B = -L'$, where the total length L' is now given by:

$$L' = 2\left(t_1 - (t_2 + t_2')\sin\left(2\alpha - 3\pi/2\right)\right). \tag{C.10}$$

Solving for f_2' we obtain our second condition:

$$f_2' = -\frac{f_1^2 \pm \sqrt{f_1^2(f_1^2 + 4f_1t_2' + 2t_2'L')}}{2f_1 + L'}. \tag{C.11}$$

Only equations (C.8) and (C.11) need to be satisfied for this modified cloaking system now. However, these form transcendental equations because L' is a function of t_1 (Equation (C.10)). At this point, we can solve for t_1 and f_2' numerically.

It is important to note that the equations above assume that all the lenses are infinitely thin. In reality, lenses have thicknesses, and this can make a large difference in obtaining the correct solutions for Equation (2.1). Hence, the calculations for our implementation required that we take a step further to correct Equations (C.8) and (C.11) using 'thick' lenses.

We simulated a symmetric cloaking system that we experimentally built, the details of which are given in the section C.1.4. Again, we used the calculated values for a perfect paraxial cloak, for our real ray simulation in CODE V. This is shown in Figure C.4(a). Field-of-view was the same as Figure C.2 ($-3.5°\sim+3.5°$), but the entrance pupil was increased to 40 mm. This allows more light to enter, which improves the resolution and 'speed' of the optical system. Even without any separate CODE V optimization, we see a marked improvement over the previous, simpler design in Figure C.2(a). The rays are closer to where they need to be, and the size of the rays exiting the system has not increased much even compared to Figure C.2(b).

Finally, we demonstrate the ease of scalability of our design for any cloaking size. We only need to scale all radii of curvature, lengths, and entrance pupil by the same factor. In Figure C.4(b), we simply doubled all of these parameters to obtain double the cloaking space.

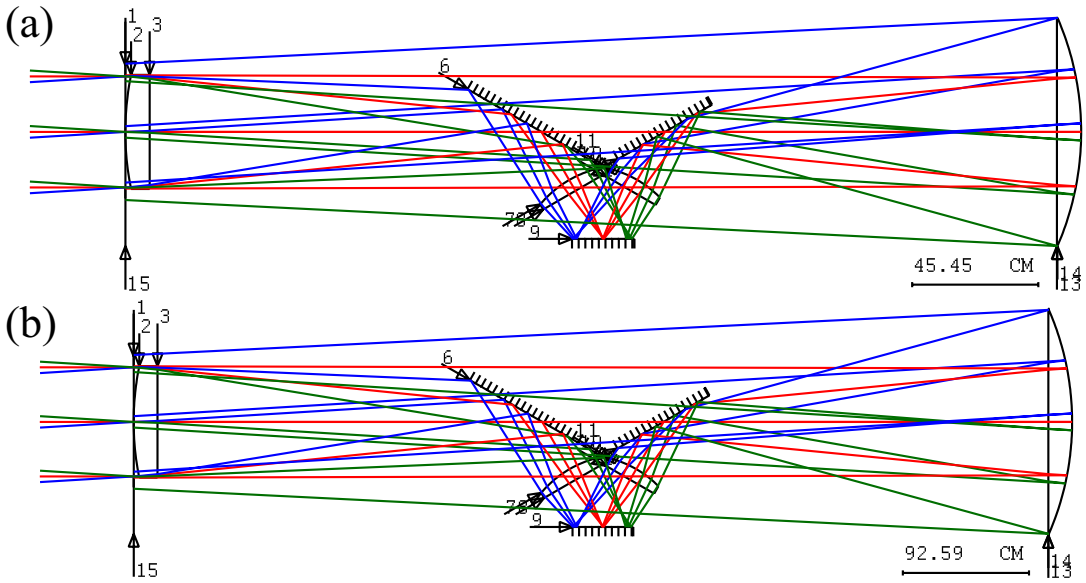

Figure C.4: Simulations for rotationally symmetric version of our initial cloak. (a) Cloaking Design 3 with four lenses. Entrance pupil is 40 mm, with field-of-view $-3.5°\sim3.5°$. Diameter of last lens needs to be > 82 mm for no vignetting. **(b)** Scaling of Design 3 by factor of 2. By doubling optical curvatures, lengths and pupil, we obtain double the cloaking diameter.

C.1.3 Limitations of Design

The design shown here, in particular Figure C.4(a), was experimentally tested. Though not clear when viewing a 2D projection of the simulations, as shown in Figures C.4, rays in other planes in 3D will be inverted. This made the design to work only in a 2D plane with off-the-shelf optics that we used. To make it work in 3D, a dove prism was necessary. Another more elegant, but expensive correction, would be to use custom-optics to make all the elements of the system completely rotationally symmetric about an axis that connects the centers of the first and last lenses. In order to explore simpler designs that might be achievable with readily available optics, we investigated whether other solutions were possible and easy to build. This then led to an all lens solution provided in Chapter 2 [5].

C.1.4 Methods for Design

Here we provide the details of the design for our experimental and simulated design in Figure C.4(a). For the first lens and last lenses (1 and 5), we used BK-7 lenses from Edmund Optics with $f_1 = 200$ mm (radius of curvature 103.4 mm) and thickness 8.74 mm. For the two middle lenses ($2'$ and $3'$), we used BK-7 lenses that were 4.5 mm thick with power close to what was optimized through simulations. The calculations were based off of the center wavelength of 587.6 nm. Using a tilt angle of $\alpha = 150$ degrees for mirror 2, and $t_2 = t_2' = -20$ mm, we solved for t_1 and f_2'. The result was that $t_1 = 141$ mm and $f'2 \approx 75$ mm (radius of curvature 38.8 mm). This was after some iterations of adjusting parameters, since we wanted to match a readily available 75 mm focal length lens. The overall length of the system was then $L' = 340$ mm. Additionally, we made various small changes to the base design to find an optimal setup.

D Appendix: Digital Integral Cloak- Supplementary Material

This document provides supplementary information to "Digital integral cloaking" (Chapter 4). Detailed specifications and measurements for our setup and demonstration are provided here. Additional principles and theory are provided to help clarify our work.

D.1 Methods

Here we describe in detail the experimental setup, measurements, and specifications.

D.1.1 Object space

The 'input plane' is where the sensor lied for the input camera (Sony DSC-RX10), and is parallel to the mechanical scanner/slider on which the input camera was mounted. The 'output plane' is where the display screen (Apple iPad mini 4) lied, along with the lenticular lens mounted on the display. The output plane is parallel to the input plane and the two planes are separated by a distance L (L was 13 cm

for our demonstration). The background objects consisted of four sets of colored blocks with the dimensions shown in Table D.1 (see also Figures 4.3(a) and 4.3(b)). For horizontal (**x**) separations between the blocks, the farthest sides of the dark

Table D.1: Object dimensions. Distance is from the input plane to the center of the objects, depth is the longitudinal (**z**) dimension, width is the horizontal (**x**) dimension, and height is the vertical (**y**) dimension. (All length units are in cm.)

Objects	**Distance**	**Depth**	**Width**	**Height**
Back wall (w/ black cover)	98			
Dark green blocks	87.6	3.8	3.8	33
Red blocks	70	5.7	2.5	35
Lime green blocks	47	3.8	3.8	33
Yellow blocks	40.6	3.8	3.8	29

green blocks and the red blocks were 9 cm apart, and the farthest sides of the lime green blocks and the yellow blocks were 18 cm apart. The blocks, from the back side of the dark green blocks to the front side of the yellow blocks, spanned a total depth of about 51 cm. The distance from the front face of the yellow blocks to the camera sensor at the input plane was 39 cm.

D.1.2 Input surface

We provide details of the input surface (at $z = z_i$) that collects the rays for propagation using Equation (4.1).

Input scan hardware

To capture the input images at the input plane, we used a digital camera (Sony DSC-RX10) for our 'input camera.' The Sony DSC-RX10 had a 1 inch 20.2 MP

Exmor sensor for low lighting, and a f/2.8 Carl Zeiss Vario-Sonnar T* 24-200mm lens with 8.3x optical zoom. It was mounted on a mechanical slider (from Varavon) that scans horizontally at a fixed speed, which can be adjusted. Visualization 4.1 shows ∼58 cm of travel on the scanner, but only $(W_s + 2L\tan(FOV_l/2)) = 18.5$ cm was necessary for our setup. Here, $W_s = 12$ cm was the active screen width of the display (Apple iPad mini 4), and $FOV_l = 29°$ was the field-of-view (FOV) of the output lenslet array (20 cylindrical lens-per-inch array from Micro Lens Technology).

Input scan video

Visualization 4.2 shows the actual scan by the input camera (Sony DSC-RX10), which was used for generating our cloaked image (Figures 4.3(c)-(f)), but modified to reduce the file size: Same 1920x1080 pixels frame size, but sped up by 500%, frame rate reduced to 30 frames/second from 60 frames/second, and bitrate reduced to 5 Mbps from 26 Mbps, compared to the original. With this input scan in Visualization 4.2, we captured 60 frames per second, while scanning at 6.35 mm/s. The input camera was focused at infinity, zoomed completely out (giving maximum spatial view), and stopped down to f/10. The field-of-view for the camera was measured to be about 60° and 33° for the horizontal and vertical dimensions, respectively.

D.1.3 Ray propagation processing

Without the propagation of the input rays to the output rays for $L \neq 0$, our system would not be a cloaking system, but rather a 3D display system. This propagation of rays over a finite distance is then a simple but important characteristic of a cloak. After collecting the images from the input video scan, the video frames

were processed using our code (written in C++) on our laptop (Lenovo Thinkpad W540).

Steps to propagate rays

Each input video frame was assigned an input ray position x_i, that is given by the position of the input camera at the time the frame was captured. Each 'view' represents an input ray angle θ_i, which corresponded to a horizontal pixel position of the input video frame. Each valid input ray was then propagated using Equation (4.1) with $y \to x$, $(z_f - z_i) \to L$, while assuming ambient air ($n = 1$). If the calculated output ray fell on a valid display pixel (in our case, an RGB subpixel), then the image pixel information for this input ray was mapped to the output display pixel. This then completed the ray propagation for the cloak.

Inverting propagation

For digital cloaking, it may be useful to invert Equation (4.1):

$$\begin{cases} y_i = y_f - (z_f - z_i)\tan\theta_f, \\ \theta_i = \theta_f \end{cases} \tag{D.1}$$

Equations (D.1) show us how to find the detector pixel that should be used for the display pixel positioned at $y = y_f$, $z = z_f$. For example, we can first select detector subpixels that collect rays of the same angle ($\theta_i = \theta_f$), color, and any other desired attributes as the output ray. Out of these candidate subpixels, we then select the one that has transverse (y) position closest to y_i, and longitudinal (z) position closest to z_i, where y_i and z_i satisfy Equations (D.1). Graphically, we can extend the dotted arrow in Figure 4.1(b) backward until it intersects the cloaking surface, and then find the nearest matching subpixel.

Vertical scaling

Since our demonstration was a 2D cloak that used cylindrical lenses, the vertical pixel positions of the background objects were fixed. This implies that the vertical size, or magnification, relative to the screen size will be constant, even if the observer changes position only in the 2D **x**-**z** plane. However, we can at least match the vertical magnification for a particular observer distance and object depth combination, which is what we did. Specifically, for our demonstrations shown in Figures 4.3 and 4.4, our code matched the vertical size of objects that were 65.4 cm from the input plane (in the $-\mathbf{z}$ direction), which corresponded roughly to the middle of all four sets of blocks. This object plane would then theoretically match in vertical size when an observer was 185.4 cm from the output plane (in the $+\mathbf{z}$ direction).

D.1.4 Output surface

We now describe the display (output) plane of our cloak.

Output display

The output display monitor we used was an Apple iPad mini 4. The display was an LED-backlit LCD monitor, with an active screen size of 20 cm (=7.9 inch) in the diagonal direction. The display pixel size was 2048 x 1536 resolution, at 326 pixels-per-inch (PPI). We assumed the display pixels were square pixels, which was a fairly good assumption. This gives a width of 12.0 cm, and a height of 16.0 cm for the active screen size, in portrait mode. The 3 RGB (Red, Green, Blue) subpixels that composed 1 display pixel, were long in the vertical direction and short in the horizontal direction when the iPad mini was in portrait mode. This is why we used the display screen in portrait mode with the slanted lenslet array at an angle of 3 pixels vertically down, and 1 pixel horizontally across.

Output lenslet array

The 20 cylindrical lens-per-inch array from Micro Lens Technology we used was a very thin (0.41 mm) sheet of plano-convex lenses. This was so we could manually adjust the separation distance between the lenslet array and the display screen. The lenslet array was mounted on a transparent glass that was 2.3 mm thick, using the adhesive layer on the flat side of the lenslet array. The distance between the lenslet array and the screen was adjusted so that the LCD screen pixels lied at the back focal plane of the lenslet array. The field-of-view of the output lenslet array (FOV_l) given by the manufacturer was 29°.

Slanted RGB subpixel imaging

The cylindrical lenses of the output lenslet array were slanted at an angle of 3 pixels vertically down, 1 pixel horizontally across. This then uses the 3 RGB subpixels of the display to gain 3 times the horizontal angular resolution (in number of 'views'), at the sacrifice of vertical resolution. Our particular combination of slanted lenslet array and display monitor generated 51.5 discrete 'views' over 29° of viewing angles (field-of-view).

With this slanted setup, the total number of views ($DimViewX_s$), for a given display monitor and lenslet array combination, is given by:

$$DimViewX_s = \sqrt{10} \cdot \frac{PPI}{LPI}. \tag{D.2}$$

PPI (pixels-per-inch) is the pixel density of the display monitor, and LPI (lens-per-inch) is the lens density of the cylindrical lenslet array used. Equation (D.2) assumes that the display pixels are uniform and square in dimension.

D.1.5 Measurements

Here we describe the details of the "measurements" that demonstrated our 2D digital integral cloak.

Horizontal (x) demonstration

The details for the horizontal demonstration shown in Figures 4.3(c)-(f), are now given. The "observer" camera (Nikon D3200) was 260 cm (along $+\mathbf{z}$) from the display screen (cloak), and scanned a total distance of 61.4 cm (along $-\mathbf{x}$) in Visualization 4.3. The center of the cloak and camera aligned (0°, or $x = 0$) at 13 seconds into the 20 second clip shown in Visualization 4.3. Viewing angles are positive when the observer camera is to the right ($x > 0$) of the cloak/display, when facing the display screen as shown in Figures 4.3(c)-(f). Both Visualization 4.3 and Visualization 4.4 were sped up by 200%, from the original videos.

Longitudinal (z) demonstration

Figures 4.4(a)-(d) showed images from varying observer positions ($z = 272$ cm, 235 cm, 203 cm, and 150 cm, for Figures 4.4(a)-(d) respectively, for the display screen located at $z = 0$). These positions then collect varying ranges of angles (or 'views') from the light rays emitted by the output cloaking display screen. Assuming that the center of the observer/camera aligns with the center of the cloaking screen, we can calculate the range of horizontal ($\mathbf{x}$) angles collected ($FOVx_{\text{observer}}$):

$$FOVx_{\text{observer}} = 2\arctan(W_s/2/z_{obs}), \tag{D.3}$$

where W_s is the horizontal width of the output display screen of the cloak, and z_{obs} is the longitudinal distance of the observer from the output screen (the output plane, which is set to $z = 0$). The resulting $FOVx_{\text{observer}}$ values were then 2.53°, 2.93°, 3.38°, 4.59°, for Figures 4.4(a)-(d), respectively.

The images shown in Figures 4.4(a)-(d) were cropped, but maintained the same pixel size as each other, just like the original images. The observer camera for these images used a tripod to maintain the same height (y), while varying the longitudinal distance z. We attempted to maintain the same horizontal position x of the observer camera, but there was a variance of several cm or so. Note that the centers of the camera and the screen must align for Equation (D.3) to be correct. However, for the small $FOVx_{\text{observer}}$ values as given in Figures 4.4(a)-(d), the range of angles should closely match to the calculated values given.

D.2 Characterization Metrics

We present details of some of the calculations made in the main text, for the metrics that were used to characterize our digital integral cloak. Since our cloak was a 2D demonstration, our analysis is limited to the horizontal ($\mathbf{x}$) and longitudinal ($\mathbf{z}$) dimensions.

D.2.1 Output surface metrics

Output spatial resolution

The limiting spatial resolution of our cloaking system was given by the output lenslet array. The spatial resolution then can simply be calculated by inverting the lens per length value of the lenslet array. So for the 20 lens-per-inch (LPI) lenslet array we used, the spatial resolution is given by 1.27 mm = 1/(20 lens/inch). This is the width of a single lens of the output lenslet array. However, this is true only if the cylindrical lenslet arrays were not slanted at an angle. Since we used RGB subpixel interlacing, we slanted our lenslet array at an angle of 1 pixel across (horizontally) to 3 pixels down (vertically). The corrected horizontal

spatial resolution (dX'_s in inches) is then given by

$$dX'_s = \frac{1}{LPI} \cdot \frac{\sqrt{10}}{3}. \tag{D.4}$$

The limiting spatial resolution of our cloak, calculated from Equation (D.4), is then 0.0527 inch = 1.34 mm.

Output display pixel spacing

The output display monitor (iPad mini 4) had a pixel density of 326 pixels-per-inch (PPI). So the pixel spacing resolution (horizontal or vertical) of the output display is 0.078 mm. Since we use RGB subpixel interlacing, we actually use the 3 RGB subpixels, giving a finer spatial resolution of 0.078/3 mm = 0.026 mm per RGB subpixel.

This small pixel resolution was used in calculating the propagated ray positions (Equation (4.1)) more precisely than the spatial resolution of the lenslet array (Equation (D.4)), for our cloaking demonstration. However, using the spatial resolution in Equation (D.4) also seemed to provide similar images, likely due to the relatively small spacing of both values compared to the observation distances.

Output angular resolution

The limiting angular resolution of our cloaking system was given by the output surface (display + lenslet array). The angular resolution ($d\theta_o$) is simply

$$d\theta_o = \frac{FOV_l}{DimViewX_s}. \tag{D.5}$$

FOV_l is the field-of-view (FOV) of the lenslet array, and $DimViewX_s$ is the total number of views from Equation (D.2). For the digital integral cloak we demonstrated, $d\theta_o = 0.56°$.

D.2.2 Input surface metrics

Ideal input system

First, the quality of input rays captured rely on the ability to separate position and angle (momentum) precisely, with no cross-talk. This is done by focusing the input camera to infinity (see Figure 4.2(a)) and 'stopping down' the aperture. The sum effect of these two steps is that a single input ray (with fixed input position and angle) is mapped to a single detector pixel.

Input spatial resolution

Recall that for the input scan we used (see Visualization 4.2), we captured 60 frames per second, while scanning at 6.35 mm/s. This high frame rate and slow scan gave a horizontal spatial resolution (dX_c) of 0.106 mm for the spacing between input camera positions:

$$dX_c = \frac{v_{scan-s}}{FPS_c}. \tag{D.6}$$

Here, v_{scan-s} is the speed of the scan in units of (length/second), and FPS_c is the frame-per-second frame rate of the input camera.

Input angular resolution

Focusing to infinity maps the same ray angles to the same detector pixels of the input camera. Hence the input ray angles are then limited by both the aberrations of the camera and the detector pixels. With a highly aberration-corrected Carl Zeiss lens, we assume aberrations were minimal. Then the horizontal input angular resolution ($d\theta_i$) is given by

$$d\theta_i = \frac{FOV_c}{DimX_f}, \tag{D.7}$$

where FOV_c is the horizontal field-of-view of the input camera, and $DimX_f$ is the total number of horizontal pixels for the input video frame. $d\theta_i$ corresponds to the uncertainty in the input ray angles. For our case, $d\theta_i \approx 60^\circ/1920 = 0.031^\circ$.

Input aperture

Next, we needed to ensure that each transverse object position was mapped to separate detector pixels as well. This can be achieved by 'stopping down' the aperture of the input camera. Doing so decreases the aperture size, reducing the transverse ($\mathbf{x}$, $\mathbf{y}$) spatial extent of the rays that are captured by the input camera. Otherwise, blurring of the input images occur, i.e., a reduced depth-of-field results. It is well known in optics and photography that smaller 'f-numbers' (=focal length/aperture size) or reduced aperture size, improves the depth-of-field, which is how clear ('in-focus') the objects appear. Ideally, the aperture size should be infinitely small, but then the amount of light entering is infinitely small, too. So we balanced this by using an f-number (f/#) = f/10.

With the input f/#, we can calculate the diameter of the input aperture stop (CA_i) used:

$$CA_i = \frac{f}{f/\#}. \tag{D.8}$$

Here, f is the focal length used. The specifications for the Sony DSC-RX10 input camera stated the focal length range to be f = 8.8 - 73.3 mm. Since we had zoomed all the way out, we used f= 8.8 mm. This then gives an input aperture size CA_i=0.88 mm. CA_i gives roughly the range of transverse spatial positions of the objects that are captured for each detector pixel of the input camera. This is particularly true when the lens is focused to objects at infinity, since only a single collimated ray bundle will enter the lens and be focused onto a single detector pixel (ignoring diffraction and aberrations). So CA_i in this way is proportional to the blurring of objects in the input images.

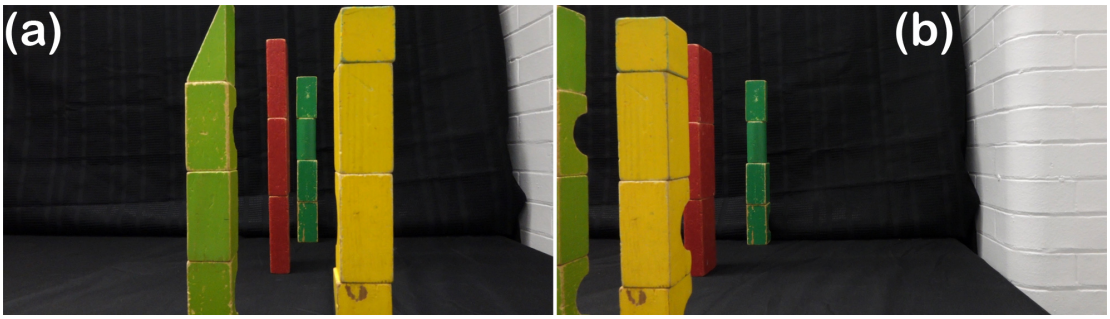

Figure D.1: (a)-(b) Input scan video frames. Snapshots at (a) 11 second, and (b) 17 second from Visualization 4.2. Large depth-of-field of the input scan is demonstrated, with objects from 39 cm to 98 cm (back wall) from the camera (input plane).

The number to compare to CA_i would be the aperture set by the output surface, which is given by the spacing of a single lens in the output lenslet array (1.34 mm), or the output spatial resolution (Equation (D.4)). Again, the output lenslet array can be seen to be the limiting element for spatial resolution and blurring of objects in the cloak. It is worth noting that CA_i is different than the positional uncertainty of the input camera; the latter is the uncertainty for each input ray position, and is given by the input spatial resolution (Equation (D.6)) of the camera scan we determined earlier (0.106 mm).

Input depth of field

Here we discuss the depth-of-field of our input system briefly. Figure D.1 shows snapshots of the input scan used for our cloaking system (see Visualization 4.2). We can see that all the blocks, even the groove lines in the white wall, and the patterns on the back wall are in good focus. Again, the input camera was not the limiting factor for our cloaking system, as we could achieve several meters of depth-of-field easily, but the display (output) surface limited both the spatial and angular resolutions, and hence also what object depths that could be shown clearly.

D.2.3 Other system metrics

Sensitivity to misalignment

Misalignment in hardware setup and imprecise propagation calculations can reduce the cloak quality. These can physically be manifested in skewed angles, shifts in object positions, or mismatching speeds of object movements as seen on the cloak, when compared to the actual background without the cloak. Our system seemed to be most sensitive at the output surface. This is mainly due to the high pixel density (326 pixels-per-inch) of the output display. So the horizontal spatial sensitivity (dx_{mis}) of an unslanted lenslet array to be misaligned on the display is such that a 0.078 mm change in position will shift the 'view' seen by an observer. For slanted lenslet arrays, which is what we used, dx_{mis} is 3 times more sensitive (0.026 mm).

Ideally, the angle of the lenslet array should align exactly along the display pixel line. Even 1 pixel change across the total height of the display screen will begin to cause deviations from the ideal image. So the angular sensitivity ($d\theta'_{mis}$) of the alignment of the lenslet array with respect to the display screen pixels is

$$d\theta'_{mis} = 2\arctan\left(\frac{(1/2)(3/\sqrt{10})(1/3/PPI)}{Hs_{in}}\right), \tag{D.9}$$

where PPI is the pixels-per-inch linear pixel density, and Hs_{in} is the active display screen height in inches. Equation (D.9) is for slanted lenslet array mounting on the display. For unslanted lenslet mounting, the $(3/\sqrt{10})$ factor in arctan should be removed. For our demonstrated digital integral cloak with slanted lenslets, $d\theta'_{mis} = (8.8 \times 10^{-3})^{\circ}$, We can see that increased resolution of displays used require increasingly careful mounting of the lenslet array on the display screen, in both relative positioning and angular alignment.

Other factors

Other causes of reduced image quality for the cloak include non-uniform bending of the lenslet array plane toward or away from the display screen, and aberrations of the lenslet arrays themselves. Since easily accessible lenslet arrays are spherical or cylindrical in curvature, even spherical aberrations are not corrected. These aberrations effectively increase the depth and transverse size of the focal point of the lenslet arrays. The result is that the display pixels will not be in focus and multiple display pixels will mix, causing blurring of the output image. Even simple lens optimizations of the lenslet array surfaces should improve the cloaking quality.

D.3 Additional discretized cloaking designs

We suggest a few other methods for discretized cloaking, than the digital integral cloak we presented in Chapter 4.

D.3.1 Passive optical fiber cloak

Optical fibers or other optics, with good anti-reflection coatings, can be used to collect and transmit analog measurement values. Some advantages of this include cloaking in a passive (rather than active) manner, and that its spectrum can be continuously broadband. A disadvantage is that the cloakable volume will be reduced by the fibers now occupying some of this space. The amount of fiber can be reduced by using micro-arrays of objective lenses to couple the input light into the fibers, but at the price of cost and decreased resolution.

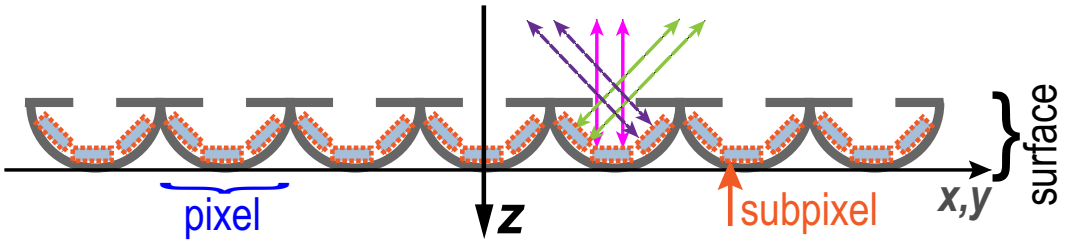

Figure D.2: Lensless 'integral cloaking' surface. Cross-section view shown. Detector and/or display subpixels can be placed on curved pixels. The top layer, which has holes for rays to pass, can be made to absorb light, or also detect incident light to calculate and compensate for irradiance losses.

D.3.2 Lensless digital integral cloak

Additionally, a discretized cloak without lenses is possible by using curved surfaces for detection and emission of rays. This is similar to one of the original methods proposed by Lippman for integral photography [80]. An example surface of such a cloak is shown in Figure D.2. This method might be easier to mass-produce and align than integral cloaking with lenses, and its field-of-view will not be limited by lens curvatures (although limited in other ways).

D.3.3 Digital integral cloak with 25 inch display monitor

Figures D.3(a) and D.3(b) show the setup for our 2D integral cloak. For the image capture (input) plane, we used a large field-of-view camera, mounted on a mechanical slider that scans horizontally at a fixed speed (see Visualization 4.1-HP25bw). Rays from the camera are processed by a computer that uses Equation (4.1) ('y' replaced by 'x') to determine the output rays for each display pixel. We used a 25 inch (diagonal) color monitor overlaid by a cylindrical lenslet array (10 lenses/inch) for the display (output) plane of the cloak. Both monitor and lenslet array were commercially available. By slanting the cylindrical lenses, we utilized the 3 RGB subpixels to gain 3 times the horizontal angular resolution

(in number of 'views'), at the sacrifice of vertical resolution [69]. Our particular combination of slanted lenslet array and display monitor generated 28 discrete 'views' over 48° of viewing angles (field-of-view). Each 'view' corresponds to a discrete ray angle/momentum that can be displayed for our system. The input plane (camera + slider) and display screen were separated by $L \approx 9.5$ inches (See Figure D.3(b)). The background objects (books and poster) ranged from 8.5 inches to 12.5 inches away from the input plane. For a 3D integral cloak, a fly's eye lens with spherical lenses on a 2D plane will work, as suggested initially. The bottleneck for a 3D version will likely be the input plane, as raster scanning over the 2D (**x**-**y**) plane would be necessary if using a single camera. A faster method, though more costly, would be to use a 2D array of detectors, combined with a fly's eye lenslet array, as initially shown in Figure 4.2(b).

Figures D.3(c)-(f) show a demonstration of this 2D integral cloak. A camera at a fixed height (y) and fixed distance z from the cloak was placed on a slider to scan horizontally (x). This camera was about 120 inches (along **z**) from the display screen, and scanned a total distance of 38 inches (along **x**) in Visualization 4.2-HP25bw. Figures D.3(c)-(f) show 3/4 of the total video, so correspond to about 13.5° range of viewing angles. The objects behind the cloak match in horizontal alignment and size (magnification) for varying depths of objects (from the cloak). The vertical magnification matched for a particular observer distance and object depth combination only, since this was a 2D cloak that used cylindrical lenses. In our case, we matched for the object depth of the "UR" poster, so that its vertical size was matched from the observation point near that of Figures D.3(c)-(f). However, if spherical fly's eye lenslet arrays are used for a full 3D integral cloak, the vertical alignment and magnification will match for varying object and observer distances. Figures D.3(g)-(i) show images from varying observer positions ($z = 66$ inch, 129 inch, and 232 inch, for (g), (h), and (i), respectively, for display screen at $z = 0$). As an observer moves closer to the cloak, a larger amount of

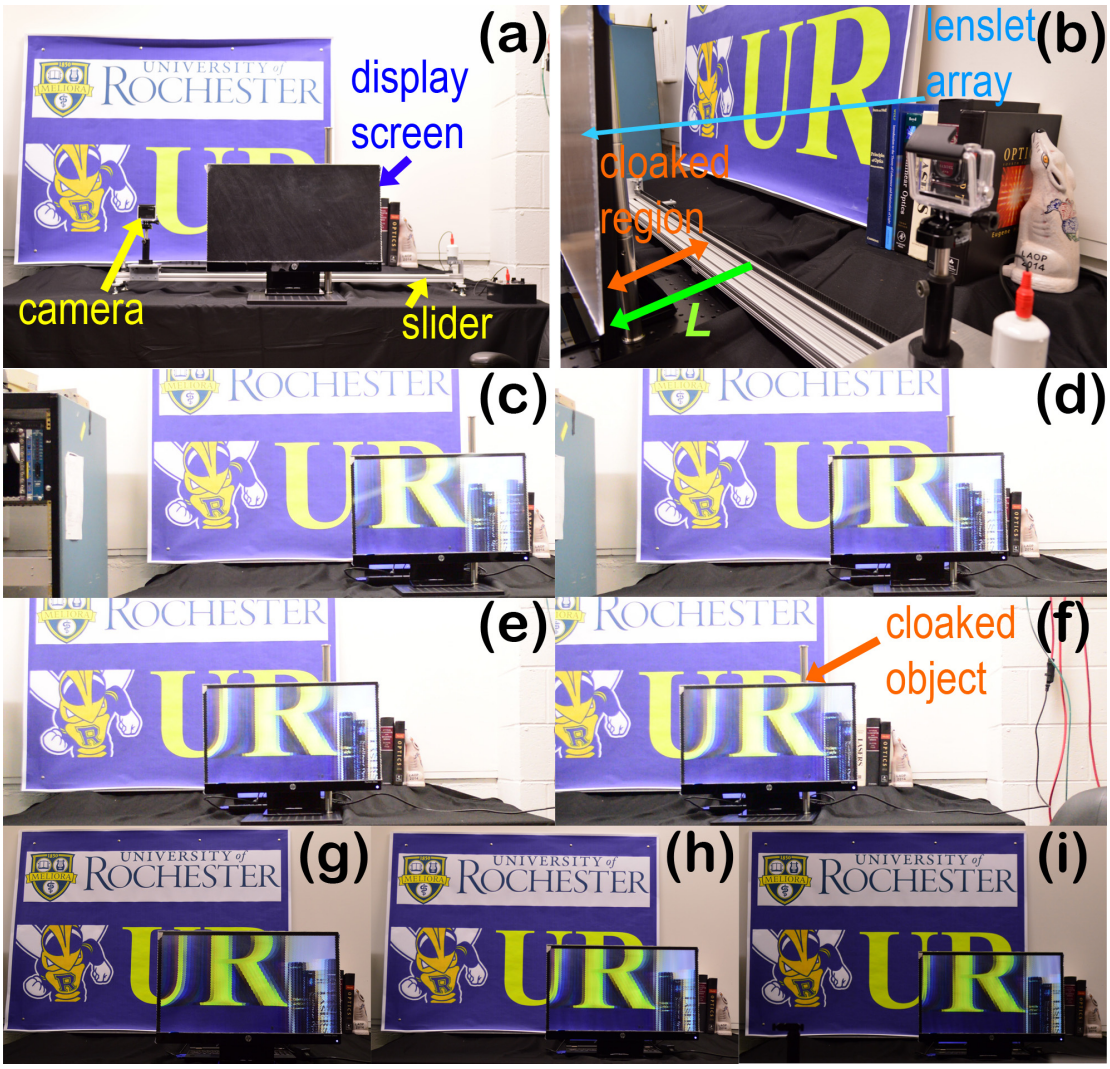

Figure D.3: (a)-(b) Integral cloak setup. Using cylindrical lenslet arrays, a 2D implementation is shown. A camera on a slider (input plane) scans horizontally to gather input rays. The lenslet array on the display screen, together (output plane) emit rays according to Equation (4.1). The space between the input plane and output plane (separated by a distance L) is the cloaked space. **(c)-(f) Integral cloak horizontal (x) demonstration.** Screen shots by a camera that moved horizontally across the room (see Visualization 4.2-HP25bw). The displayed output on the screen horizontally aligns with the background objects (poster and books), as the observer (camera) moves left or right (over ≈13.5° range). A rod placed between the input and output planes is cloaked. **(g)-(i) Integral cloak longitudinal (z) demonstration.** Observer (camera) at different distances in front of the display screen of the cloak. The horizontal field-of-views displayed on the screen were (g) 19°, (h) 10°, and (i) 5°. Images shown were zoomed and cropped to be similar in size. The field-of-view displayed on the cloaking screen changes to make the screen appear absent/cloaked.

the background scene is shown by the cloak. This is as expected for a cloak that appears as if absent (transparent).

Index